AFOSR-TR- 86-0848

STRUCTURAL RESEARCH SERIES 8601 - BOULDER, 1986

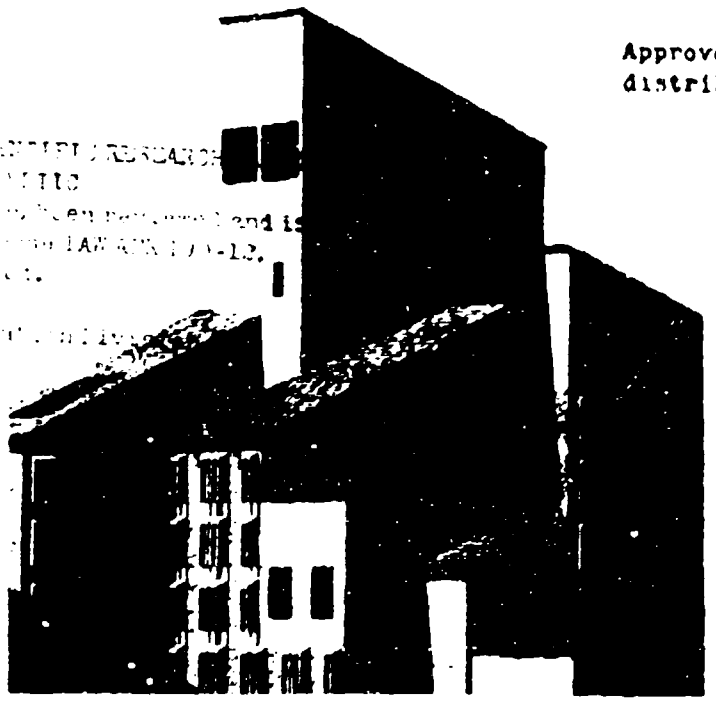

FINITE ELEMENTS AND LOCALIZED FAILURE

Final Technical Report

by

Kaspar Willam and Stein Sture

Department of Civil, Environmental,
and Architectural Engineering

College of Engineering
and Applied Science

University of Colorado, Boulder

UNCLASSIFIED
SECURITY CLASSIFICATION OF THIS PAGE

REPORT DOCUMENTATION PAGE

1a REPORT SECURITY CLASSIFICATION: UNCLASSIFIED	1b. RESTRICTIVE MARKINGS: Unrestricted
2a SECURITY CLASSIFICATION AUTHORITY	3 DISTRIBUTION/AVAILABILITY OF REPORT: Approved for Public Release; Distribution Unlimited
2b DECLASSIFICATION/DOWNGRADING SCHEDULE	
4 PERFORMING ORGANIZATION REPORT NUMBER(S)	5. MONITORING ORGANIZATION REPORT NUMBER(S): AFOSR-TR- 86-0848
6a NAME OF PERFORMING ORGANIZATION: UNIVERSITY OF COLORADO; 6b. OFFICE SYMBOL (If applicable): CEAE Dept.	7a. NAME OF MONITORING ORGANIZATION: AFOSR
6c ADDRESS (City, State and ZIP Code): CIVIL, ENVIRONMENTAL AND ARCHITECTURAL ENGRG. BOULDER, CO 80309-0428	7b. ADDRESS (City, State and ZIP Code): Bld 410 BAFB DC 20332
8a NAME OF FUNDING/SPONSORING ORGANIZATION: AIR FORCE OFFICE OF SCIENTIFIC RESEARCH; 8b. OFFICE SYMBOL (If applicable): AFOSR/NA	9. PROCUREMENT INSTRUMENT IDENTIFICATION NUMBER: AFOSR-82-0273
8c ADDRESS (City, State and ZIP Code): BOLLING AFB, DC 20332	10 SOURCE OF FUNDING NOS: PROGRAM ELEMENT NO 61102F; PROJECT NO. 2302; TASK NO. C2; WORK UNIT NO: UNCLASSIFIED
11 TITLE (Include Security Classification): FINITE ELEMENTS AND LOCALIZED FAILURE	
12 PERSONAL AUTHOR(S): KILLAN, KASPAR J. and STURE, STEIN	
13a TYPE OF REPORT: Final; 13b. TIME COVERED: FROM 8/1/82 TO 10/31/85	14 DATE OF REPORT (Yr., Mo., Day): Dec. 31, 1985; 15 PAGE COUNT: 137
16 SUPPLEMENTARY NOTATION	
17 COSATI CODES: FIELD / GROUP / SUB GR	18 SUBJECT TERMS (Continue on reverse if necessary and identify by block number): STRAIN-SOFTENING, LOCALIZATION OF FAILURE, POST-PEAK EXPERIMENTS, COMPOSITE FRACTURE MODEL, FINITE ELEMENT ANALYSIS OF PLAIN CONCRETE COMPONENTS

19 ABSTRACT (Continue on reverse if necessary and identify by block number)

The final technical report summarizes the activities and major results of the research project, "Finite Elements and Localized Failure". The report is divided into an administrative and into a technical part which describe the research efforts and technical findings in the following three areas:

(i) Post-peak laboratory experiments on plain concrete specimens in tension, low confined compression and direct shear,

(ii) Development of the "Composite Fracture Model" for the homogenization of failure within an elementary volume of finite dimension

(iii) Computational aspects of quasistatic and dynamic post-critical response analysis within the frame work of fracture energy equivalent strain-softening plasticity calculations.

20 DISTRIBUTION/AVAILABILITY OF ABSTRACT: UNCLASSIFIED/UNLIMITED ☒ SAME AS RPT ☐ DTIC USERS ☐	21 ABSTRACT SECURITY CLASSIFICATION: UNCLASSIFIED
22a NAME OF RESPONSIBLE INDIVIDUAL: Lt. Col. Lawrence D. Hokanson	22b TELEPHONE NUMBER (Include Area Code): 202/767-4935; 22c OFFICE SYMBOL: AFOSR/NA

DD FORM 1473, 83 APR EDITION OF 1 JAN 73 IS OBSOLETE

UNCLASSIFIED
SECURITY CLASSIFICATION OF THIS PAGE

Table of Contents

1. SUMMARY

The project on "Finite Elements and Localized Failure" was comprised of research on three different levels:

(i) Experimental Work:

Stroke controlled post-peak experiments on plain concrete specimens which were subjected to direct tension, triaxial compression and direct shear.

(ii) Constitutive Work:

Homogenization of localized failure due to tensile cracking and frictional slip in the form of the "Composite Fracture Model" which describes the degradation of strength within an elementary volume of a fracture energy equivalent continuum.

(iii) Computational Work:

Stabilization of strain-softening computations of localized failure within solids subjected to tensile cracking and/or shear faulting.

2. RESEARCH OBJECTIVES

The principal objective of the research project on "Finite Elements and Localized Failure" was the limited ductility or rather the "fragility" of particulate composites such as concrete under low confinement. This facet of the material behavior controls the strength and deformability of indeterminate structures which exhibit substantial reserves as long as sufficient ductility accompanies the localization of failure.

Within this endeavour several critical issues had to be addressed in order to gain insight into the fundamental aspects of brittle-ductile fracture. Since failure is a structural rather than a local constitutive process involving stress redistribution and non-uniform deformation, the research efforts encompassed several closely interrelated tasks on the experimental, the constitutive as well as the computational level.

2.1 Experimental Issues

1. Under what condition does concrete failure reduce to a local constitutive issue such that the degradation of strength and stiffness on the structural level does directly reflect the effects of localized strain-softening?
2. To what extent is progressive concrete failure a surface driven fracture phenomenon of singular macrodefects rather than the result of distributed microdefects within a volume driven damage process?
3. Is there a transition between brittle fracture and ductile flow which separates softening from the hardening response regime and where is it located?

4. Are tensile cracking and shear faulting separate failure mechanisms due to debonding and decohesion or is the development of shear bands simply the result of coalescing tensile cracking?
5. Is dilatancy a frictional mechanisms associated with the loss of normality or is it simply another facet of fracture under mixed mode conditions?
6. To what extent is brittle failure the result of tensile straining rather than tensile stressing?
7. Is the loss of strength in the post-peak regime accompanied by simultaneous degradation of stiffness which in turn introduces strong elastic-plastic coupling?

2.2 Constitutive Issues

1. Can the differences of discrete and distributed failure analysis be reconciled by incorporating fracture energy concepts into the strain-softening formulation of "equivalent" continua?
2. Can a "nonlocal" constitutive formulation be developed which captures the transition of failure from tensile cracking to shear faulting which gradually diffuses into continuous hardening under increasing confinement?
3. Is failure an anisotropic phenomenon which requires storage and monitoring of vector- or tensor- valued state variables instead of scalars only?
4. Can the elastic-plastic coupling be neglected as a first approximation or do we have to account for the simultaneous degradation of strength as well as stiffness?

5. Is there a necessity for rate sensitive constitutive formulations such as viscoelasticity or viscoplasticity in order to assure positive definiteness of the underlying constitutive operators?
6. Does the strain-space setting of strain-softening plasticity resolve the difficulties of stable peak and post-peak descriptions or is the latter simply an issue of the driving control variables?

2.3 Computational Issues

1. Can the computational difficulties of discrete fracture analysis with continuously changing fracture topologies be resolved by "equivalent" strain-softening formulation of the constitutive behavior?
2. What is the basic difference between the proposed composite fracture model and the discrete crack analysis in fracture mechanics with regard to fracture energy release rate computations?
3. To what extent do progressive failure computations within the proposed composite fracture model circumvent the topological difficulties of the fictitious crack model of Hillerborg et al. and those of the imbricate continuum theory by Bazant et al.?
4. What are the restrictions for uniqueness and stability of contained strain-softening computations with regard to the maximum mesh size?
5. What are the numerical requirements for capturing localization and propagation of contained strain-softening regions within a solid?

6. To what extent can post-peak response predictions of strain-softening computations be stabilized by displacement or arc-length control of the underlying incremental/iterative solution strategy?

3. SIGNIFICANT ACCOMPLISHMENTS

The diverse research efforts on "Finite Elements and Localized Failure" resulted in several significant accomplishments which are summarized below within three groups of activities:

3.1 Experimental Results

Three different sets of experiments were carried out to examine the post-peak response behavior of plain concrete specimens subjected to direct tension, triaxial compression and direct shear loading histories. All experiments were carried out with a servo-controlled MTS-testing system in order to study the load-displacement response and fragility behavior of concrete failure under low confinement and the localization of failure regions when the specimen was loaded into the post-peak regime.

a. Direct Tension Experiments

The principal results of these experiments are illustrated in Figs. 1, 2, 3 and 4. The response curves depict the axial force-displacement (stroke) behavior when NX-size cylindrical concrete specimens of D = 54 mm diameter and H = 108 mm height were subjected to monotonic loading histories with partial unloading.

The experimental observations support the following conclusions:

(i) Concrete failure in direct tension is an extremely brittle fracture phenomenon which is difficult to control in a stable fashion if unnotched specimens are utilized.

(ii) Tensile cracking is clearly a fracture energy dominated process in which the energy release per unit of newly generated crack surface plays a fundamental role. In fact the direct tension

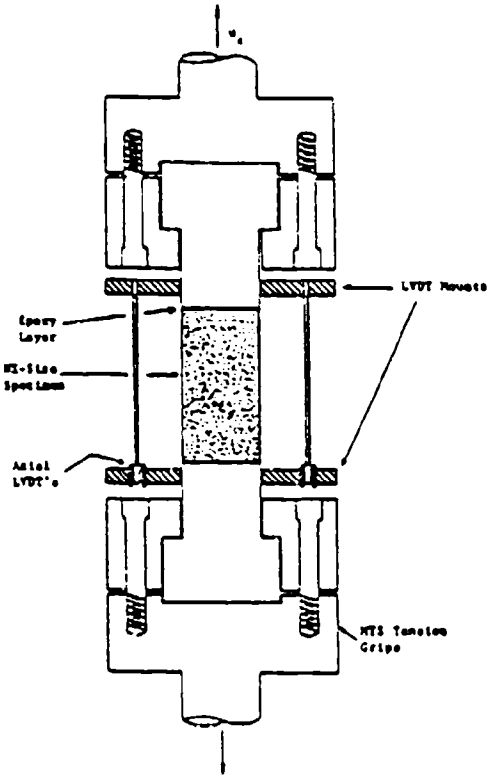

Figure 1 Direct Tension Apparatus

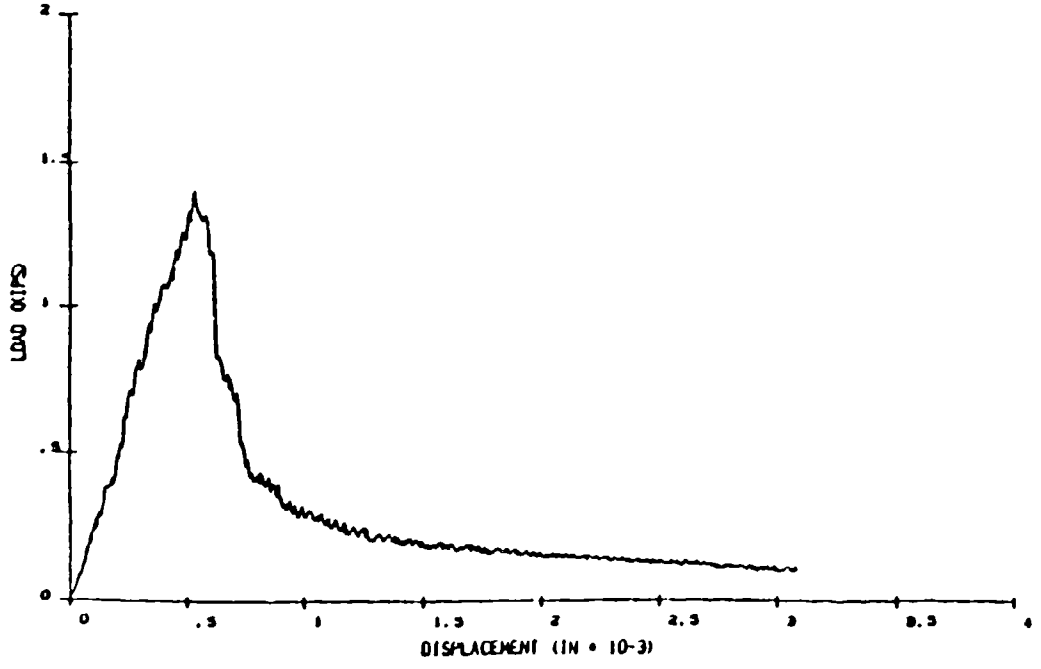

Figure 2 Direct Tension Test of Full Size NX-Specimen

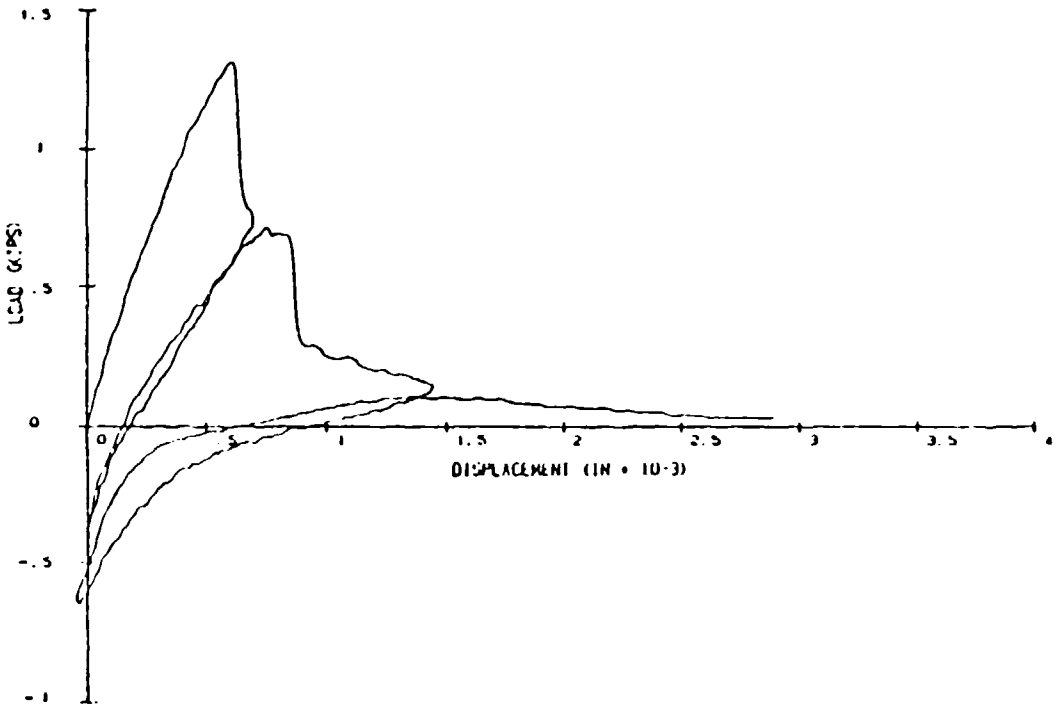

Figure 3 Cyclic Tension Test of Full Size NX-Specimen

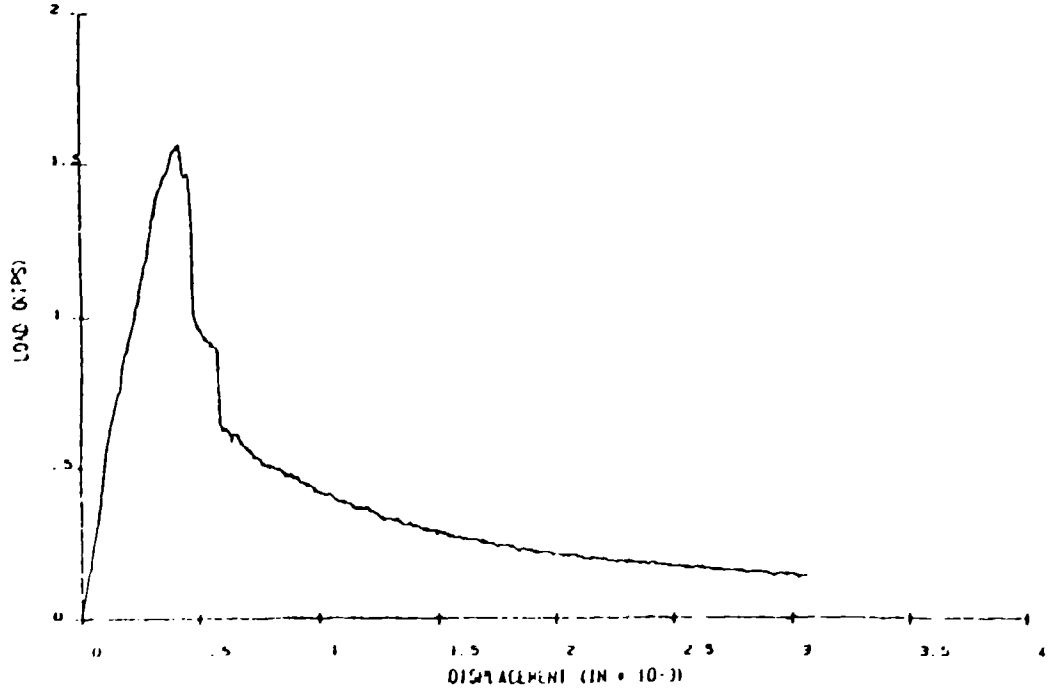

Figure 4 Monotonic Tension Test of Half Size NX-Specimen

experiments with unnotched cylindrical concrete specimens of different height clearly support the hypothesis of a constant fracture energy release rate in tension, i.e. G_f^I = const.

(iii) The degradation of tensile strength during debonding consistently follows an exponential decay function when the nominal tensile stress is plotted versus the overall extension of the tension specimen.

(iv) The tensile fracture mechanism fully supports the formation of a singular macrodefect which is oriented perpendicular to the direction of major principal stress, while the contiguous regions of the specimens unload elastically. As a result, the overall extension of the tension specimens furnishes a global measure of the crack opening displacement during tensile debonding.

(v) The degrading bond strength is fully recoverable under cyclic loading-unloading conditions. Separation takes place along an extremely tortous crack surface with strong "aggregate interlock" in direct tension.

(vi) There is considerable degradation of tensile stiffness in the post-critical response regime, i.e. the unloading-reloading branches indicate a progressive reduction of the slope near zero residual strength.

(vii) Direct tension experiments on cylindrical test specimens of different height and constant cross-section support the fracture energy release concept of a single macrodefect rather than the damage concept of distributed microdefects. Representative

values for the fracture energy release rate of low strength concrete with f'_c = 22.1 MPa are in the range of G_f^I = 60 N/m for full height and halfheight specimens

$$G_f^I = -\frac{\partial U_f^t}{\partial A_t} = -\int_{u_r} \sigma_n \, du_z = 56 \text{ to } 62 \text{ N/m} \qquad (1)$$

b. Triaxial Compression Experiments

The principal results of these experiments are illustrated in Figs. 5, 6, and 7 which depict the axial force-displacement (stroke) and the lateral versus the axial displacement (stroke) response when NX-size cylindrical concrete specimens were subjected to confined triaxial compression. The experimental observations support the following conclusions:

(i) The strength and ductility increase dramatically with increasing confining stress.

(ii) There is a distinct transition from brittle to ductile fracture, whereby the softening failure mechanism gradually transforms into continuous hardening.

(iii) The partial unloading branches during axial loading in the pre- and post-peak regime indicate surprisingly little degradation of stiffness.

(iv) The lateral deformations illustrate the strong frictional dilatation which diminishes rapidly with increasing confinement.

(v) The failure mode changes gradually from "compressive splitting" under uniaxial compression to inclined shear faulting under

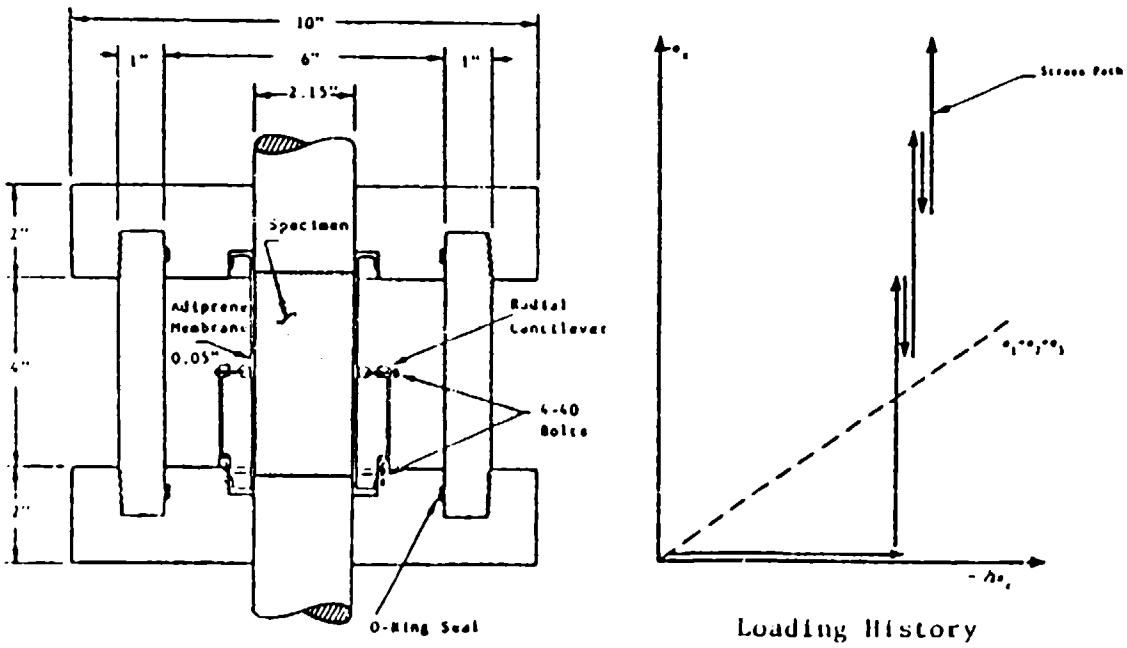

Figure 5 Triaxial Compression Apparatus

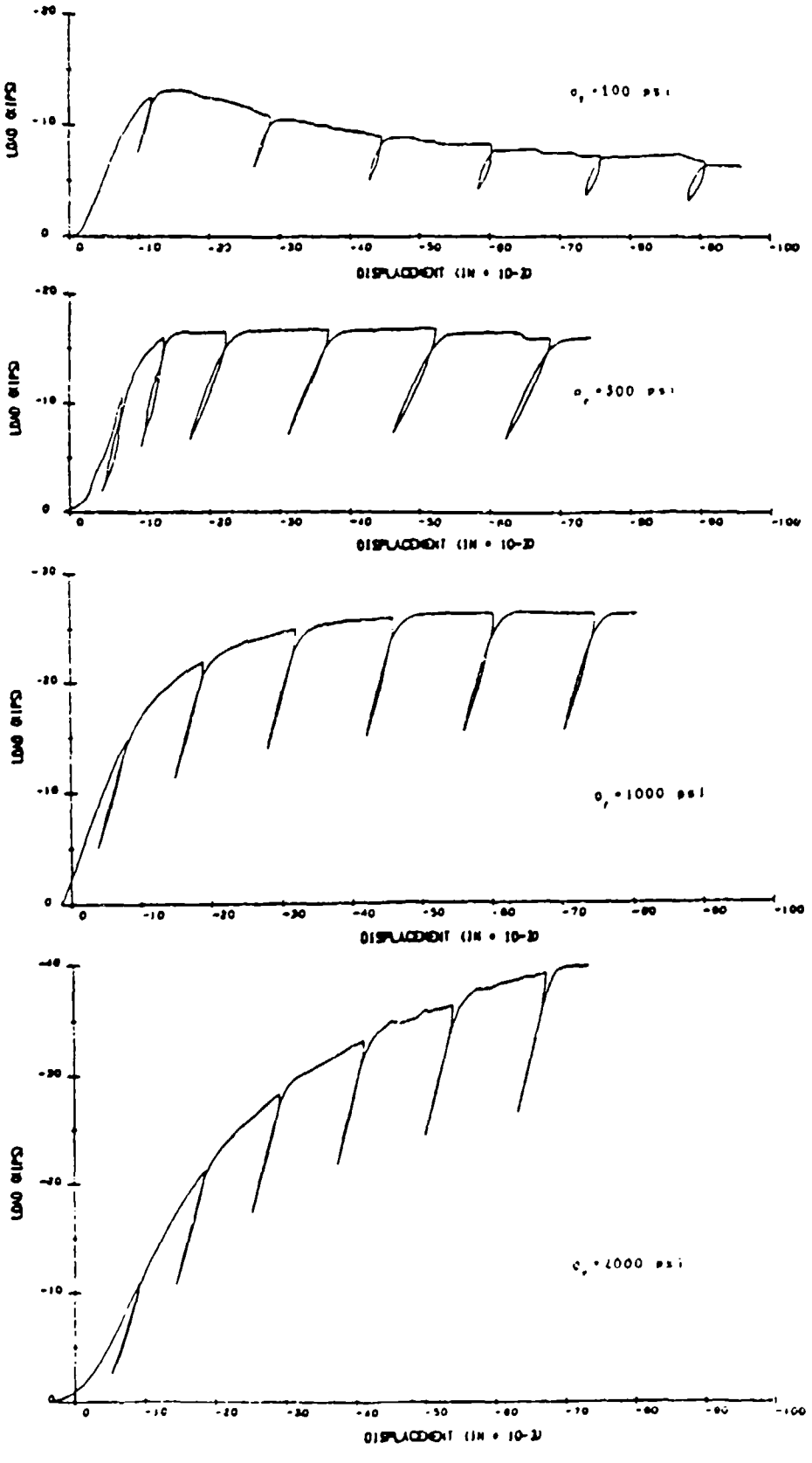

Figure 6 Conventional Triaxial Compression Tests with Partial Unloading

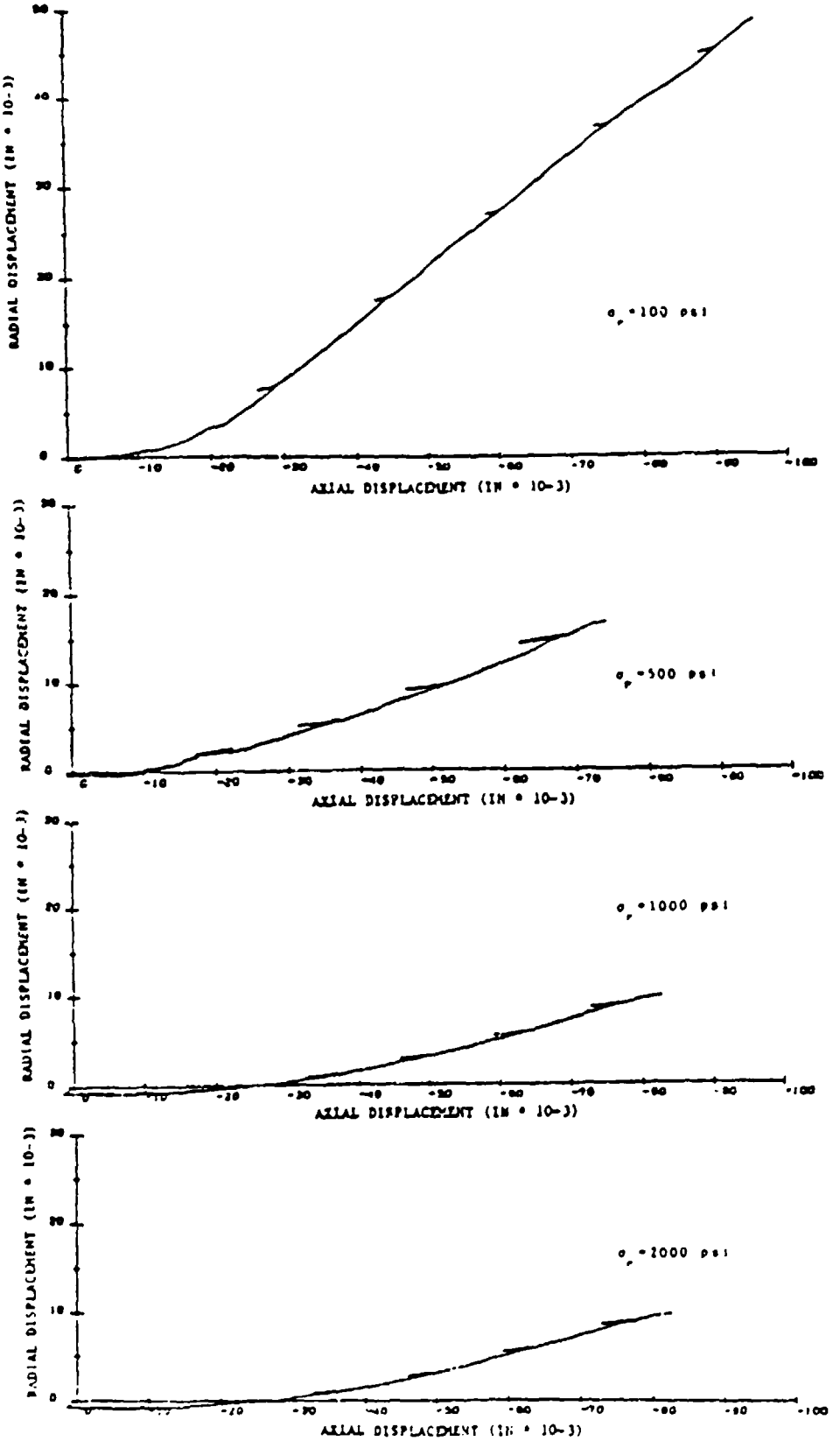

Figure 7 Dilatation Response of Conventional Triaxial Compression Tests with Partial Unloading

increasing confinement. Beyond the transition point failure transforms slowly into diffuse damage within the entire specimen.

(vi) The modulus of toughness provides a first approximation of the strain energy release during compressive splitting in unconfined compression when the energy dissipation in the hardening regime is discarded

$$U_f^c = \int_{u_p}^{u_r} P_z \, du_z \approx -10.91 \text{ Nm} \tag{2}$$

In view of the compressive splitting mode of failure, the crack surface area is ill-defined. However, if we assume that the fracture energy release rate $G_f^I = 60$ N/m controls the splitting mode of failure the unknown crack surface area A_c can be evaluated from

$$G_f^I = - \frac{\partial U_f^c}{\partial A_c} \quad \rightarrow \quad A_c \approx 0.18 \text{ m}^2 \tag{3}$$

This value is almost hundred fold the cross-sectional area of the cylindrical test specimen which corresponds to the crack surface area in the direct tension test

$$A = A_t = 2.29 \times 10^{-3} \text{ m}^2 \tag{4}$$

Fig. 8 summarizes these fracture energy interpretations of the post-peak experiments which are consistent with the 8-10 fold increase of uniaxial compressive strength over the tensile strength.

Direct Tension Test:

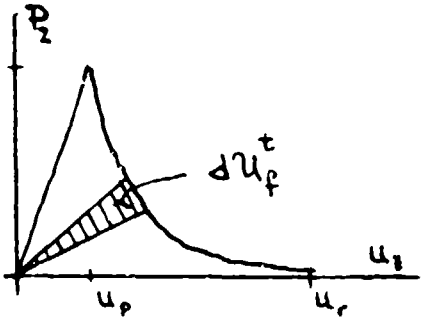

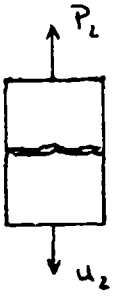

$A_t = 2.29 \times 10^{-3}\ m^2$

$G_f^I = -\frac{\partial U_f^t}{\partial A_t} = 60\ N/m$

$U_f^t = 0.14\ Nm$

Uniaxial Compression Test:

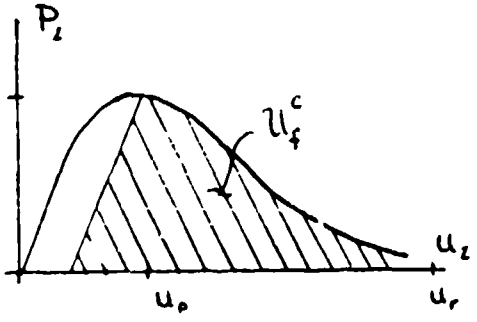

$A_c = ?$

$U_f^c = -10.9\ Nm$

$G_f^I = -\frac{\partial U_f^c}{\partial A_c} \div A_c = 0.18 m^2$

Direct Shear Test:

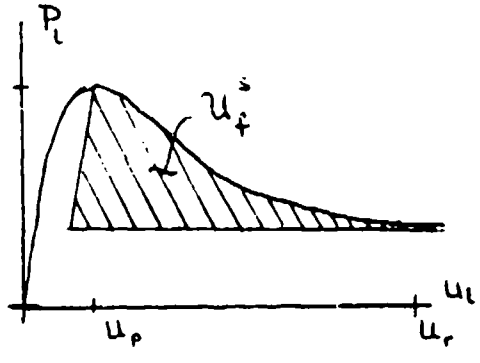

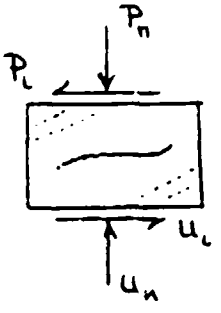

$A_s = 2.06 \times 10^{-2}$

$U_f^s = -50 Nm$

$G_f^{II} = -\frac{\partial U_f^s}{\partial A_s} = 2430\ Nm$

Figure 8 Fracture Energy Release Calculations

c. Direct Shear Experiments

The principal results of these experiments are illustrated in Figs. 9, 10 and 11 which depict the experimental set up and the nominal shear stress versus relative lateral displacement response. To this end prismatic concrete specimens of the size 103 x 117 x 204 mm were subjected to different normal confining pressures and subsequently sheared. The experimental observations support the following conclusions:

(i) The peak strength and residual strength values exhibit a substantial increase with increasing confining pressure in accordance with the concept of frictional materials. The residual shear strength does not increase proportionally with the confining pressure indicating that the angle of internal friction decreases with confinement.

(ii) Spontaneous energy release under low confinement diminishes with increasing confinement level in favor of a stable post-peak response throughout the shearing process.

(iii) The contained failure process in the direct shear specimen is initiated by distributed tensile cracking well before reaching peak strength. This initial cracking phase is followed by compressive strut-action at peak and subsequent localization of a discrete shear band due to mixed mode fracture at the residual strength level.

(iv) The highly non-homogeneous failure process during mixed mode fracture requires inverse identification of the underlying

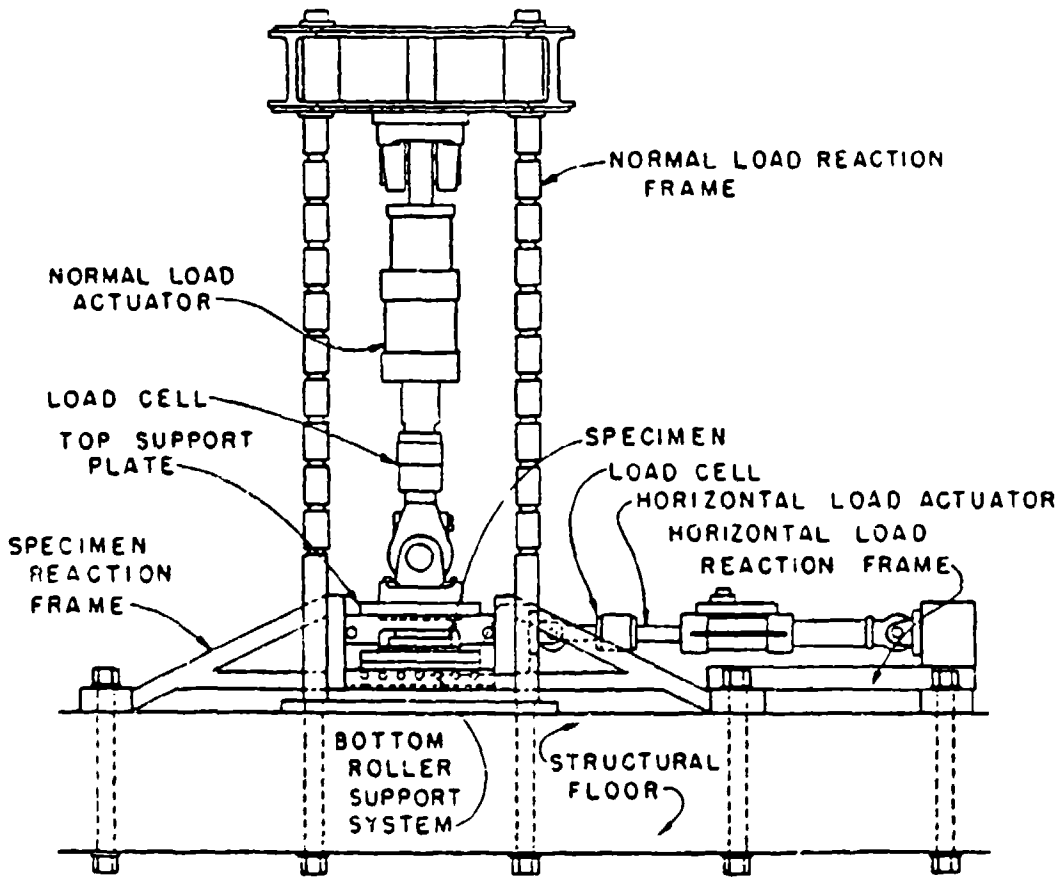

Fig. 9 Direct shear apparatus. Side view of shear device and support system.

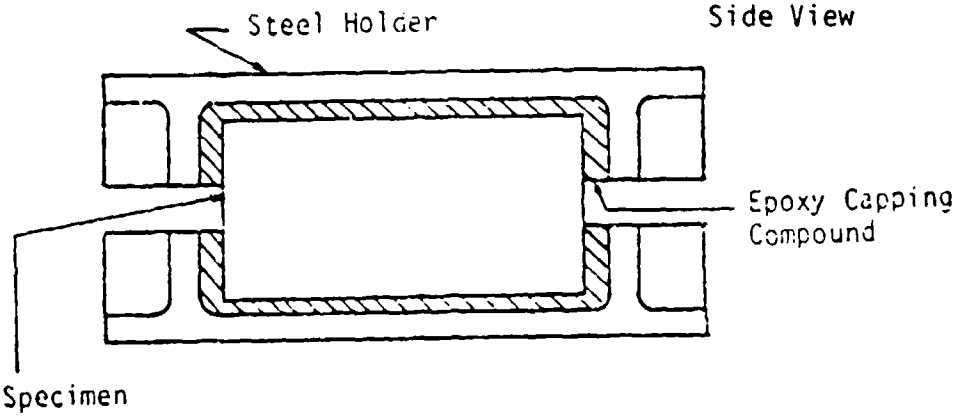

(iv)

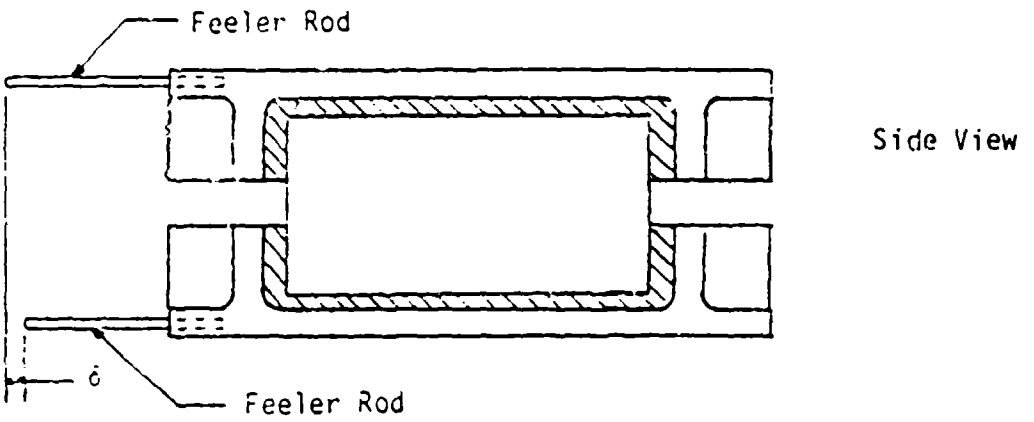

(v)

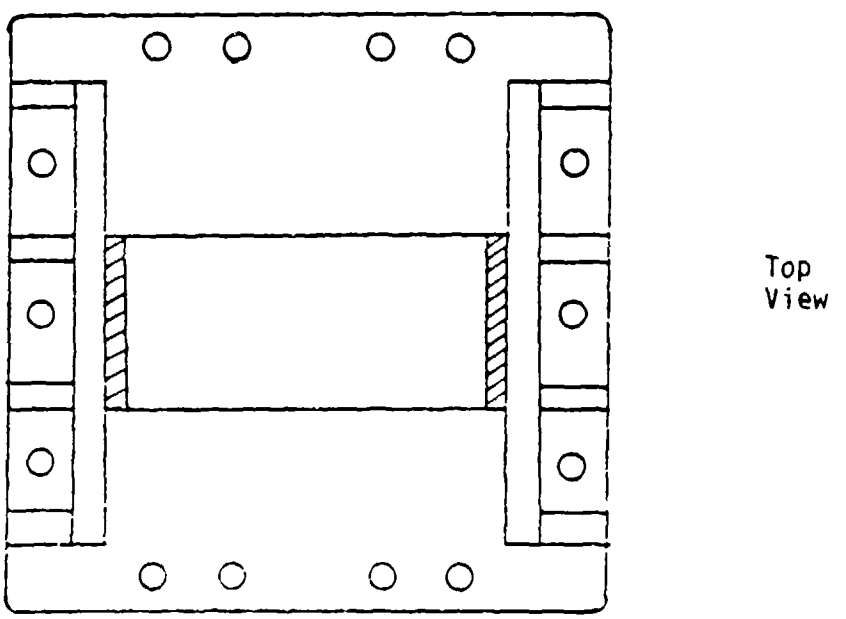

(vi)

Fig. 10 Configuration of shear box compartments for narrow specimens, (iv, vi) and location of relative displacement LVDT feeler rods in later experiments (v).

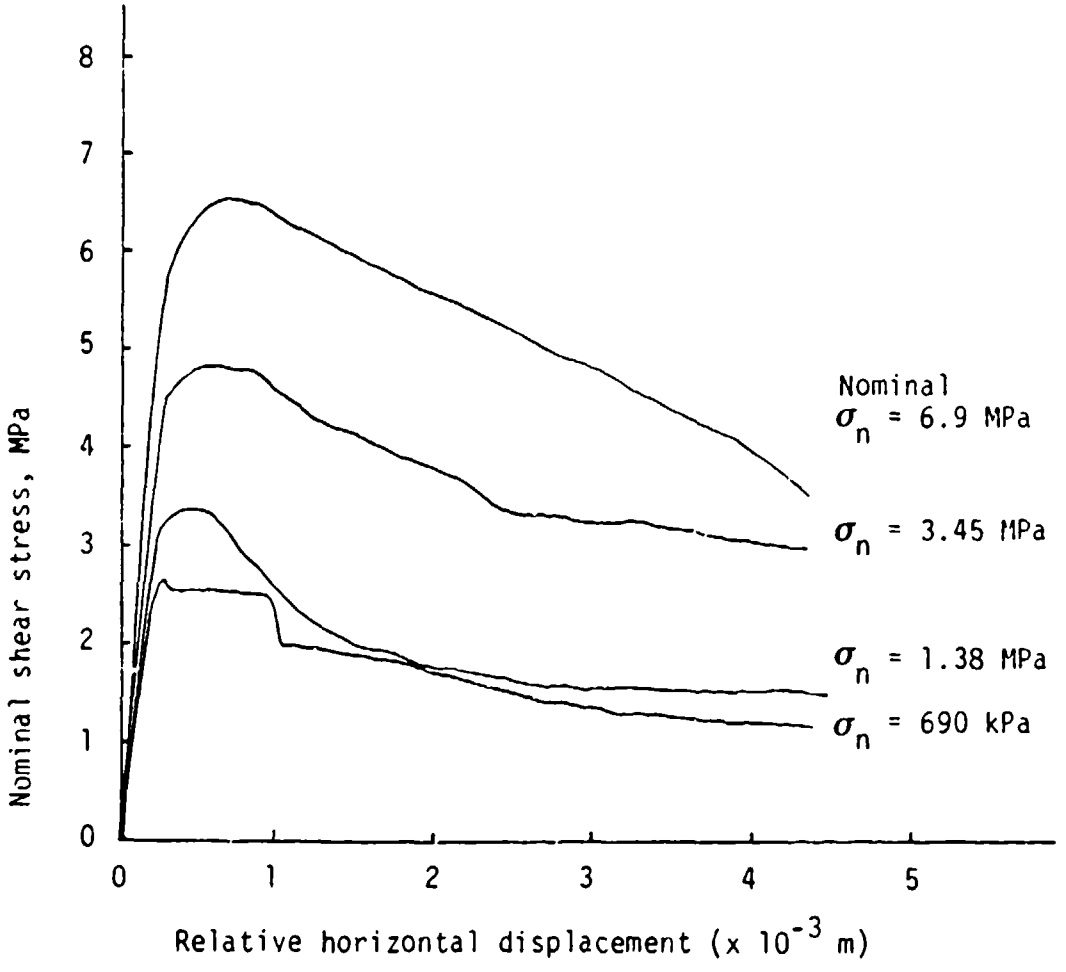

Fig. 11 Nominal shear stress-relative displacement response curves for concrete specimens in the direct shear apparatus.

material parameters in order to interprete the response behavior and in particular the "fragility" of the specimen.

(v) The traditional measures of ductility in terms of the ratio between the modulus of resilience and the modulus of toughness is of little meaning particularly since continuous shearing takes place at the residual strength level in form of relative rigid body translation of the upper versus the lower portion.

(vi) The fracture energy release rate for developing the shear band provides a more appropriate measure of ductility which remains fairly insensitive of the level of confining normal stress. The area under the descending portion of the lateral force-lateral displacement diagram provides a first approximation of the strain energy release rate for Mode II fracture when the energy dissipation in the pre-peak regime is discarded

$$U_f^S = \int_{u_p}^{u_r} P_l \, du_l + \int_{v_p}^{v_r} P_n \, du_n \approx -50 \text{ Nm} \qquad (5)$$

The second term in Eq. 5 represents the release due to shear dilatancy in the post-peak regime which contributes less than 20% to the energy balance in the case of a normal confining pressure of σ_n = 1.38 MPa. Fig. 8 illustrates the interpretation of the post-peak response in terms of fracture energy considerations for Mode I and Mode II failure. Since the fracture surface at the residual strength level

corresponds to the cross-sectional area, the fracture energy release rate for mode II type failure follows from eq. 5

$$G_f^{II} = - \frac{\partial U_f^S}{\partial A_S} \approx 2430 \text{ N/m} \qquad \text{with } A_S = 2.06 \times 10^{-2} m^2 \qquad (6)$$

which is almost fifty times the fracture energy release rate for tensile cracking, $G_f^I \approx 60$ N/m. This large value is consistent with the large increase of strain energy release in compression and lends itself to a fracture mechanics interpretation of the direct shear test with a well defined slip surface because of the box confinement. Clearly, in view of the different orders of magnitude of G_f^I and G_f^{II}, concrete failure will always be preceded by tensile cracking. However, the post-peak behavior in direct shear is controlled by the separate fracture mechanism of decohesion which is responsible for the formation of a distinct shear band when the inclined compressive struts are sheared. It is interesting that the "structural aspects" of the direct shear test clearly support two distinct fracture mechanisms in spite of the complexity of this experiment.

(vii) Interpretation of the underlying softening mechanism is complicated by the interaction of debonding during tensile cracking in the pre-peak regime and the subsequent decohesion during shearing of the compressive struts in the post-peak regime. Parametric finite element studies clearly indicated that these mechanisms are distinctly different and that the

degradation of shear strength in the post-peak regime is primarily controlled by decohesion rather than debonding.

(viii) During shearing the confined specimen is subjected to substantial dilatancy which results in considerable vertical uplift during softening in the post-peak regime.

(ix) There is little change in the shear strength degradation for nominal confinement levels between $0.69 \leq \sigma_n \leq 6.9$ MPa. In fact mode II type fracture of concrete is always preceded by tensile cracking and thus mobilizes failure below the transition point for brittle-ductile fracture.

3.2 Constitutive Results

The principal modelling effort was directed towards the development of strain-softening relations for tensile cracking and frictional slip with the understanding that strain-softening does not constitute a local material property. The fracture energy concept of G_f = const was introduced in order to homogenize the surface dominated failure mechanism within an elementary volume element of finite dimension. For mode I type cracking this infers that the fracture energy of opening a discrete crack of surface dA_t is equivalent to the energy released during straining the elementary volume dV_e in tension up to rupture

$$G_f A_t = \int_{A_t} \sigma_t \, du_f \quad dA_t = \int_{V_e} \phi^t \, d\epsilon_f dV_e \tag{7}$$

This fracture energy equivalence furnishes the relationship between the crack opening displacement du_f in the cracked discontinuum and the tensile fracture strain $d\epsilon_f$ of the homogenized continuum

$$du_f = \frac{V_e}{A_t} d\varepsilon_f \tag{8}$$

A_t/V_e is a measure of the crack density which lends itself to the interpretation of crack spacing $h_t=V_e/A_t$. Fig. 12 illustrates the composite fracture model for uniaxial tension. In this case the homogenization of a single tensile crack within the elementary volume does not require further explanation, it remains to be said that the generalization to two- and three dimensions is fairly straight forward. In fact the composite fracture theory was successfully adopted to develop a fracture energy based strain-softening plasticity model for tensile cracking, see Appendix B. In this case the equivalent tensile fracture strain ε_f was utilized as control variable in order to monitor strain-softening of the fracture energy equivalent continuum in terms of the following relationship between the softening moduli E_f-E_d

$$E_f = \frac{d\sigma_t}{d\varepsilon_f} = \frac{d\sigma_t}{du_f}\frac{V_e}{A_t} = E_d h_t \tag{9}$$

Note that the strain-softening modulus E_f is directly expressed in terms of the fracture modulus $E_d = \frac{d\sigma_t}{du_f}$ which represents the post-peak slope in terms of the primary test variables, the nominal strength σ_t = P/A and the overall crack extension u_f. In this context the characteristic length $h_t = V_e/A_t$ converts the "crack-opening displacement" into equivalent tensile strain of the homogenized continuum.

Except for this novel definition of the softening modulus E_f the resulting strain-softening plasticity model follows the established

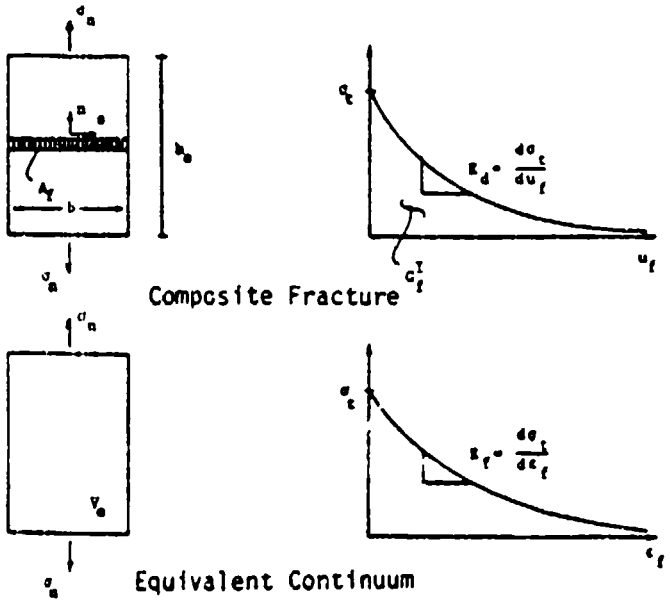

Fig. 12 Composite Fracture Model

concepts of plasticity theory and leads to the following incremental stress-strain relationship

$$\dot{\phi} = \mathbb{E}_T \dot{\epsilon} \qquad \text{where } \mathbb{E}_T = \mathbb{E} - \frac{\mathbb{E}\, m\, m^t \mathbb{E}}{E_f + m^t \mathbb{E}\, m} \tag{10}$$

For isotropic degradation of the tensile strength $\sigma_t = \sigma(\varepsilon_f)$ a single softening relationship suffices to monitor the cracking status in all directions in terms of the equivalent tensile fracture strain

$$\dot{\varepsilon}_f = \sqrt{\langle \dot{\varepsilon}_1 \rangle_f^2 + \langle \dot{\varepsilon}_2 \rangle_f^2 + \langle \dot{\varepsilon}_3 \rangle_f^2} \tag{11}$$

In view of the inherent directionality due to tensile cracking this is clearly a gross simplification which is, however, conservative since the major stress component $\sigma_1 = \sigma_t$ controls the degradation of tensile strength. Extension to anisotropic softening along the three principal direction does not introduce conceptual difficulties but requires eparate monitoring of three independent strain-softening processes. However, the usual assumption of permanent crack-memory does require special provisions for "induced anisotropy" such as kinematic rules, back-stress meaures etc. in order to accommodate rotation of the crack directions during rotation of the principal directions.

The "main accomplishment" of the constitutive development was the generalization of the composite fracture theory from Mode I type cracking to mixed mode fracture. In fact compressive splitting as well as strain-softening during shear-faulting under triaxial compression could be reconciled within the format of the fracture energy based strain-softening plasticity model delineated in Appendix B. The increase

of strength and ductility with increasing confinement was accomplished via the Leon generalization of the Mohr-Coulomb criterion plus tension cut-off and the adoption of ε_f in Eq. 11 as control variable for tensile softening. Thereby the tensile strength degrades simultaneously with the internal cohesion, while the internal friction increases in order to retain a residual strength envelope which passes through the transition point of brittle-ductile failure. The softening modulus E_f diminishes to zero with increasing confinement since the value of the characteristics length h decreases rapidly in compression

$$h = \frac{dV}{dA} \approx \frac{G_f^I}{G_f^{II}} h_t \qquad \text{where } G_f^{II} >> G_f^I \tag{12}$$

It is particularly appealing that softening in compression as well as tension can be unified within the concept of the composite fracture theory, whereby the equivalent tensile fracture strain ε_f is the main control variable for the entire failure process.

3.3 Computational Results

Recent computational issues have focused on the well-posedness of quasistatic and dynamic strain-softening computations and the underlying uniqueness and stability of the numerical results. In the context of the research on "Finite Elements and Localized Failure" these issues had to be addressed because of the structural aspects of strain-softening computations. In other words, stable overall response behavior of the structure is only possible if the strain-softening regime is "contained" within the intact elastic portion of the structure and if the solution is

stabilized by displacement or general arc-length control. Therefore, spatial localization of the material instabilities is of crucial importance for the stable control of the overall structural response. It is this strong interaction between the space and time (load) domain which is critical for the survival of the numerical failure simulation. The papers in Appendices C and D summarize the fundamental aspects of quasistatic and dynamic failure analyses with the aid of one dimensional model problems.

Considering the incremental energy balance between the intact elastic storage region $V-V_f$ and the energy release region V_f the difficulties of progressive failure computations become apparent.

$$\underbrace{\frac{1}{2}\int_{V-V_f} \dot{\sigma}^t \dot{\epsilon}\, dv}_{\text{Adsorption}} + \underbrace{\frac{1}{2}\int_{V_f} \dot{\sigma}^t \dot{\epsilon}\, dV}_{\text{Release}} = \underbrace{\frac{1}{2}\int_{S_\sigma} \dot{p}_s^t \dot{u}\, ds}_{\text{Positive}} + \underbrace{\frac{1}{2}\int_{S_u} \dot{p}^t \dot{u}_s\, ds}_{\text{Positive/Negative}} \qquad (13)$$

The finite element discretization of the space domain demonstrates clearly the equivalence between the crack driving force in fracture mechanics of discrete crack extension and the equivalent fracture load due to progressive strain-softening in the homogenized continuum.

$$dR_f = \int_V \frac{dB^t}{dA}\, \sigma\, dV \simeq \int_{V_f} B^t d\sigma_f dV \qquad (14)$$

$$\text{where} \qquad G_f = - r^t\, dR_f$$

$$\text{and} \qquad d\sigma_f = E\, d\epsilon_f$$

The principal difference between the discrete and the distributed fracture approach centers around the role of the crack surface area dA, which is in the first case the primary control variable while the strain-softening region V_f is only a secondary result of distributed failure analysis. In the latter case the geometric extent of the failure zone is only defined indirectly in terms of the "loading condition" in the displacement (strain) driven computational algorithm

$$m^{t}\mathbf{E}\,\dot{\boldsymbol{\varepsilon}} > 0 \tag{14}$$

This condition has to be interpreted for load increments which are truly finite, and it leads to the concept of for "iterative reversibility" in order to allow for elastic unloading. This aspect is of utmost importance, if elastic snap-back and sharp localization of the strain-softening regime are to be captured.

Appendix D describes a dynamic model problem which illustrates strain-softening effects and localized deformation trapping in the case of wave propagation in an axial force member. The bar was subdivided into 9, 21 and 97 finite elements of equal length and subjected to constant end velocities $c = \pm 0.5\, c_p$ amounting to 50% of the acoustic wave speed. Fig. 13 describes the lay-out of the model problem in which the predictions of the traditional strain-softening approach with E_f = const. (independent of mesh size) were compared with those of the composite fracture model with G_f = const. (mesh size dependent value of the strain-softening modulus, $E_f \neq$ const.).

The resulting stress histories are depicted in Fig. 14 which clearly demonstrates the strong mesh-sensitivity of the traditional E_f = const. approach. In fact Fig. 15 illustrates the rapid decrease of the

fracture energy which diminishes to zero with decreasing mesh size, i.e. $G_f \to 0$ as $h \to 0$ when $E_f = \text{const.}$ On the other hand the composite fracture model maintains fracture energy release rates which remain constant irrespective of the mesh size. Fig. 16 illustrates the time history of strain localization at the center of the tension specimen for the three idealizations. Clearly, it is primarily a question of spatial resolution to capture tensile cracking by strain-softening of an equivalent continuum. It is rather intriguing that both strain-softening models reproduce the actual separation phenomenon in the form of deformation trapping in the center element, whereby the conventional strain-softening approach with $E_f = \text{const.}$ leads to a more pronounced strain localization according to the analytic solution of strain singularity in a domain of measure zero, i.e. $\varepsilon \to \infty$ as $h \to 0$. Obviously, both continuum models cannot capture the actual separation and concomitant displacement discontinuity of the center of the bar, however, both strain-softening formulations simulate the fracture process in the form of deformation trapping, whereby the composite fracture model maintains a constant fracture energy release rate irrespective of the mesh size.

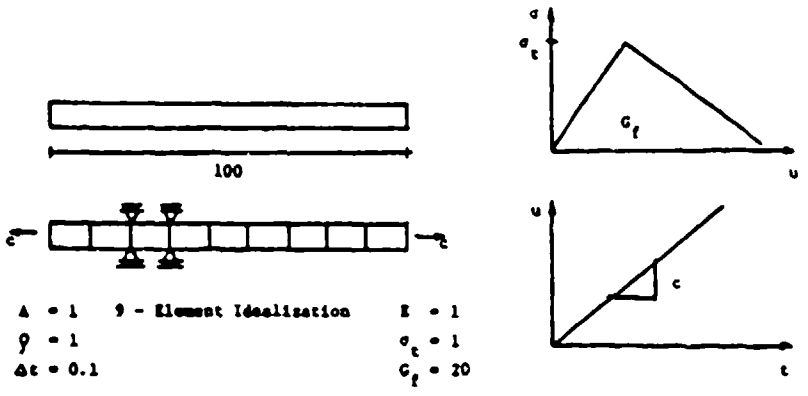

Fig.13 Dynamic Model Problem

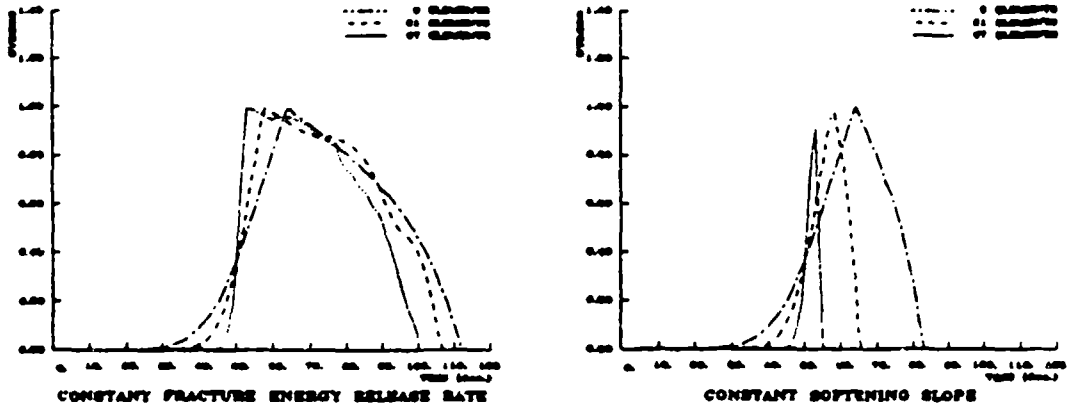

Fig. 14 Global Response Behaviour

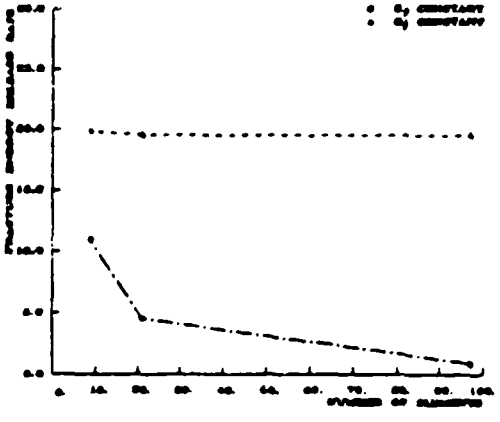

Fig.15 Mesh Sensitivity of Fracture Energy

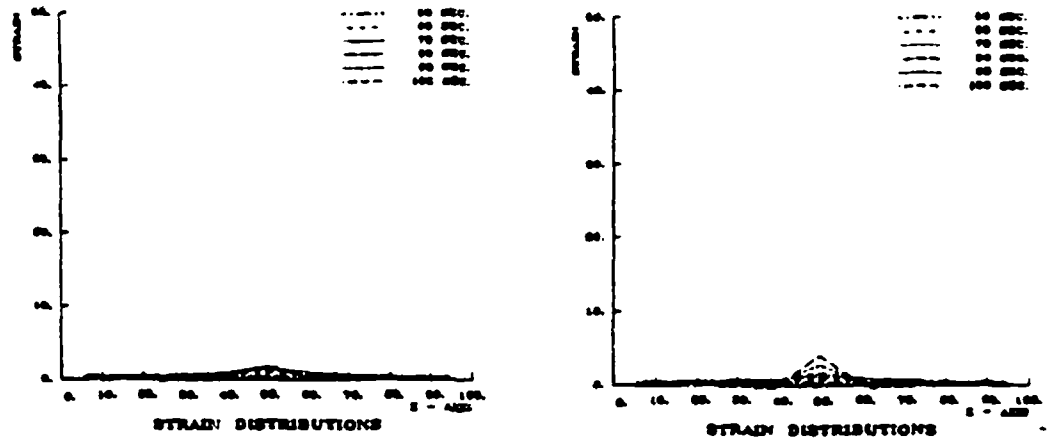

9 - Element Idealization

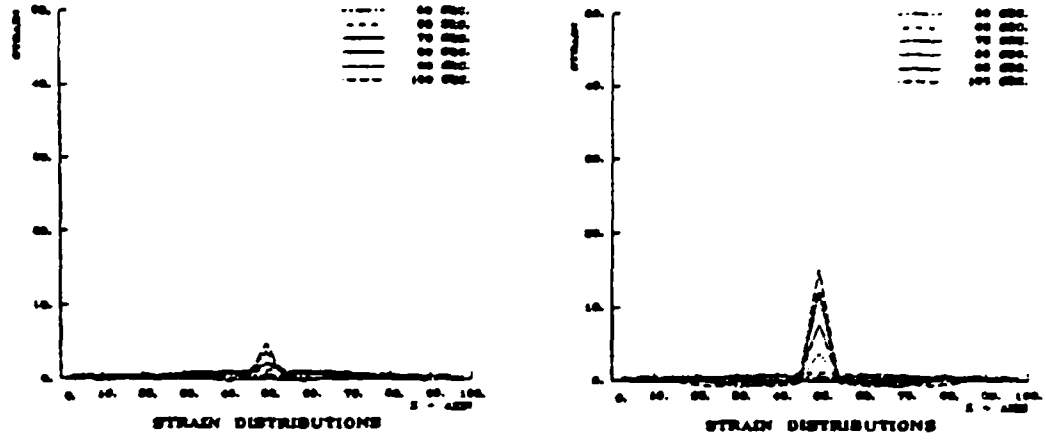

21 - Element Idealization

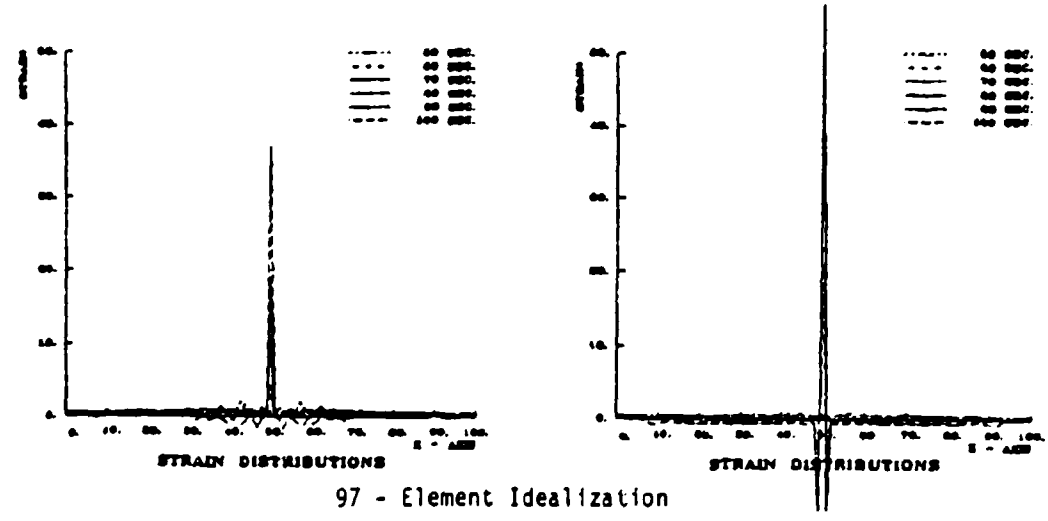

97 - Element Idealization

Composite Fracture Model

Constant Strain Softening

Fig.16 Localization of Tensile Failure

4. LIST OF TECHNICAL PUBLICATIONS

In the course of the research on "Finite Elements and Localized Failure" the following papers were or are in the process of being published in technical conference proceedings and technical Journals.

4.1 Technical Papers

[1] Christensen, J., Ickert, K., Stankowski, T., Sture, S. and Willam, K., "Numerical Modeling of Strength and Deformation Behavior in the Direct Shear Test", Intl. Conf. Constitutive Laws for Engineering Materials, Tucson, Jan. 10-14, 1983, Proc. eds C.S. Desai and R.H. Gallagher, University of Arizona (1983), pp. 537-544.

[2] Christensen, J. and Willam, K., "Finite Element Analysis of Concrete Fracture in Shear", Air Force Symp. Interaction of Non-Nuclear Munitions with Structures, Colorado Springs, May 10-13, 1983, Proc. Part I (1983), pp. 101-106.

[3] Sture, S., "Experimental Modeling of Strength and Deformation Behavior of Concrete in Direct Shear", Air Force Symp. Interaction of Non-Nuclear Munitions with Structures, Colorado Springs, May 10-13, 1983, Proc. Part I (1983), pp. 95-100.

[4] Willam, K., "Experimental and Computational Aspects of Concrete Fracture", Intl. Conf. Computer Aided Analysis and Design of Concrete Structures, Split, Sept. 17-21, 1984, Proc. eds. F. Damjanic, E. Hinton, D.R.J. Owen, N. Bicanic, V. Simonic, Pineridge Press, Swansea (1984), pp. 33-70.

[5] Bicanic, N., Sture, S., Hurlbut B. and Day, S., "On the Prediction of the Peak and Post-Peak Behavior of Concrete Structures", Intl. Conf. Computer Aided Analysis and Design of Concrete Structures, Split, Sept. 17-21, 1984, Proc. eds. F. Damjanic, E. Hinton, D.R.J. Owen, N. Bicanic, V. Simonic, Pineridge Press, Swansea (1984), pp. 245-260.

[6] Willam, K., Bicanic, N. and Sture, S., "Constitutive and Computational Aspects of Strain-Softening and Localization in Solids", ASME-WAM'84 Symp: Constitutive Equations: Macro and Computational Aspects, New Orleans, Dec. 10-14, 1984, ASME Symp. Volume G00274, ed. K. Willam, New York (1984), pp. 233-252.

[7] Willam, K. and Sture, S., "A Composite Fracture Model for Localized Failure in Cementitious Materials," 2nd Air Force Symp. Interaction of Non-Nuclear Munitions with Structures, Panama City Beach, Florida, April 15-18, 1985, Proc. (1985), pp. 272-277.

[8] Willam, K., Hurlbut, S. and Sture, S. "Experimental and Constitutive Aspects of Concrete Failure", U.S.-Japan Symp. Finite Element Analysis of Reinforced Concrete Structures, Tokyo, may 21-24, 1985, Proc. Part I (1985), pp. 149-171. Revised paper will be published in ASCE Volume on Finite Element Analysis of Reinforced Concrete Structures, New York (1986).

[9] Willam, K., Pramono, E. and Sture, S., "Stability and Uniqueness of Strain-Softening Computations," Europe-U.S. Symposium Finite Element Methods for Nonlinear Problems, NIT Trondheim, Norway, Aug. 12-16, 1985 Paper will be published in Special Conference Volume by Springer Verlag, Berlin, Heidelberg (1986).

[10] Willam, K., Bicanic, N., Pramono, E. and Sture, S., "Composite Fracture Model for Strain-Softening Computations for Concrete", Int. Conf. Fracture Mechanics of Concrete-Fundamentals and Applications, EPF Lausanne, Switzerland, Oct. 1-3, 1985, Paper will be published in Conference Proceedings by Elsevier Science Publishers, Amsterdam (1986).

For speedy disemination of the different results of the Air Force project several research reports were published within the "Structural Research Series" of the Department of Civil, Environmental and Architectural Engineering at the University of Colorado, Boulder.

4.2 Technical Reports

[1] K. Willam, S. Sture, N. Bicanic, J. Christensen and B. Hurlbut, "Identification of Strain-Softening Properties and Computational Predictions of Localized Fracture", Structures Research Series 8404-Boulder, 1984, pg. 192.

[2] K. Willam, N. Bicanic and S. Sture, "Constitutive and Computational Aspects of Strain-Softening and Localization in Solids," Structures Research Series, 8406 - Boulder, 1984, pg. 20.

[3] K. Willam, B. Hurlbut and S. Sture, "Experimental and Constitutive Aspects of Concrete Failure", Structures Research Series 8502 - Boulder 1985, pg. 29.

[4] K. Willam, E. Pramono and S. Sture, "Stability and Uniqueness of Strain-Softening Computations", Structures Research Series 8503 - Boulder, 1985, pg. 24.

[5] K. Willam, N. Bicanic, E. Pramono and S. Sture, "Composite Fracture Model for Strain-Softening Computations of Concrete", Structures Research Series 8506 - Boulder, 1985, pg. 14.

In addition the following three master theses were published in report form in order to record pertinent results of the on-going Air Force project.

[6] J. Christensen, "Computational and Experimental Investigation of Concrete Failure in Shear", M.Sc. Thesis, CEAE Department, University of Colorado, Boulder, 1983, pg. 232.

[7] S.E. Day, "A Softening Plasticity Model for Concrete", M.Sc. Thesis, CEAE Department, University of Colorado, Boulder 1985, pg. 215.

[8] B.S. Hurlbut, "Experimental and Computational Investigation of Strain-Softening in Concrete", M.Sc. Thesis, CEAE Department, University of Colorado, Boulder, 1985, pg. 128.

5. LIST OF PROFESSIONAL PERSONNEL

During the funding period 1982-85 the Air Force project, "Finite Elements and Localized Failure" provided continuous financial assistance for the following personnel:

(i) Two Principal Investigators:	Kaspar Willam Stein Sture
3 Academic Years: 3 Summers:	10 and 15% release time for two PI 1 and 2 months summer support for two PI
(ii) Post-Doctoral Research Associate:	Nenad Bicanic (Senior Lecturer at Dept. of Civil Eng., University of College, Swansea)
1 Academic Year:	100% support for one RA
(iii) Research Assistants:	James Christensen (Martin Marietta Aerospace, Denver, CO) Shari Day (Failure Analysis Assoc., Palo Alto, CA) Bryan Hurlbut (Applied Mechanics Inc., Lakewood, CO) Eddy Pramono
3 Academic Years: 3 Summers:	50% support for two students/AY 2 months support for two students/summer
(iv) Laboratory Assistants:	Hourly Employees
3 Years:	500 hrs/year
(v) Secretarial Help:	Part-time Assistance
3 Years:	15% support for one secretary p.a.

During the funding period three research assistants completed their Master of Science degree, each with a substantial thesis involving experimental, constitutive as well as computational research. In the meanwhile, all three master students are placed in challenging positions at the aerospace industry and computer-oriented consulting firms. The fourth research assistant started his Ph.D. studies in Summer 1984 and should complete his dissertation within another 1.5 years.

6. LIST OF ORAL PRESENTATIONS

In view of the strong interest on concrete failure the principal investigators participated very actively in workshops, conferences and international symposia in order to present early results of the Air Force project on "Finite Elements and Localized Failure". In fact, one of the principal investigators organized a Symposium on "Constitutive Equations: Macro and Computational Aspects" during the ASME Winter Annual Meeting 1984, New Orleans Dec. 10-14, 1984 with 17 papers and a set of substantial Conference Proceedings of 272 pages. The chronological list below summarizes the presentations of technical meetings and university seminars during the funding period 1982-1985.

6.1 International Conferences

1. "Numerical Modeling of Strength and Deformation Behavior in the Direct Shear Test", Intl. Conf. Constitutive Laws for Engineering Materials, Tucson, Arizona, Jan 10-14, 1983.

2. "Finite Element Analysis of Concrete Failure in Shear", Air Force Symp. Interaction of Non-Nuclear Munitions with Structures, U.S. Air Force Academy, Colorado Springs, May 10-13, 1983.

3. "Experimental Modeling of Strength and Deformation Behavior of Concrete in Direct Shear", Air Force Symp. Interaction of Non-Nuclear Munitions with Structures, U.S. Air Force Academy, Colorado Spring, May 10-13, 1983.

4. "Finite Element Modeling of Concrete Failure in Shear", 4th ASCE - Engineering Mechanics Specialty Conference, Purdue University, Lafayette, May 23-25, 1983.

5. "Computational Stability and Uniqueness of Strain-Softening Materials", W. Prager Symposium on Mechanics of Geomaterials, Northwestern University, Evanston, Sept. 11-15, 1983.

6. "Strain-Softening, a Material Property, that is the Question?" ASCE Spring Convention, Atlanta, Georgia, May 14-18, 1984.

7. "Composite Damage Model for Localized Fracture", 5th ASCE - Engineering Mechanics Specialty Conference, University of Wyoming, Laramie, Aug. 1-3, 1984.

8. "Continuous Fracture Computations and Strain Localization in Cementitious Solids Subjected to Tension and Shear", XVIth IUTAM Congress of Theoretical and Applied Mechanics, Lyngby, Denmark, Aug. 19-25, 1984.

9. "Experimental and Computational Aspects of Concrete Fracture, Intl. Conf. Computer Aided Analysis and Design of Concrete Structures", Split, Yugoslavia, Sept. 17-21, 1984.

10. "Constitutive and Computational Aspects of Strain-Softening and Localization in Solids", ASME-WAM'84 Symp. Constitutive Equations: Micro, Macro and Computational Aspects, New Orleans, Dec. 10-14, 1984.

11. "A Composite Fracture Model for Localized Failure in Cementitious Materials", 2nd Air Force Symp. Interaction of Non-Nuclear Munitions with Structures, Panama City Beach, Florida, April 15-19, 1985.

12. "Experimental, Constitutive and Computational Aspects of Concrete Failure", U.S.-Japan Symposium on Finite Element Analysis of Reinforced Concrete Structures, Tokyo, May 21-24, 1985.

13. "Computational Modeling of Material Softening", 2nd Joint ASCE/ASME Mechanics Conference, Albuquerque, June 23-26, 1985.

14. "Stability and Uniqueness of Strain-Softening Computations", Europe-US Symposium Finite Element Methods for Nonlinear Problems, NIT Trondheim, Norway, Aug. 12-16, 1985.

15. "Computational Modeling of Distributed and Localized Fracture", 8tn Intl. Conf. Structural Mechanics in Reactor Technology, Aug. 19-23, 1985.

16. "Composite Fracture Model for Strain-Softening Computations of Concrete", Int. Conf. Fracture Mechanics of Concrete-Fundamentals and Applications, EPF Lausanne, Switzerland, Oct. 1-3, 1985.

6.2 Workshops and University Seminars

1. "Finite Element Modelling of Concrete Failure in Shear", Graduate Seminar at Northwestern University, Evanston, May 20, 1983.

2. "Computational Aspects of Concrete Mechanics," US-Dutch Cooperative Research Symposium, Delft University of Technology, Delft, June 22-24, 1983.

3. "Nlchtlineare Stoffmechanik und Finite Elemente" Graduate Seminar, University of Innsbruck, June 29, 1983.

4. "Finite Elements and Localized Failure", US-AFWL Material Properties Meeting, Albuquerque, Oct. 3, 1983.

5. "Strain-Softening, Experimental and Computational Aspects", U.S. Army Waterways Experiment Station, Vicksburg, Jan. 17, 1984.

6. "Experimental Results on Concrete Failure", Workshop on Inelastic Deformations and Failure Modes, Northwestern University, Evanston Nov. 18-21, 1984.

7. "Experimental and Computational Aspects of Strain-Softening", Hardy Cross Lecture, University of Illinois at Urbana-Champaign, April 19, 1985.

8. "Strain-Softening Computations of Brittle Failure Processes", Graduate Seminar at Lund Institute of Technology, Lund, Sweden, Aug. 16, 1985.

9. "Experimental, Constitutive and Computational Aspects of Concrete Failure," Seminar at Applied Mechanics Division, Sandia National Laboratories, Albuquerque, Nov. 8, 1985.

7. NEW FINDINGS

The research effort on "Finite Elements and Localized Failure" led to a better understanding of brittle-ductile failure phenomena in particulate composites such as concrete. Most of the findings were listed in Section 3 above under the heading of significant accomplishments on the experimental, the constitutive and computational fronts.

The most important result of the investigation on concrete fragility is that concrete failure is a fracture driven process in which the nominal tensile strain plays an instrumental role to homogenize the effect of coalescing microdefects into a single macrodefect. In fact strain-softening is not a local material phenomenon but rather the consequence of distributing the degradation effects of microdefects in an elementary but finite volume. Therefore, the principal issue of extracting useful fragility information from servo-controlled post-peak experiments on laboratory specimens centers around the homogenization of the fracture process in the discontinuum by an equivalent strain-softening continuum.

To this end a series of servo-controlled experiments were performed on cylindrical and prismatic concrete specimen[illegible] provided unique data of concrete strength and deformation behavio[illegible]ell as fragility when subjected to direct tension, triaxial compression and direct shear. The experiments furnished quantitative evidence on the brittle-ductile transition of cylindrical failure which diffuses entirely under sufficient confinement. The different tests, also substantiated two different failure modes, (i) a planar failure mode under direct tension

and direct shear due to progressive debonding and decohesion, and (ii) a cylindrical failure mode under triaxial compression due to simultaneous decohesion and increase of internal friction. The two different failure modes support the concept of tensile strain as the control variable for the degradation of strength, whereby planar failure is caused by the single value of major principal strain, while axisymmetric or cylindrical failure is the result of double valued major principal strains.

For interpretation of these failure phenomena the "Composite Fracture Theory" was developed which resorts to the fracture energy release rate in order to monitor the fracture process in an elementary volume of finite size by "equivalent" strain-softening. In this way the fracture mechanics of tortuous cracking in brittle solids is replaced by fracture energy equivalent strain-softening. In fact the traditional format of strain-softening plasticity could be readily adopted, except for the new definition of the strain-softening modulus E_f in terms of the fracture energy release-rate G_f and the crack density per unit volume

$$E_f = \frac{d\sigma_t}{d\varepsilon_f} = \frac{d\sigma_t}{du_f}\frac{du_f}{d\varepsilon_f} = E_d \frac{V_e}{A_t}$$

where $$E_d = \frac{d^2 G_f^I}{du_f^2} \qquad \text{with } G_f^I = \int_{u_r} \sigma_t \, du_f$$

and $$\frac{dV_e}{dA_t} = h_t$$

The resulting tangential material law

$$\dot{\sigma} = \mathbb{E}_T \dot{\varepsilon} \qquad \text{where} \qquad \mathbb{E}_T = \mathbb{E} - \frac{\mathbb{E}\, m\, m^t \mathbb{E}}{E_f + m^t \mathbb{E} m}$$

maintains constant fracture energy release rate when the elementary volume is subjected to fracture up to rupture where the stress reaches the residual strength level. Although the composite fracture model was initially developed for tensile cracking it was further extended to include the prevalent strength and failure phenomena in compression, such as "splitting compression" and "shear faulting". Beyond the brittle-ductile transition point the strain-softening formulation reverts to strain-hardening during which volume driven damage accumulation replaces the surface driven fracture process. As a result the composite fracture model covers the entire spectrum of failure phenomena of concrete, starting from brittle tensile cracking under Mode I type fracture, to increasingly ductile fracture up to continuous hardening beyond the transition point under sufficiently high confinement.

The ensuing strain-softening computations of fracture energy equivalent elastic plastic solids lead to stringent prerequisites of the numerical simulation procedure. The spatial discretization with finite elements is limited by mesh size restrictions for local stability and the numerical integration has to make proper provisions for elastic unloading in order to allow for snap-back and concomitant strain localization in load increments which are truly finite. Contained fracture calculations require numerical stabilization with displacement and/or arc length control with computational strategies which are sufficiently robust to survive local instabilities and which are on the other hand sufficiently sensitive to detect failure of the overall structure.

8. CONCLUDING REMARKS AND FUTURE WORK

Considerable progress was made in improving the understanding of concrete fragility. Novel post-peak experiments were performed in unnotched concrete specimens which demonstrated the brittle-ductile transition of failure. In addition the composite fracture theory was developed in order to monitor the fracture energy release rate within the framework of strain-softening plasticity. The computational issues of contained strain-softening computations were addressed in quasistatic and dynamic environments.

Several issues remain, however, unresolved and deserve further attention:

(i) For a better understanding of the actual failure process in particulate composites such as concrete "mesomechanical" studies are needed on the experimental as well as computational level. In this case concrete could be resolved into its constituents, the aggregate, the hardened cement paste and the interface in order to examine the mesomechanical aspects of damage and fracture in particulate composites. In view of the experimental difficulties with SEM, CAT-SCAN X-ray, hypersonic and acoustic emission techniques a probabilistic numerical simulation would provide valuable information on the internal microprocesses and the associated macrophenomena in conjunction with a substantial experimental data base.

(ii) The "anisotropy" or rather the load history effects of failure should be studied in more detail in view of the strong directionality of damage and fracture and the large difference in ductility between planar and cylindrical failure. To this

end servo-controlled laboratory experiments could provide very valuable information for loading histories involving large rotations of the loading direction.

(iii) The stabilization of contained strain-softening computations deserves immediate attention. The development of robust algorithms for post-critical response calculations is of great practical importance for reliable fragility analyses of actual structures.

APPENDIX A

APPENDIX A

"Constitutive and Computational Aspects of Strain-Softening and Localization in Solids"

by

Kaspar Willam, Nenad Bicanic and Stein Sture

Paper presented at ASME/WAM'84 Symposium Constitutive Equations: Micro, Macro and Computational Aspects, New Orleans, Dec. 10-14, 1984; Published in ASME Symposium Volume G 00274, K. Willam ed., New York (1984), pp. 233-252.

CONSTITUTIVE AND COMPUTATIONAL ASPECTS OF STRAIN-SOFTENING AND LOCALIZATION IN SOLIDS

Kaspar J. Willam

Nenad Bicanic*

Stein Sture

Department of Civil, Environmental and Architectural Engineering

University of Colorado, Boulder

Campus Box 428, CO 80309, U.S.A.

*Department of Civil Engineering, Zagreb, Yugoslavia

ABSTRACT

The current study examines the degradation of strength in cementitious materials loaded in tension and shear. Based on experimental observations a strain-softening model is developed which encompasses both continuous decohesion due to distributed microdefects as well as the fracture energy release rate concept for single macrodefects. Distributed and localized fracture are combined in the composite damage model of an equivalent homogenized continuum of finite dimension. In one case the model reduces to the traditional strain-softening formulation of continuous damage mechanics. In the other case it furnishes a non-local softening law which depends on the characteristic fracture dimension as well as the fracture configuration.

The performance of the composite damage model is illustrated with experimental data of the direct tension and triaxial compression tests on WX-size mortar specimens. Post-critical response predictions illustrate that the fracture energy release rate should remain invariant if localized tensile cracking is to be captured. In contradistinction, the shear-softening law should be a constant fracture property if distributed fracture is to be described in the form of frictional slip.

These basic concepts for distributed and localized fracture are subsequently utilized to formulate a comprehensive triaxial fracture model for both tensile debonding and frictional decohesion in cementitious solids. These two mechanisms are described by a non-associative Mohr-Coulomb formulation with tension cut-off in which the tensile strain-softening is controlled by the critical fracture energy release rate. The performance of the overall model is verified by experimental results obtained in the direct shear test in which both tensile cracking as well as frictional slip take place interactively similar to contained fracture processes in highly indeterminate structures.

1. INTRODUCTION

In the recent past a vigorous debate has been concerned with the postcritical or post-peak strength behavior of engineering materials. In particular the limited ductility of cementitious materials has been of considerable interest; advocates of continuous strain-softening models have been in open conflict with the fracture mechanics proponents on this issue. Clearly, the computational advantages of the smeared approach provide the predominant argument in favor of the continuous damage models in which progressive decohesion due to distributed microde-

fects is described by an equivalent strain-softening behavior of a homogenized continuum. On the other hand, serious questions arise with regard to the validity of computational predictions in the case of fracture localization when the structural integrity is determined by the severity of a single macrodefect. This type of failure has been traditionally the realm of fracture mechanics in which the initiation and propagation of a single discontinuity is considered the determining factor.

The main objective of the present investigation is to compare the conflicting strategies and to reconcile the fundamental differences of strain-softening and fracture mechanics. To this end, a composite damage formulation will be developed which embodies the basic concepts of single and distributed fracture events. On one end of the spectrum the composite damage model enforces a fracture energy release rate which is constant in the case of a highly localized discrete discontinuity. On the other end of the spectrum it reduces to the continuous damage theory for distributed fracture. The constitutive formulation follows strain-softening plasticity theories in which the non-associated flow rule is recast into a non-local fracture rule which includes the characteristic fracture dimension of the fracture process zone. The underlying composite damage parameters for tension and shear are calibrated from post-critical experimental data obtained from the direct tension and triaxial compression tests. These two independent sets of servo-controlled experiments are subsequently utilized to study the performance of the computational post-critical predictions with regard to their ability to capture distributed microdefects as well as single macrodefects. These two opposing concepts are implemented within the unified framework of the composite damage theory which decomposes an elementary volume into a series of intact elastic zones and/or a single damage zone in which oriented tensile cracking and frictional slip take place in a highly localized manner. The implications on the computational predictions of the post-critical behavior are then illustrated with fracture investigations of the direct tension test and the triaxial compression test on cylindrical mortar specimens for which experimental data are available for comparison. The uniqueness of the post-critical response predictions is examined with the aid of systematic mesh sensitivity studies of unnotched test specimens which exhibit pronounced softening behavior both in tension and shear.

The disjoint formats of the composite damage model are subsequently integrated into a triaxial strain-softening model of non-associated plasticity for combined fracture in tension and shear. The computational aspects of the strain driven algorithm are examined with regard to the finite increments which are used in computational implementation and analysis. To this end an implicit backward strategy is adopted which assures that the underlying non-associated fracture rule satisfies the constitutive constraints both at the beginning and at the end of the finite time interval. Particular attention is paid to the combined effect of softening in tension and in shear.

Last, the composite damage model is applied to study the postcritical response behavior of prismatic mortar specimens in the direct shear test. In this case contained fracture takes place both in the form of tensile cracking as well as frictional slip depending on the ratio between normal and tangential load levels. In this sense the direct shear test exhibits all ingredients of a highly indeterminate structure in which progressive propagation of distributed microdefects leads to an overall degradation of stiffness and strength before coalescence into a single macro-defect takes place which is ultimately responsible for the structural failure.

2. DIRECT TENSION TEST

For simplicity let us first consider the direct tension test in order to illustrate the underlying fracture mechanics issues and strain-softening concepts. Fig. 1 depicts the basic experiment layout and the response curve for linear-elastic, perfectly brittle behavior. The critical fracture energy release rate G_c follows the energy balance relation which reduces for prescribed displacement boundary conditions to the simple expression

$$G_c = -\frac{d\Pi}{dA} = \frac{\sigma_f^2 \ell}{E} \qquad (1)$$

where Π denotes the total potential energy, σ_f the ideal strength of a flawless crystalline material and dA the change of crack surface [1]. In the spirit of the Griffith concept of brittle fracture G_c corresponds to the surface energy density γ, while the characteristic crack dimension ℓ defines the range of the interatomic bond forces in the order of the lattice spacing for ideally cohesive and crystalline materials.

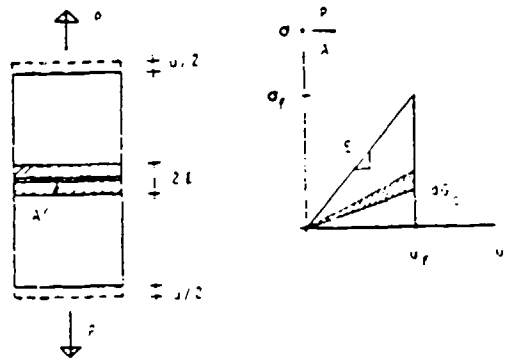

Fig.1 Direct tension test of ideally brittle material

In the case of cementitious materials the question arises if the fracture energy release rate G_c is a proper material property which characterizes the tensile cracking independently of the particular geometry and boundary conditions. In fact, this issue was raised previously in the context of fragmentation of rocks by Paul von Rittinger in 1867 [2] who stated that the newly created surface area is directly proportional to the energy expended during fracture, i.e. G_c = constant. In the recent past, this fundamental fracture mechanics concept was adopted by Hillerborg et al [3] in formulating the fictitious crack band model for concrete. This discrete fracture strategy was extended by Bazant et al [4] to formulate the crack band theory for distributed fracture within a process zone of finite width. Along similar lines the experimental and computational fracture studies by Ingraffea and Saouma [5] were based on the equivalent fracture postulate of a critical stress intensity factor to constitute an invariant fracture property.

In view of this fundamental issue let us examine whether the fracture mechanics hypothesis applies to tensile cracking of cementitious materials and how it can be incorporated into the strain-softening formulation of an equivalent continuum. To this end let us consider the actual experimental data of the direct tension test shown in Fig. 2. We recall that the cylindrical mortar specimen is tested in a very stiff, servo-controlled MTS-apparatus which maintains stable displacement control in the post-critical response regime. In fact, no noticeable change of the geometry occurs during the entire test except for a fine cleavage crack which becomes visible only at the residual load level. At this stage the unnotched mortar specimen separates into two competent parts, while the crack opening displacement localizes within the single crack band between them.

In the absence of noticeable geometric distortions before separation of the specimen into two parts, the elementary uniaxial interpretation of the direct tension data leads to the following stiffness and strength properties in terms of nominal stress and strain measures:

$$E = \frac{\sigma_f}{\epsilon_f} = 6{,}895 \text{ MPa}; \quad \sigma_f = \frac{P_f}{A} = 1.59 \text{ MPa}; \quad \epsilon_f = \frac{u_f}{L} = 2.30 \times 10^{-4} \qquad (2)$$

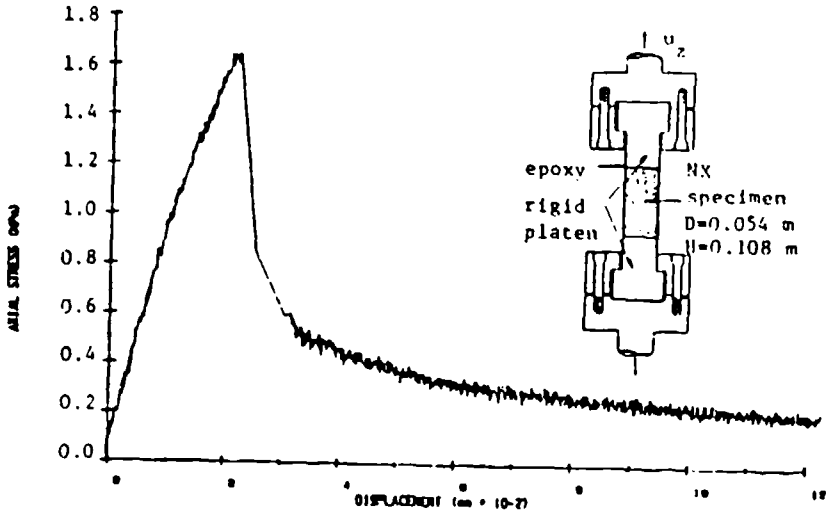

Fig. 2 Direct tension of NX-size specimen

Assuming that the actual strain localization during tensile cracking can be replaced by an equivalent uniform distribution of microdefects over the gauge length L we can extract the strain-softening modulus

$$E_s = 0.82\ E = 5{,}653\ \text{MPa} \tag{3}$$

which remains constant in the case of a bilinear stress-strain idealization of the pre-and post-critical response behavior. Clearly if E_s would be a "proper" material property it should have the same value for each material particle within the gauge length. Obviously this is not the case since E_s is based on a nominal strain measure equal to the overall axial displacement divided by the specimen height which contains a single tensile crack. In other words the strain-softening modulus E_s is a structural property intimately tied to the particular test configuration and fracture condition. Therefore, it cannot be extended right away to different geometries and boundary conditions witnout a rational concept benind this extrapolation. In fact, the equivalent strain-softening model infers that distributed cracking takes place in a truly finite volume of material in which non-local theories for continuous media with microstructure simulate progressive fracture [6], [7].

On the other hand the displacement-controlled formation of a single crack band in the direct tension specimen can be used to determine the critical fracture energy release rate in tension $G_{c,t}$. According to Petersson [8] the integral of nominal normal stress-displacement curve shown in Fig. 2 yields a first order approximation of the critical fracture energy release rate in tension for the particular mortar undet consideration

$$G_{c,t} = \int_0^{u_r} \sigma_z \, du_z \approx 44\ \text{N/m} \tag{4}$$

This value agrees fairly well with other fracture mechanics data reported for concrete and mortar [8]. The characteristic fracture dimension is in this case

$$\lambda_t = \frac{G_{c,t}\ E}{\sigma_t^2} = 0.12\ \text{m} \tag{5}$$

which is definitely several orders of magnitude beyond the lattice spacing of crystalline solids. In fact λ_t is of the same order of magnitude as the entire NX-size specimen which gives rise to the question if the fracture energy release rate is a "proper" fracture property. If we adopt the notion of a fracture process zone with degrading material properties characterized by E_d, then an elementary series model of the uniaxial tension specimen [9] yields the following value for the width d_t of the characteristic fracture process zone

$$d_t = \frac{E_d}{E} \lambda_t \tag{6}$$

This result indicates that the actual width of the fracture process zone d_t may be considerably smaller than λ_t, depending on the ratio between the tangential material stiffness in the damage zone and the elastic properties of the undamaged zone. However, it appears that the width of the fracture band d_t will be still sufficiently large such that the validity of the underlying fracture mechanics concept must be questioned.

2.1 Composite Damage Model for Tensile Cracking

In order to compare the computational response predictions resulting from the constant strain-softening formulation as opposed to the constant fracture energy release rate strategy, we resort to the composite damage model illustrated in Fig. 3 (See also refs. [9-11]).

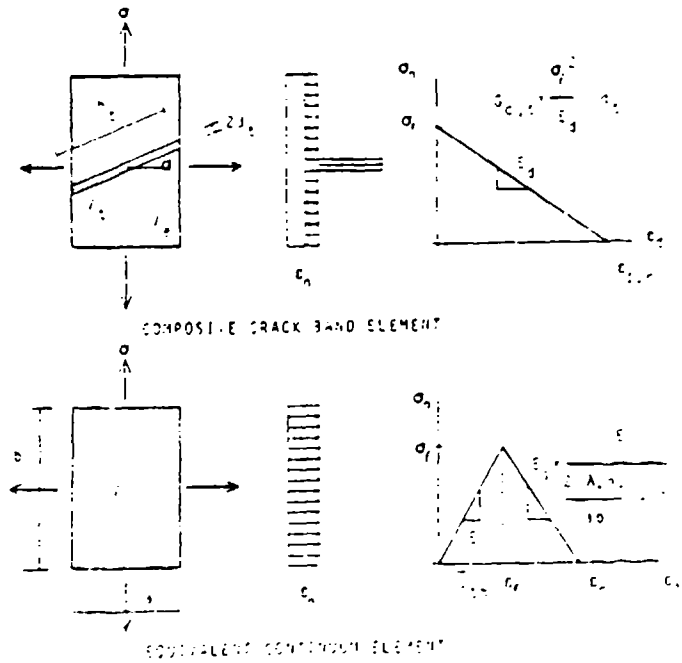

Fig. 3 Composite damage model for tensile cracking

In the case of tensile cracking the elementary volume V is composed of the undamaged elastic zone V_e and the localized crack band V_t of width d_t and length h_t in which oriented microcracking is confined. Resorting to the maximum stress criterion for cracking, the orientation of the tensile crack band is defined by the angle α between the reference axis and the minor principal stress direction. Figure 3 depicts a typical rectangular geometry of the elementary volume of thickness c

$$V = V_e + V_t \qquad \text{where} \qquad V = a\,b\,c \quad \text{and} \quad V_t = 2\,d_t h_t c \tag{7}$$

In this case $2d_t$ denotes the width of the tensile crack band and h_t the length within the elementary volume, where

$$h_t = \frac{a}{\cos\alpha} \qquad \text{or} \qquad h_t = \frac{b}{\sin\alpha} \tag{8}$$

whichever is smaller.

For straining up to rupture the energy release of the composite damage element is confined to the localized crack band because of full unloading of the elastic zone. In the simple case of linear degradation of the tensile strength σ_f, the tensile energy release of the composite element follows from

$$\Delta U_t^{CE} = \frac{1}{2}\frac{\sigma_f^2}{E_d}\,V_t = \frac{\sigma_f^2}{E_d}\,d_t\,h_t\,c \tag{9}$$

The critical fracture energy release rate for opening the crack band with the surface $\Delta A_t = h_t c$ results in

$$G_{c,t} = \frac{\Delta U_t^{CE}}{\Delta A_t} = \frac{\sigma_f^2}{E_d}\,d_t = \frac{\sigma_f^2}{E}\,\lambda_t \qquad \text{where} \quad \lambda_t = \frac{E}{E_d}\,d_t \tag{10}$$

The energy dissipation characteristics of the equivalent continuum element in which the crack band is distributed uniformly are defined by

$$\Delta U_t^{EQ} = \frac{1}{2}\left(\frac{\sigma_f^2}{E} + \frac{\sigma_f^2}{E_s}\right) V \tag{11}$$

From the equivalence of the energy release during cracking $\Delta U_t^{CE} = \Delta U_t^{EQ}$ the softening modulus E_s in tension depends on the fracture energy release rate $G_{c,t}$ or the alternative characteristic fracture dimension λ_t as well as the crack geometry

$$E_s = \frac{E}{\dfrac{2G_{c,t}}{\sigma_f^2}\dfrac{h_t}{ab} - \dfrac{1}{E}} = \frac{E}{\dfrac{2\lambda_t h_t}{ab} - 1} \tag{12}$$

This expression clearly demonstrates that the strain-softening modulus E_s of the equivalent continuum element depends also on the geometry of the elementary volume and thus exhibits a pronounced size effect. In other words, E_s varies with the mesh size of the particular finite element layout if the fracture energy release rate $G_{c,t}$ and the respective characteristic fracture dimension λ_t constitute invariant fracture properties. As a result the fracture mechanics concept leads to a non-local format of the equivalent softening relation which is fundamentally different from the local constitutive formats of strain-softening plasticity and continuous damage mechanics [12,13].

Before we turn to the computational study let us consider the material identification of the composite damage model. Contrary to previous proposals of Bažant et al [4] the equivalent softening modulus in Eq. 12 is completely defined by two parameters, the initial tensile strength σ_f and the fracture energy release rate $G_{c,t}$ or the alternative fracture dimension λ_t. In this case there is no need to speculate on the width of the blunt crack band d_t or the material behavior E_d in the localized damage zone. In fact the equivalent strain-softening expression reduces to the following relationship in the case of the direct tension test of Section 2.1.

$$E_s^1 = \frac{E}{\dfrac{2\lambda_t}{b^1} - 1} \qquad \text{where} \quad \lambda_t = 0.12\,a \qquad \text{and} \qquad h_t = a \text{ for } \alpha = 0 \tag{13}$$

Recall that b^1 denotes the height of the elementary volume and defines the size transverse to the crack band. Clearly the maximum size of the mesh layout is re-

stricted to $b^1 \leq 2\lambda_c = 0.24$ m which results in perfectly brittle softening of the equivalent continuum element with $E_s = \infty$. On the other hand a decrease of mesh size would lead to a corresponding increase of ductility. In fact virtually ideally plastic behavior with $E_s = E/100$ is obtained if the height of the elementary volume reduces to $b^1 = 2.4$ mm.

On the other hand we may ask ourselves under what condition the constant strain-softening approach and the constant fracture energy release rate concept coincide. In the case of our particular tension test this corresponds to the question for what size of b^1 do we recover the softening modulus in Eq. 3.

$$\frac{E^1_s}{E} = 0.82 = \frac{1}{\frac{2\lambda_c}{b^1} - 1} \tag{14}$$

The characteristic dimension of the fracture process zone $\lambda_c = 0.12$ m and the height $b^1 = 0.108$ m of the elementary volume will reproduce exactly the constant softening modulus. We recall that $b^1 = 0.108$ corresponds to the height of the actual test specimen in Fig. 2. This brings us back to the initial interpretation of the post-critical response data in terms of the nominal softening model and the alternative fracture energy formulation for the localized crack band. While the constant strain-softening approach is strictly valid only for the particular test configuration under consideration, the constant fracture energy release rate concept provides a rational methodology for translating this result to other test configurations with a single crack band.

2.2 Post-Critical Response Computations of Direct Tension Test

During the discussion of the direct tension test data it was observed that both the continuous strain-softening approach as well as the discrete fracture approach raised serious questions with regard to their validity. In the first case it was doubtful if the strain-softening of a continuum would be able to capture a single macrodefect. In the second case it was questionable if a constant fracture energy release rate would be applicable to specimen sizes of the order of the characteristic fracture dimension.

For this reason let us investigate the post-critical response predictions of the direct tension test using the composite damage model presented above. To this end the upper half of the cylindrical NX specimen in Fig. 2 is idealized with three different meshes of biquadratic elements. The initial axial load-displacement relation corresponds to the bilinear idealization of the uniaxial tension test, whereby the specimen is loaded under displacement control with radial restraints at the loading platens.

Figure 4 depicts the computational response predictions for the case of constant fracture energy release rate in tension i.e. $G_{c,t} = 4.5$ N/m. The reference solution agrees fairly closely with the results of the square 4 x 8 mesh as well as the rectangular 2 x 4 and 4 x 2 idealizations in which the softening modulus is adjusted according to Eq. 13 in order to enforce a constant fracture energy release rate. The constant fracture energy release rate formulation captures the strain localization in the single crack band fairly well. Figures 5 and 6 clearly illustrate the overall motion and the redistribution of strains and stresses within the tensile test specimen during the formation of the single macrodefect. In fact, the comparison between the results at peak strength and the solution at low residual strength demonstrates the consequences of strain localization which initiates at the right top corner of the tension specimen because of the stress concentration due to radial restraint at the loading platen.

In contrast the computational post-critical predictions for the case of constant softening modulus $E_s = 0.82\ E$ exhibit the almost perfectly brittle response shown in Fig. 7. This excessive decrease of ductility is a direct consequence of the mesh refinement which introduces multiple cracking into the idealization instead of a single macrocrack. The simple expression in Eq. 13 demonstrates clearly that decreasing the mesh height, i.e., $b^1 = 0.054$ m, implies an equivalent increase of λ_c and the conjugate fracture energy release rate $G_{c,t}$ if E_s is to remain constant. As a result the energy dissipation

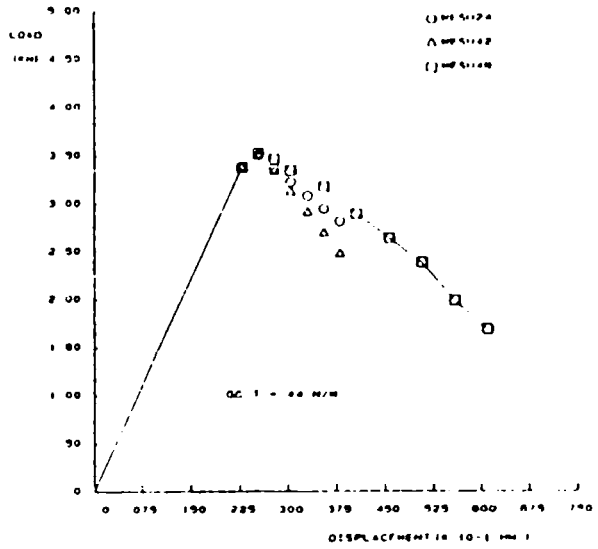

Fig. 4 Numerical predictions for $G_{c,t}$ = constant

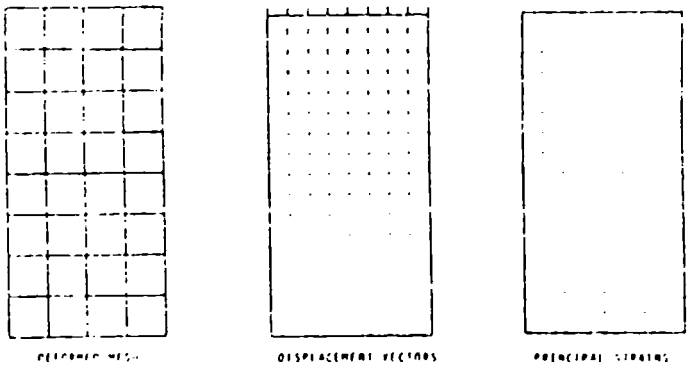

Fig. 5 Direct tension test - peak response at load step 3

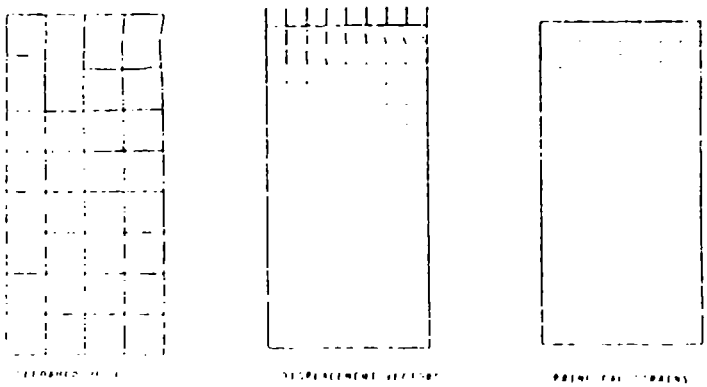

Fig. 6 Direct tension test - post-critical response at load step 13

capacity of the specimen diminishes to the limiting condition of elastic perfectly brittle response behavior if the height of the specimen is subdivided into a refined mesh. In fact, this conclusion is fairly obvious if we recall that the initial softening slope $E_s = 0.82\ E$ was calibrated by the elementary idealization of the direct tension test in terms of nominal stress and strain, whereby the axial strain was based on the gauge length of the entire specimen height containing a single tensile crack. Consequently, it is illusory to capture the actual localization of the tensile crack band with the constant strain-softening model.

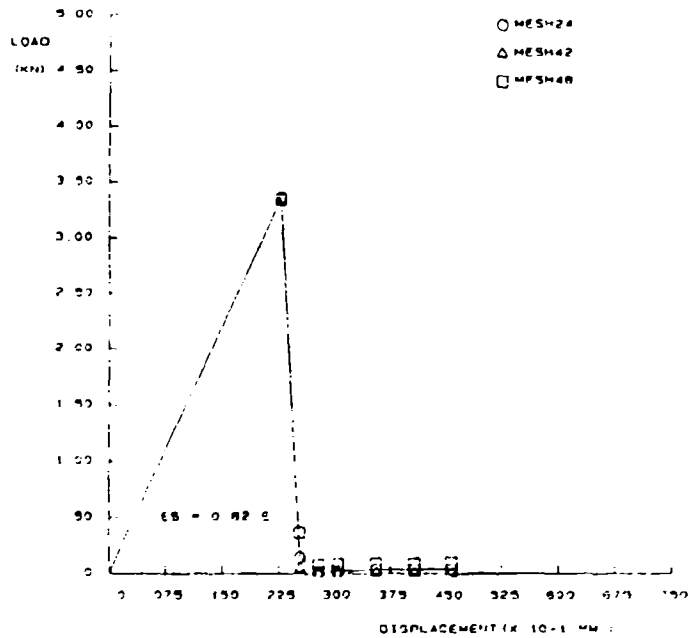

Fig. 7 Numerical predictions for E_s = constant

3. TRIAXIAL COMPRESSION TEST

While the fracture mechanics concepts have been widely accepted for tensile micro-cracking, there is considerable debate with regard to shear fracture of concrete and geomaterials. In fact, most geotechnical failure computations are based on the traditional notion of hardening/softening plasticity theories [14,15], while prominent applied mechanicians advocate fracture mechanics models for the development of shear bands in geophysical applications [16,17,18].

In cementitious materials such as concrete the situation is aggravated by the heterogeneous composition of the mesostructure which leads, for example, to splitting tensile failure under uniaxial compression. Moreover, the traditional shear tests normally result in a tensile cracking mode of fracture if brittle materials are considered. In fact a frictional slip mode of failure can only be observed under sufficiently high confining stresses. For this reason, the conventional triaxial compression test is examined below, in which a constant confining stress is applied first before the specimen is failed under axial loading.

Figure 8 illustrates the MX-size specimen and a typical response curve which was obtained in the servo-controlled triaxial Hoek cell developed at the University of Colorado, Boulder for post-critical response studies [9]. The following material parameters were extracted from a series of triaxial compression tests at different confining pressures

Stiffness: $G = 2{,}873$ MPa
$\nu = 0.20$

Strength: $C_0 = 2.868$ MPa
$\phi_0 = 41.3°$ (15)

For simplicity let us assume that the degradation of strength is primarily a result of decohesion while the internal friction remains constant. Therefore, at the residual strength level the cohesion reduces to zero, $C_r = 0$, and the angle of internal friction retains its initial value, $\phi_r = 41.3°$.

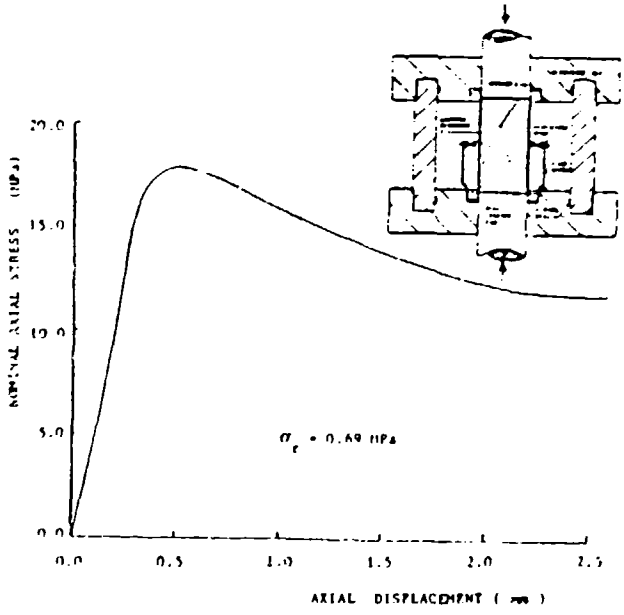

Fig. 9 Triaxial compression test of NX-size specimen

If we replace the localization of the shear band by an equivalent uniform distribution of microdefects over the gauge length, then we can interpret the softening branch in terms of the shear softening modulus

$$G_s = 0.05\ G = 143.6 \text{ MPa} \quad (16)$$

As a result the pre- and post-critical response behavior is idealized by a bilinear stress-strain relation followed by perfectly plastic behavior at the residual strength level. Again the definition of the strain-softening modulus G_s is a structural property which is intimately tied to the particular test and fracture configuration. Therefore, it is questionable if and how this parameter can be applied to different geometries and boundary conditions.

On the other hand, the displacement controlled development of a single shear band in the triaxial compression specimen can be utilized to calibrate the critical fracture energy release rate in shear. According to Palmer and Rice [19] the integral under the nominal shear stress-tangential displacement curve yields a first order approximation of the critical shear fracture energy release rate for the particular mortar under consideration. Let us assume that a homogeneous stress state prevails within the specimen up to the formation of a single shear band which is inclined according to the Mohr-Coulomb slip condition at the angle $\vartheta = \pi/2 + \phi/2$ with the major axis of principal stress. Furthermore, if we neglect the effect of elastic shear deformations within the two portions of the specimen

separated by the shear band shown in Fig. 8, then the critical shear fracture energy release rate can be evaluated by the elementary expression

$$G_{c,s} = \int_0^{\bar{u}_r} \tau \, d\bar{u} = \int_{u_0}^{u_r} \frac{(\sigma_r - \sigma_z)}{2} \frac{\sin 2\theta}{\sin\theta} \, du_z = 2{,}452 \text{ N/m} \qquad (17)$$

This extremely large value is a direct result of the tenfold increase of strength and ductility in compression versus tension. The magnitude agrees with first order approximation of $G_{c,s}$ when calibrated from alternative test data of the direct shear test. The conjugate value for the characteristic fracture dimension is defined by the analogous expression for tensile cracking in Eq. 5

$$\lambda_s = \frac{G_{c,s} \, G}{(\tau_f - \tau_r)^2} = 1.465 \text{ m} \qquad (18)$$

If we adopt again the notion of a fracture process zone with degraded material properties G_d then the width of the shear band is actually

$$d_s = \frac{G_d}{G} \lambda_s \qquad (19)$$

However, we still face a fracture process zone which is extremely large and of the same size as the specimen height. Therefore, in the case of frictional slip it is highly questionable if the fracture mechanics of a single shear band governs the post-critical response behavior.

3.2 Composite Damage Model for Frictional Slip

For the sake of a unified approach towards shear softening, let us resort to the composite damage model illustrated in Fig. 9, see also refs. [9-11].

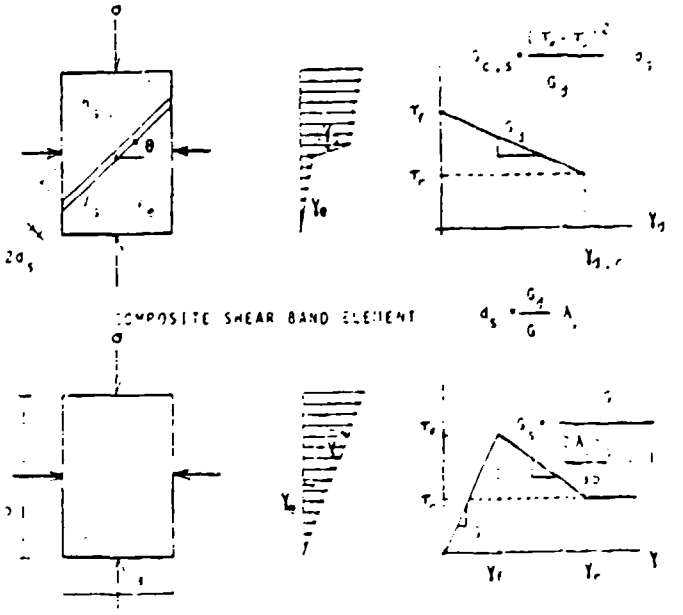

Fig. 9 Composite damage model for frictional slip

The elementary volume V is again composed of the undamaged elastic zone V_e and the localized shear band V_s of width d_s and length h_s in which oriented slip is confined. Resorting to the Mohr-Coulomb condition of frictional slip, the orientation of the frictional shear band is defined by the angle $\theta = \phi/2 + \pi/4$ with the major axis of principal stress. Elementary geometry yields for the rectangular configuration of the elementary volume

$$V = V_e + V_s \qquad \text{where} \quad V = a\,b\,c \quad \text{and} \quad V_s = 2d_s h_s c \tag{20}$$

In this case $2d_s$ denotes the width and h_s the length of the shear band within the elementary volume, where

$$h_s = \frac{s}{\cos\theta} \qquad \text{or} \qquad h_s = \frac{b}{\sin\theta} \tag{21}$$

whichever is smaller.

For straining up to rupture the energy release of the composite element is confined to the localized shear band. In the simple case of linear degradation of the cohesion the shear energy release of the composite element follows from

$$\Delta U_s^{CE} = \frac{(\tau_f-\tau_r)^2}{2G_d} V_s = \frac{(\tau_f-\tau_r)^2}{G_d}\, d_s h_s c \tag{22}$$

The critical fracture energy release rate for advancing the shear band by the surface $\Delta A_s = h_s\, c$ is then

$$G_{c,s} = \frac{\Delta U_s^{CE}}{\Delta A_s} = \frac{(\tau_f-\tau_r)^2}{G_d}\, d_s = \frac{(\tau_f-\tau_r)^2}{G}\,\lambda_s \quad \text{where} \quad \lambda_s = \frac{G}{G_d}\, d_s \tag{23}$$

The energy dissipation characteristics in the equivalent continuum element are defined by

$$\Delta U_s^{EQ} = \frac{(\tau_f-\tau_r)^2}{2}\left(\frac{1}{G} + \frac{1}{G_s}\right) V \tag{24}$$

From the equivalence $\Delta U_s^{CE} = \Delta U_s^{EQ}$ the softening modulus G_s in shear depends on the fracture energy release rate $G_{c,s}$ or the characteristic fracture dimension λ_s and the crack geometry according to

$$G_s = \frac{1}{\dfrac{2G_{c,s}}{(\tau_f-\tau_r)^2}\dfrac{h_s}{ab} - \dfrac{1}{G}} = \frac{G}{\dfrac{2\lambda_s h_s}{ab} - 1} \tag{25}$$

This expression clearly demonstrates that the shear softening modulus G_s of the equivalent continuum element depends on the geometry of the elementary volume and thus exhibits a pronounced size effect. In other words, G_s depends on the particular finite element mesh layout if the fracture energy release rate $G_{c,s}$ and the respective characteristic fracture dimension λ_s constitute invariant fracture properties. As a result, the underlying fracture mechanics concept leads to a non-local format of the equivalent softening relation which is fundamentally different from the local constitutive theories of strain-softening plasticity and continuous damage mechanics.

We conclude that the composite damage models for tension and shear have essentially the same structure. In both cases the fracture energy release concept results in a non-local format of the equivalent softening continuum.

Before turning to the computational study let us consider again the particular aspects of the triaxial compression test examined previously in Section 3.1. In this case the shear softening modulus expression of Eq. 25 reduces to

$$G_s^1 = \frac{G}{\dfrac{2\lambda_s}{a^1 \sin\theta} - 1} \qquad \text{where } \lambda_s = 1.465\ \text{m} \ \text{ and } \ \theta = 65.65^0 \tag{26}$$

Recall that $h^1 \sin\theta$ denotes the size of the elementary volume transverse to the shear band. Clearly for reasonable values of b^1 with regard to the NX-size specimen we obtain increasingly ductile behavior, i.e. $G_s \to 0$ as $b^1 \to 0$. In fact, for a single element idealization of the entire specimen with b = 0.108 m we find that $G_s = 0.017\ G$ which is somewhat smaller than the initial interpretation of the post-critial response data in terms of the nominal shear softening modulus, $G_s = 0.05\ G$. However, from this simple result it should be apparent that a convergence study with successive mesh refinement will result in increasingly ductile response predictions if λ_s remains invariant. Alternatively, we should ask ourselves what would happen if the constant fracture energy release concept were to be applied to the solution of different boundary value problems in view of the large value of $\lambda_s = 1.465$ m. Clearly if sufficiently large geometries would be considered, the opposite effect would take place. In fact for increasing b^1 values increasingly brittle post-peak predictions would result, whereby the maximum mesh size for b^1 is restricted by the condition

$$\frac{2\lambda_s}{b^1 \cos\theta} \geq 1 \qquad (27)$$

For $\lambda_s = 1.465$ m this condition results in the limiting value for $b^1 < 7.106$ m and the respective restriction for $h^1 < 3.216$ m for perfectly brittle conditions, i.e. $G_s = \infty$. In other words a constant fracture energy release analysis of large-scale geotechnical problems would result in a mesh size restriction in the order of meters.

3.2 Post-Critical Response Computations of Triaxial Compression Test

In view of the different interpretation of the experimental data in the post-critical regime, let us examine the computational response predictions for the compression test using the composite damage model above. The upper half of the cylindrical NX specimen is idealized with three different mesh layouts of biquadratic elements. The axial load-displacement relation corresponds to the bilinear idealization of the triaxial compression test, whereby the specimen is loaded under axial displacement control with radial restraints at the loading platens and radial confinement $\sigma_r = 0.69$ MPa.

Figure 10 illustrates the computational response predictions for the case where the softening modulus remains invariant, i.e. $G_s = 0.05\ G$. The numerical results indicate that the post-critical response is virtually independent of the particular mesh-size and underestimates the ductility of the idealized test data in Fig. 8. This conclusion coincides with previous observations [10,11] for distributed shear fracture which can be summarized by stating that the constant softening formulation yields post-critical response predictions which are quite consistent and independent of mesh size. The constant softening modulus formulation captures fracture in the form of a shear cone and radial splitting within the compression specimen. Figures 11 and 12 clearly illustrate the overall motion and the strain localization along the cone, whereby the axisymmetric idealization imposes some restriction on the failure mode. However, the comparison between the results at peak strength and the solution at the residual strength level clearly demonstrates the formation of the compressive shear cone at the loading platen and the subsequent radial splitting at mid-height.

In contradistinction the basic fracture mechanics postulate of an invariant energy release rate leads to the results depicted in Fig. 13. The excessive ductility during the formation of the shear band leads to a post-critical response prediction which exhibits very little softening. The reason for the increased ductility has been discussed in the context of Eq. 26. In fact, the large value of the characteristic fracture dimension $\lambda_s = 1.465$ m simply indicates that there is no localization of a single shear band possible in the NX-size test specimen with a height of 0.108 m. In other words the entire specimen constitutes the fracture process zone which is mobilized in the energy exchange during shear failure. As a result the constant softening modulus formulation for uniformly distributed microdefects is, in this case more appropriate.

We conclude that frictional slip type fracture takes place in cementitious materials in a far more distributed fashion than tensile cracking. In fact, a

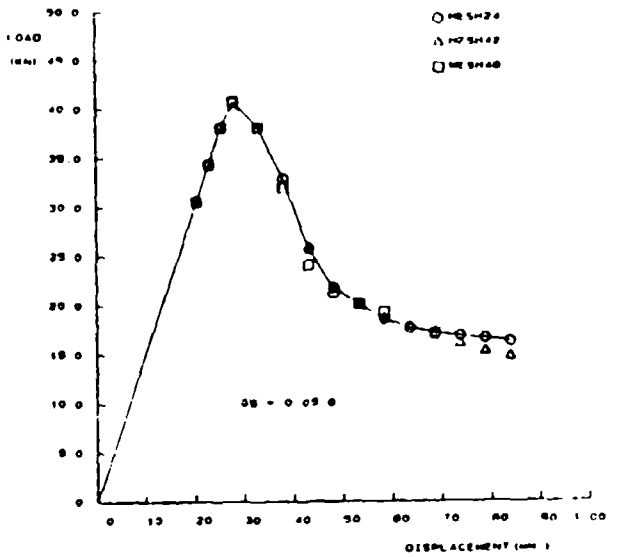

Fig. 10 Triaxial compression test - numerical predictions for σ_3 constant

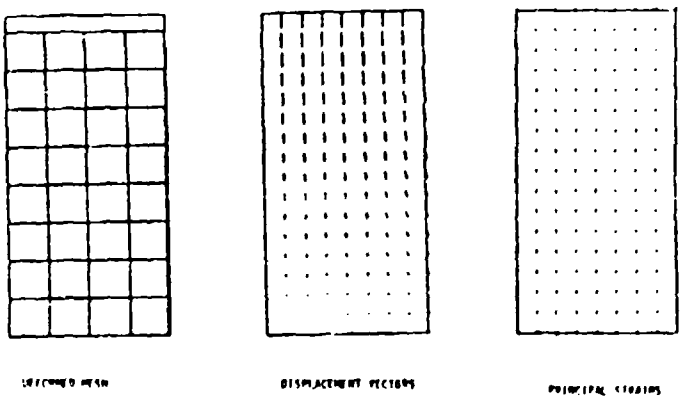

Fig. 11 Triaxial compression test - peak response at load step 4

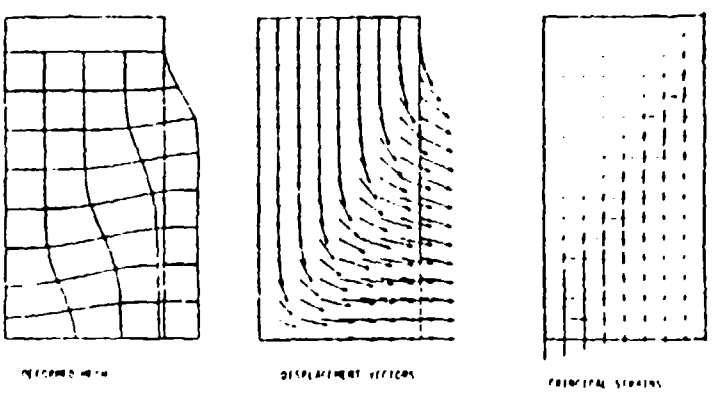

Fig. 12 Triaxial compression test - post-critical response at load step 15

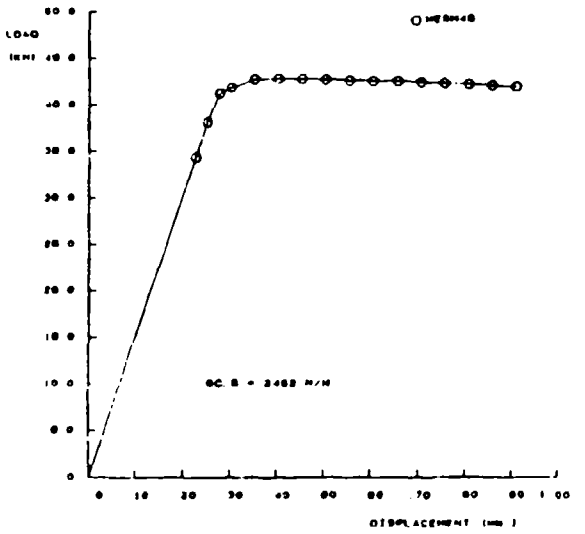

Fig. 13 Numerical predictions for $G_{c,s}$ = constant

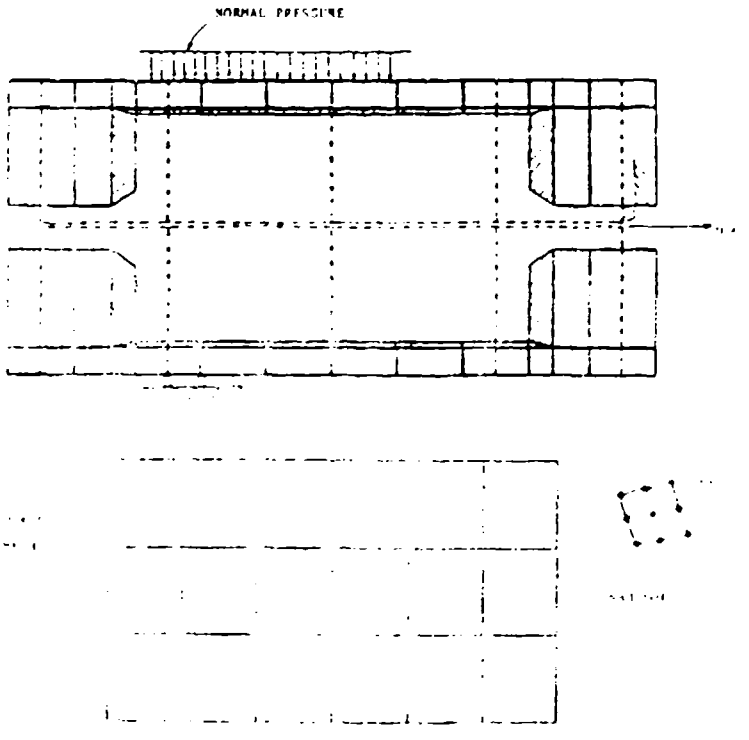

single shear band develops only under sufficiently confined conditions when premature cracking is suppressed by compressive stress states. Therefore the fracture mechanics hypothesis of a constant fracture energy release rate in shear is not of immediate concern for traditional structures but is of paramount interest in geotechnical and geophysical applications.

4. DIRECT SHEAR TEST

In the final example let us examine the post-critical behavior of the direct shear test specimen in which both tensile cracking and frictional slip take place simultaneously. In this case distributed fracture is contained by the two steel box compartments, whose motions are monitored by two servo-controlled actuators in the stiff shear test frame built at the University of Colorado, Boulder [20]. In this sense the direct shear test specimen constitutes a miniature structure in which contained fracture propagates in a manner that is similar to the failure behavior in confined structures of high indeterminacy. The normal pressure is applied to a prescribed load level and held constant during the subsequent tangential loading monitored under displacement control in order to capture the full post-critical response branch down to the residual load level. Depending on the ratio of normal to tangential load level the full range of predominantly tensile cracking to highly confined frictional slip is mobilized within the "shear test" specimen.

From the different test results reported in Ref. [10] we consider the prismatic 0.204 x 0.102 x 0.117 m mortar specimen tested at the normal pressure σ_n = 1.379 MPa. The test specimen is bonded to the steel box compartments with the aid of an epoxy compound in order to ensure full contact on the tensile sidewalls of the shear box. Because of the planar mode of fracture a two-dimensional plane strain idealization is used to model the specimen and contiguous shear box. The finite element mesh layout includes the actual test specimen as well as the upper and lower shear box compartments in order to ensure that the tangential displacement control lies in the prevalent shear plane at mid-height of the specimen. The idealization of the direct shear test is shown in Fig. 14 for the 3 x 6 mesh of the specimen. Altogether 683 degrees of freedom were used to interconnect 78 biquadratic isoparametric elements which include the idealization of the steel box and the loading frame in order to avoid overturning effects due to eccentric tangential loading, see also ref. [21].

The composite damage model for tensile cracking and frictional slip are combined for describing constant softening or alternatively constant fracture energy release in tension and shear. The actual properties of the mortar specimen were calibrated before in the context of the direct tension and triaxial compression tests. Therefore the direct shear test constitutes an entirely independent example of different size which will assert the previous findings on distributed and localized fracture in tension and shear. The elastic response is defined as before by E = 6,895 MPa and ν = 0.20. The initial fracture condition is governed by the modified Mohr-Coulomb condition C_0 = 2.87 MPa and ϕ_0 = 41.3° augmented by the tension cut off σ_f = 1.59 MPa. The post-critical behavior is in one case described by the constant softening model where E_s = 0.82 E and G_s = 0.05 G and in the other case by the constant fracture energy release rates $G_{c,t}$ = 44 N/m and $G_{c,s}$ = 2,452 N/m. In addition, a third post-critical strategy is pursued in which the fracture energy release rate in tension is kept constant, $G_{c,t}$ = 44 N/m, while the shear softening modulus remains invariant, G_s = 0.05 G. For frictional slip a non-associated flow rule is used throughout in order to capture the splitting tension mode of fracture during shearing with a flow potential in the form of the maximum stress criterion. In the case of tensile cracking this flow rule reduces to the traditional associated flow rule used to monitor the growth of tensile cracking strains.

Figure 15 depicts the overall load-deformation behavior in terms of the nominal shear stress in the prevalent shear plane versus the relative tangential displacement between the upper and lower shear box compartments. The three computational predictions exhibit considerable variation as compared to the experimental results. The constant shear softening modulus approach shows the best agreement with regard to both strength and overall ductility, while the constant fracture energy formulation indicates far too ductile behavior. Clearly, in view of the

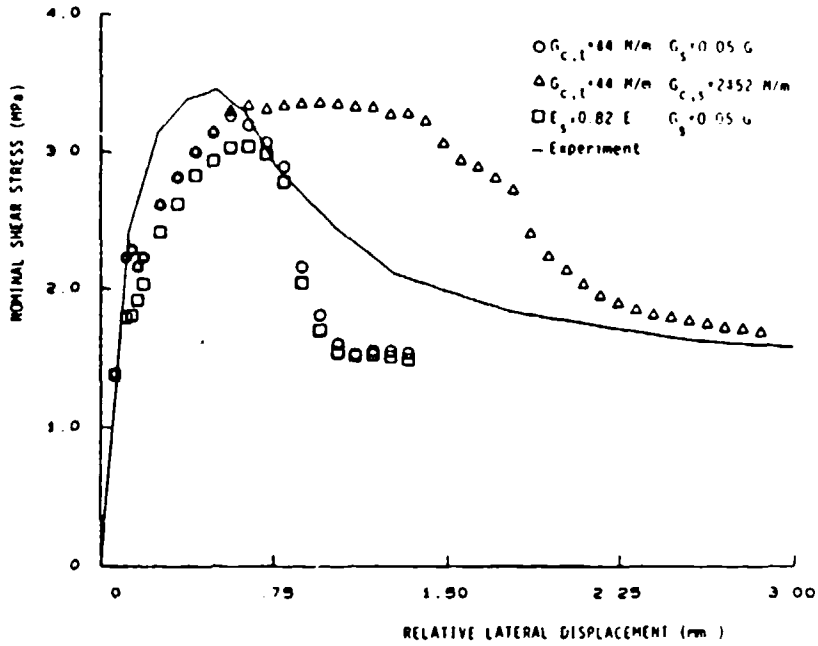

Fig. 15 Direct shear test - numerical predictions for various softening strategies

confined fracture propagation within the shear specimen one could argue that a single slip band only develops in the final stage at the residual strength level. In addition, this localized shear band involves extensive tensile cracking in a direction which differs substantially from the prevalent shear plane. Therefore, one could conclude that contained fracture is beyond the realm of fracture mechanics of single macrodefects. However, in engineering applications this final mode of fracture in cementitious materials is always accompanied by extensive zones of distributed damage in which the constant softening model prevails.

Figure 16 illustrates the shearing motion in terms of the total displacement vectors for load steps corresponding to the peak and post-critical regimes. Observe the localization into a wide shear band which is accompanied by considerable vertical dilatation due to tensile splitting. The total strain distribution is depicted in Fig. 17 at the same loading steps. The plots emphasize the localization of shear strains in the prevalent shear plane while the upper and lower portions of the specimen unload progressively. The associated stress redistribution during progressive fracturing is shown in Fig. 18 with plots of principal stresses at the two load steps. Recall that the minor principal stress is initially aligned with the vertical pressure $\sigma_n = 1.379$ MPa. It rotates upon continuous shearing by almost 80° in order to accommodate the compressive strut action between the compressive side-walls of the shear box. The initial cracking is confined to the tensile corners of the specimen and exhibits little influence on the overall response behavior. The splitting tension that is parallel to the compressive struts, leads ultimately to a single shear band at mid-height in the form of an S-shaped fracture surface.

The results clearly confirm that the direct shear test is definitely not a simple material test when cementitious materials are considered. In fact, the contained mode of fracture results in a complex combination of tensile cracking and frictional slip which is highly distributed before final localization of a macrodefect takes place.

DISPLACEMENT VECTORS

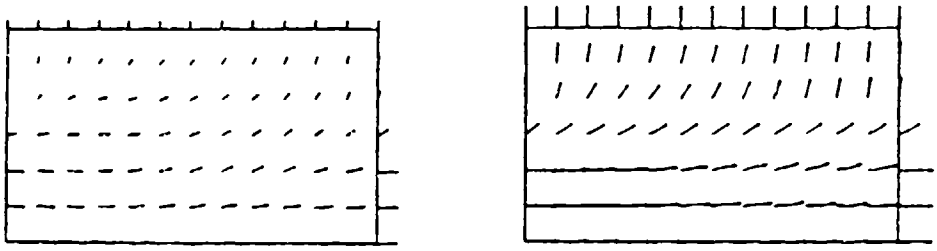

Fig. 16 Motion of the direct shear test specimen

PRINCIPAL STRESSES

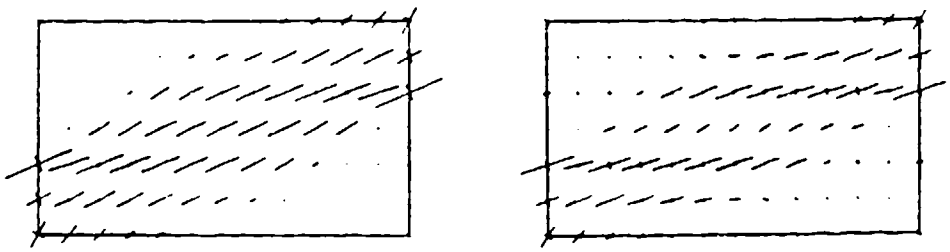

Fig. 17 Stress redistribution within direct shear test specimen

PRINCIPAL STRAINS

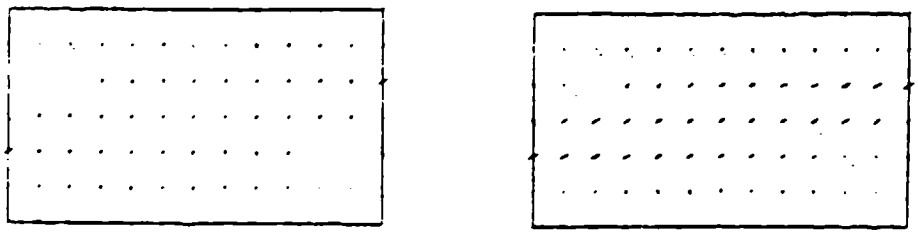

Fig. 18 Strain redistribution within direct shear test specimen

5. CONCLUDING REMARKS

The principal result of the proposed composite damage model is a unified approach towards localized and distributed fracture in the form of tensile cracking and frictional slip. In the case of localized fracture the composite damage model provides a non-local softening law of the equivalent continuum which depends on the characteristic fracture dimension as well as the geometric configuration of the fracture band within the elementary volume of finite dimension. In fact, the composite damage model recovers in this case the constant fracture energy release concept without resorting to the fracture mechanics of discrete macrodefects. On the other end of the spectrum the composite damage model degenerates to the continuous damage theory of distributed fracture when the volume fraction of localized damage approaches unity. In this case the softening modulus E_s of the equivalent continuum constitutes a local material property which holds pointwise and is independent of the particular fracture configuration.

The composite damage model was applied to the post-critical response behavior of the direct tension and triaxial compression tests on cylindrical mortar specimens for which test data were available for comparison. While the constant fracture energy release concept captured the localization of a single crack band in tension, the constant softening model reproduced distributed fracture in shear.

In the final example of the direct shear test both tensile cracking as well as frictional slip modes of contained fracture were mobilized, similar to the failure behavior in highly confined structures. In this case the combination of the constant fracture release concept for tensile cracking and the constant softening formulation for shear slip furnished the best agreement with the experimental post-critical response behavior.

Clearly, the previous exposition was based on gross simplication in order to arrive at elementary algebraic relations which clearly exhibit the fundamental differences of distributed and highly localized fracture. In reality fracture is an evolutionary process in which the localized damage zone increases gradually and where the critical fracture energy release rate varies in accordance with the experimental degradation of strength in the post-critical response regime. In addition inelastic dissipation mechanisms take place which are mobilized particularly in shear. As such the composite damage model above is a first order approximation which captures the limiting conditions of the local size-independent softening relation as well as the non-local fracture energy release rate concept. For the continuous transition from distributed to localized fracture an evolutionary damage process should provide an immediate solution to combine these two extreme cases.

ACKNOWLEDGEMENT

The work was supported by the U.S. Air Force Office of Scientific Research under contract AFOSR 82-0273 with the University of Colorado, Boulder. The authors would like to thank B. Hurlbut and E. Pramono for their assistance in the experimental and computational studies.

REFERENCES

[1] Janson, J., and Hult, J., "Fracture Mechanics and Damage Mechanics, a Combined Approach," J. de Mécanique Appliquée, Vol. 1, 1977, pp. 69-84.

[2] Von Rittinger, P., "Lehrbuch der Aufbereitungskunde," Ernst und Korn, Berlin, 1867.

[3] Hillerborg, A., Modéer, M., and Petersson, P.E., "Analysis of Crack Formation and Crack Growth in Concrete by Means of Fracture Mechanics and Finite Elements," Cement and Concrete Research, Vol. 6, 1976 pp. 773-781.

[4] Bažant, Z.P., and Cedolin, L., "Blunt Crack Band Propagation in Finite Element Analysis," ASCE, Jnl. of the Engineering Mechanics Division, Vol. 105, No. EM2, 1979, pp. 297-315.

[5] Saouma, V.E., and Ingraffea, A.R., "Fracture Mechanics Analysis of Discrete Cracking," Proc. IABSE Conf. on Advanced Mechanics of Reinforced Concrete, Delft, June 2-4, 1981, pp. 393-416.

[6] Kröner, E., "Interrelations Between Various Branches of Continuum Mechanics," Mechanics of Generalized Continua, ed. by E. Kröner, Springer-Verlag, 1968, pp. 330-340.

[7] Bažant, Z.P. and Oh, B.H., "Crack Band Theory for Fracture of Concrete," Rilem, Materiaux et Constructions, Vol. 16, 1983, pp. 155-177.

[8] Petersson, P.E., "Fracture Energy of Concrete: Method of Determination," Cement and Concrete Research, Vol. 10, 1980, pp. 78-89.

[9] Willam, K.J., Sture, S., Bićanić, N., Christensen, J. and Hurlbut, B., "Identification of Strain-Softening Properties and Computational Predictions of Localized Fracture," Structural Research Series No. 8404, University of Colorado, Boulder, 1984.

[10] Willam, K.J., "Experimental and Computational Aspects of Concrete Fracture," Invited paper at Int. Conf. Computer-Aided Analysis and Design of Concrete Structures, Split, Yugoslavia, Sept. 17-21, 1984.

[11] Bićanić, N., Sture, S., Hurlbut, B., and Day, S. "On the Prediction of the Peak and Post-Peak Behavior of Concrete Structures," paper at Int. Conf. Computer-Aided Analysis and Design of Concrete Structures, Split, Yugoslavia, Sept. 17-21, 1984.

[12] Dougill, J.W., "On Stable Progressively Fracturing Solids," J. Appl. Math. Phys., ZAMP, Vol. 27, 1976, pp. 423-436.

[13] Lorrain, M. and Loland, K.E., "Damage Theory Applied to Concrete," Chapter 4.4 of Fracture Mechanics of Concrete, ed. F.H. Wittmann, Elsevier Science Publ. B.V., Amsterdam, 1983, pp. 341-369.

[14] Desai, C.S., and Siriwardane, H.J., "Constitute Laws for Engineering Materials with Emphasis on Geologic Materials," Prentice-Hall, Inc., Englewood Cliffs, N.J., 1984.

[15] Resende, L., and Martin, J.B., "A Progressive Damage Continuum Model for Granular Materials," Comp. Meth. Appl. Mecn. Eng. Vol. 42, 1984, pp. 1-18.

[16] Rudnicki, J.W., and Rice, J.R.," Conditions for the Localization of Deformation in Pressure-Sensitive Dilatant Materials," J. Mechanics and Physics of Solids, Vol. 23, 1975, pp. 371-394.

[17] Costin, L.S., "A Microcrack Damage Model for Brittle Rock," Sandia Report SAND 83-1590, 1983.

[18] Pietruszczak, St. and Mroz, Z., "Finite Element Analysis of Deformation of Strain-Softening Materials," Int. J. Num. Meth. Eng., Vol. 17, 1981, pp. 327-334.

[19] Palmer, A.C. and Rice, J.R., " The Growth of Slip Surfaces in the Progressive Failure of Overconsolidated Clay," Proc. Royal Soc. London, A, 332, 1973, pp. 527-548.

[20] Christensen, J., Ickert, K., Stankowski, T., Sture, S., and Willam, K. J., "Numerical Modeling of Strength and Deformation Behavior in the Direct Shear Test," Proc. Int. Conf. on Constitutive Laws for Engineering Materials, C.S. Desai and R.H. Gallagher, eds., Tucson, AZ, 1983, pp. 537-544.

APPENDIX B

APPENDIX B

"Experimental and Constitutive Aspects of Concrete Failure"

by

Kaspar Willam, Bryan Hurlbut and Stein Sture

Paper presented at US-Japan Symposium on
Finite Analysis of Reinforced Concrete Structures
Tokyo, May 21-24, 1985; will be published in special
ASCE Volume on Finite Element Analysis of
Reinforced Concrete Structures,
New York (1986)

EXPERIMENTAL AND CONSTITUTIVE ASPECTS OF CONCRETE FAILURE

By Kaspar Willam[1], M.ASCE, Bryan Hurlbut[2], and Stein Sture[3], M.ASCE

ABSTRACT

The failure analyses of concrete structures are plagued (i) by the constitutive difficulties in describing the transition from brittle to ductile fracture of concrete under increasing confinement, and (ii) by the numerical intricacies related to structural response predictions of contained material instabilities due to strain-softening and/or due to lack of normality in conjunction with non-associated plastic flow concepts.

This paper presents novel experimental observations of post-critical response phenomena when cylindrical concrete specimens are loaded under displacement control in the form of direct tension and triaxial compression experiments. The investigation focuses on the problem whether or not "proper" material properties can be extracted from such experiments which characterize not only stiffness and strength behavior but also the ductility in the post-peak response regime. In this context a fracture energy based strain-softening plasticity formulation will be developed in terms of the fundamental Mode I type cracking which accounts for the transition from brittle to ductile fracture under increasing triaxial confinement.

INTRODUCTION

The failure behavior of cementitious materials such as mortar and concrete can be broadly classified into (i) tensile cleavage in the form of Mode I type cracking, and (ii) decohesive faulting in the form of Mode II type frictional slip. The tensile fracture mode typically leads to a sudden discontinuity at peak strength and a very brittle appearance of the load-deformation response when the direct tension experiment is considered. Recent experiments on notched concrete specimens by Reinhardt [15], Gopalaratnam and Shah [6] as well as the direct tension experiments by Hurlbut [9] on unnotched specimens all indicate that little hardening precedes the onset of cleavage failure which results in

---

[1] Professor of Civil Engineering, Campus Box 428, University of Colorado, Boulder, CO 80309, U.S.A.

[2] Staff Consultant, Applied Mechanics Incorporated, 12600 West Colfax Ave., Suite C360, Lakewood, CO 80215, U.S.A.

[3] Associate Professor of Civil Engineering, Campus Box 428, University of Colorado, Boulder, CO 80309, U.S.A.

the separation of the test specimen into two competent parts. In contrast, shear fracture exhibits far more ductile behavior, whereby hardening in the pre-peak regime is followed by a gradual softening regime during the process of progressive decohesion down to the residual strength level which is characterized by granular friction only. The triaxial compression experiments on concrete by van Mier [13] and Hurlbut [9] illustrate clearly the increase of ductility with increasing confining pressure. In fact the splitting tension mode of failure in uniaxial compression transforms gradually into a faulting mode of failure with increasing confinement and ultimately diffuses into distributed damage throughout the entire specimen. As a result under sufficiently high confinement there is a third response regime which does not exhibit any softening whatsoever and which is governed by compactive hardening due to pore collapse and related inelastic processes of the composite microstructure of concrete.

Since the failure of plain and reinforced concrete structures depends to a large extent on the ductility and thus the governing post-peak response characteristics of the concrete the main thrust of this investigation is directed towards the softening behavior. We will focus on recent experimental evidence obtained at the University of Colorado within a series of displacement controlled post-critical experiments on low strength concrete specimens featuring shear dilatancy, hardening as well as softening in tension and shear. There have been various attempts to correlate these global phenomena to different processes in the microstructure such as debonding between the cement matrix and the aggregate, progressive microcracking within the cement matrix and ultimately fracture of the aggregate. Quite noteworthy is the recent work by Ortiz [14] who used the mixture theory of interacting continua to model these evolutionary processes within each phase of the composite. This development is closely related to the continuous damage formulation of Mazars [12] who expressed Mode I type cracking and Mode II type shear fracture in terms of maximum tensile strain conditions.

In the following we will concentrate on the fundamental issues of strain-softening, the transition from brittle to ductile fracture, and the decrease of shear dilatancy with increasing confinement. Special attention will be paid to the extraction of fracture properties from the post-critical response regime which are independent of a particular test geometry and the given set of boundary conditions. This task is complicated by the fact that the post-critical response behavior is accompanied by severe strain localization and actual discontinuities within the test specimen. For this purpose we will expand the composite fracture formulation which has previously been developed by the authors [19] in order to incorporate the fracture energy release rate concept within the strain-softening formulation of an equivalent elastic plastic continuum.

POST-PEAK EXPERIMENTS

In conjunction with a substantial research effort on finite elements and localized failure in cementitious materials two series of experiments were recently completed which involved stable post-critical loading of cylindrical concrete specimens in direct tension and triaxial compres-

sion, (NX size samples with D = 2.125 in. (54 mm) diameter and H = 4.25 in. (108 mm) height). The concrete mix was based on a water-cement ratio of W/C = 0.833, a mix grading of C:S:G = 1:3.16:3.19 and a maximum aggregate size of 3/8 in. (9.5 mm) which in turn gave a uniaxial compressive strength of f'_c = 3.2 ksi (22.1 MPa) at 28 days. The concrete was cast into 1 x 3 x 3 ft. (0.3 x 1.0 x 1.0 m) slabs which were kept in a fog room until testing except for the period for preparation of the specimens. The cylindrical concrete samples were cored from the slab and milled with a diamond grinding wheel to the prescribed height with a tolerance of $\Delta H = \pm 0.02$ in. (± 0.5 mm). The exposed voids at the cylindrical surface of each specimen were filled with putty in order to prevent intrusion of the elastomeric membrane into the concrete voids in the case of high confining pressures.

Two series of post-peak experiments were carried out with the aid of a MTS loading system consisting of a standard 110 kip (489 kN) loading frame with servo control and function generator units. These were comprised of a series of direct tension and a series of triaxial compression experiments which will be described below.

Direct Tension Experiment

In order to clarify our understanding of the tensile fracture mechanisms the following objectives were pursued with the aid of direct tension experiments:

(i) Uniqueness of the load-displacement response in the post-peak regime,
(ii) Progressive damage and stiffness degradation during loading and unloading cycles, and
(iii) Size effects related to different height specimens.

A special technique was developed by Hurlbut [9] to stabilize the post-critical response behavior of the cylindrical tension specimens. The basic difficulty of maintaining stable post-peak control was resolved by incorporating two axial Linear Virtual Displacement Transducers (LVDT) which were attached to the loading platen as illustrated in Fig. 1. In contrast to the recent tension tests by Reinhardt [15] and Shah [6] unnotched specimens were utilized in order to avoid any bias towards fracture mechanics by introducing a well defined macrofect in the sample to start with. Therefore the actual location of tensile cracking was undetermined and the stroke of the loading actuator had to be controlled by the two axial LVDT's in order to monitor the post-peak response behavior. In return a premature fracture mechanics interpretation of the tensile cracking process was avoided and the question of a volume versus surface dominated failure process could be explored.

It is important to keep in mind that the tensile test specimen was placed into the loading frame 12 hrs before actual testing. The cylindrical sample was attached to the specially prepared solid loading platens by means of a thin layer of a high strength structural epoxy cured during the 12-hr. period under a slight compressive load of P_z = -100 lbs (-445N). Clearly the epoxy layer provided some lateral

restraint and was therefore responsible for a non-uniform stress state near the end section. In fact, the stress concentration at the corner of the specimen-platen interface led in some cases to premature bond failure or delamination.

Fig. 2 depicts the axial load-extension response of a typical direct tension experiment conducted at a displacement rate of 1.67×10^{-6} in/sec. (4.24×10^{-8} m/sec). We observe a nearly linear ascending branch up to the peak load. At this point the axial tension suddenly decreased without noticeable formation of a crack. Upon close inspection a single transverse hairline crack appeared around the periphery of the sample at an overall axial displacement of 1.5×10^{-3} in. (0.04 mm) when the residual tensile strength diminished to near zero load level. At that time the specimen had separated into two competent parts which remained entirely intact. Upon continuous loading the increasing displacements reflected simply further crack opening accompanied by rigid body movement of the two separated portions of the specimen.

Considering the reproducibility of the post-critical response branch under monotonic loading the question arises if the residual tensile strength can be recovered during loading-unloading cycles and if the associated stiffness is affected by the degrading strength. Loading-unloading experiments were performed in order to explore the residual tensile strength and the associated tangent stiffness. Fig. 3 depicts the resulting load-displacement response when the stroke is reversed to zero displacement and subsequently increased again. The plot illustrates clearly that tensile bonds still remain intact in the softening branch and that the residual tensile strength is fully recovered during reloading. In fact the post-peak load-displacement response curve approaches that of the monotonic experiment very much along the line of strain-softening elastic-plastic behavior with substantial permanent deformations. We observe a slight decrease of elastic stiffness in the first cycle and a substantial reduction when the tensile crack has fully developed very much along the results on notched tension specimens reported recently by Reinhardt [15]. There is some elastic-inelastic coupling, however, it is not nearly so pronounced as to fully support the progressive fracturing theory of Dougill [5] or the continuous damage theory of Mazars [12], Janson and Hult [10], Krajinovic and Fonseka [11] which resort to secant formulations and thus fully reversible deformations upon unloading.

In order to probe the fracture mechanics hypothesis of a single macrodefect an additional monotonic tension test was carried out with a specimen of half the height and the same cross-section. In the case of a constant fracture energy release rate the area under the P-u diagram (actually the nominal axial stress-extension plot) should remain constant, assuming that the tensile strength is not affected by the two different volumes and their different probability of failure. On the other hand if the concept of a continuous distribution of microdefects were to be adopted along the line of the smeared cracking approach, then the area under the P-u diagram, i.e., the strain energy dissipation during the transverse crack process should be reduced by half. Fig. 4

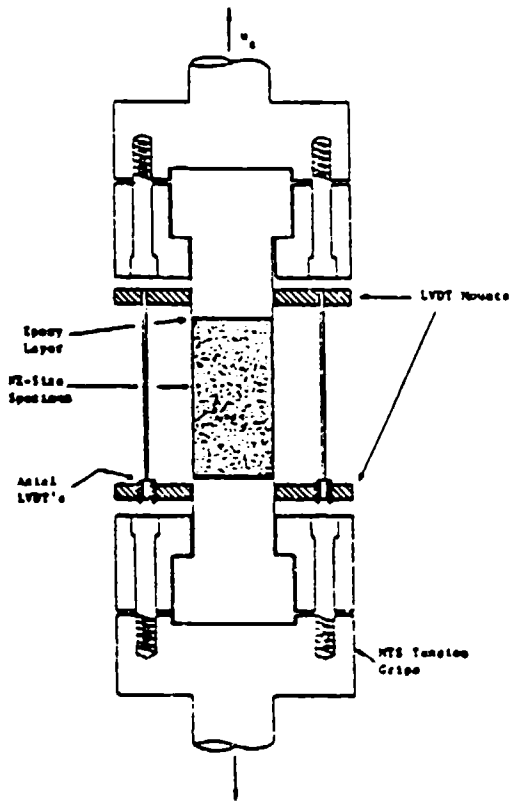

Figure 1 Direct Tension Apparatus

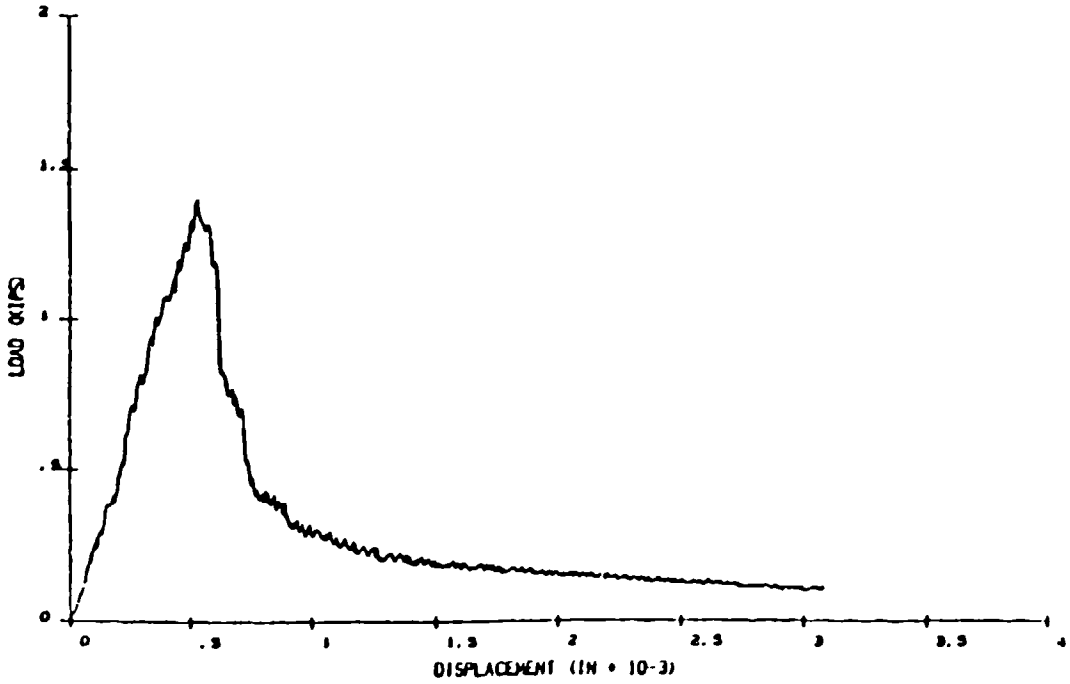

Figure 2 Direct Tension Test of Full Size NX-Specimen

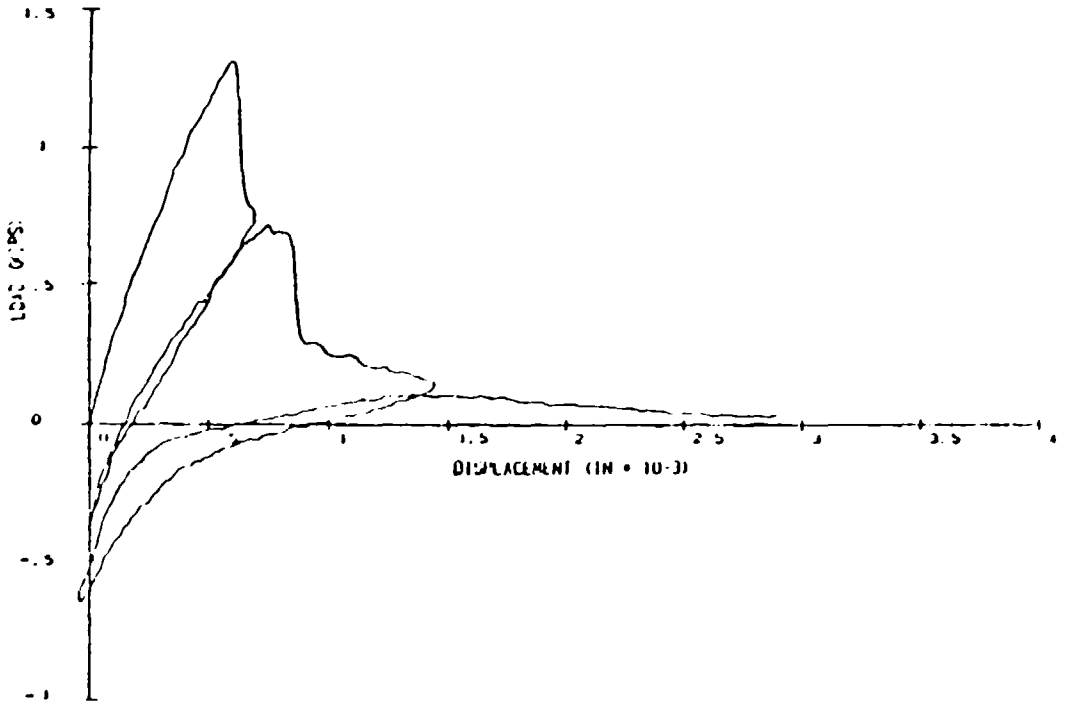

Figure 3 Cyclic Tension Test of Full Size NX-Specimen

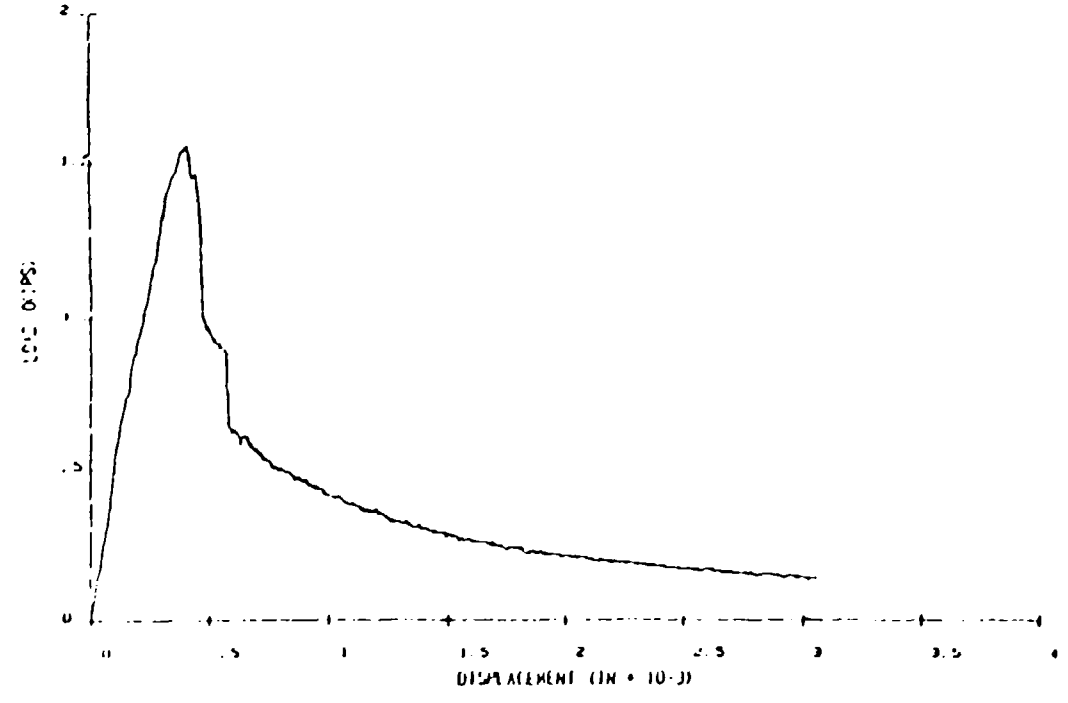

Figure 4 Monotonic Tension Test of Half Size NX-Specimen

illustrates the results of the half-size specimen test. The plot clearly indicates that the area under the P-u diagram is hardly affected by halving the height of the tension specimen. Therefore the results support the postulate of a constant fracture energy which ultimately controls the localization of distributed microdefects into a single macrodefect.

Triaxial Compression Experiments

In order to clarify our understanding of shear fracture the following objectives were pursued with the aid of axisymmetric triaxial compression experiments:

(i) Transition from brittle to ductile fracture at various levels of confinement,
(ii) Shear dilatancy during progressive shear fracture, and
(iii) Stiffness degradation during loading - unloading cycles.

Conventional triaxial compression experiments were conducted in a Hoek cell device [8] which had been modified at the University of Colorado, Boulder, in order to measure axial and lateral deformations of cylindrical NX-size specimens. The Hoek cell which is illustrated in Fig. 5 has a capacity of up to σ_r = 10 ksi (68.9 MPa) confining pressure. It is instrumented for measuring lateral deformations at the mid-height with the aid of six strain gaged cantilevers spaced at 60° intervals around the circumference. The cell pressure is provided by hydraulic fluid and is transmitted to the specimen by a flexible polyurethane membrane of 0.05 in. (1.3 mm) thickness. The confining pressure has no component in the axial direction of the cylindrical specimen. The axial load was applied with the same 110 kip (489 kN) MTS loading system with servo control and function generator units capable of stabilizing the post-critical softening branch.

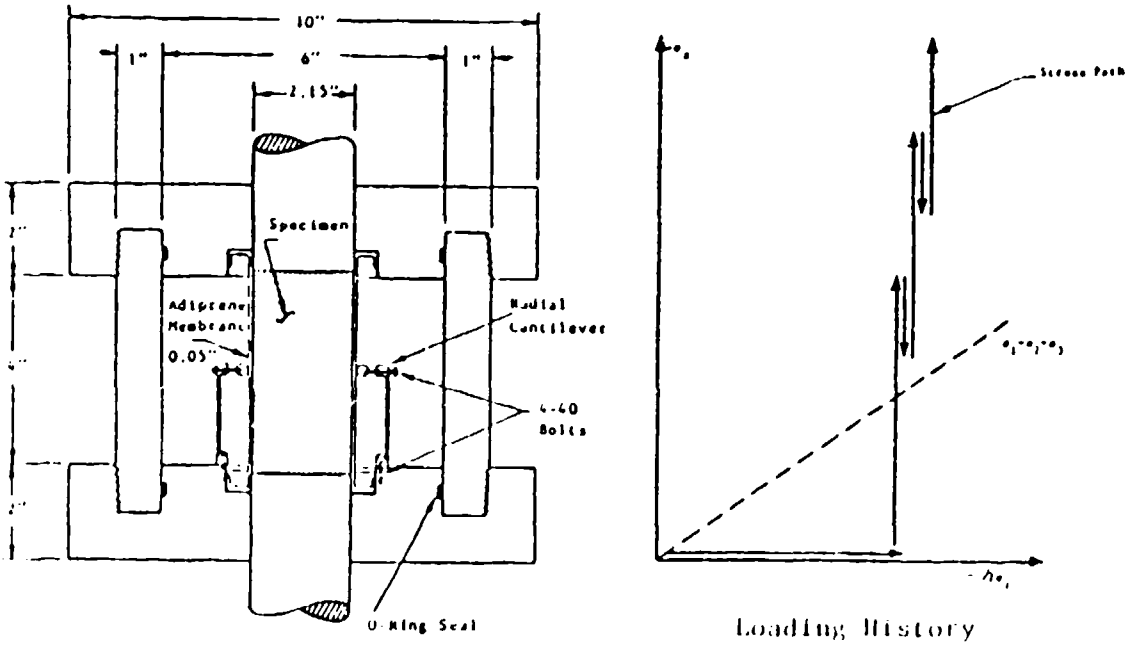

Figure 5 Triaxial Compression Apparatus

All the triaxial compression tests were conducted by pressurizing first the cell to the prescribed confining pressure which was held constant while the axial load was applied under stroke control at a displacement rate of 1.67×10^{-4} in/sec (4.24×10^{-6} m/sec).

Fig. 6 depicts the axial load-displacement behavior at four different confining levels σ_r = 100, 500, 1000 and 2000 psi (0.69, 3.45, 6.89 and 13.79 MPa). Again experimental results are plotted in the form of global load-displacement results rather than in the form of stress and strain measures since localization of fracture takes place in the softening regime which requires a proper homogenization concept. The four plots clearly demonstrate the increase of ductility with increasing confinement which suppresses the softening tendencies. The partial unloading cycles indicate very little hysteretic energy dissipation. The linear elastic unloading-reloading behavior hardly exhibits any degradation of stiffness. This suggests that the elastic-plastic coupling remains negligible and conjectures little damage accumulation of the elastic material texture not only in the pre- but also in the post-peak regime. The resulting failure modes showed a distinct transition from splitting tension under low confinement, over shear faulting under intermediate confinement, to diffuse damage at high confinement when no softening was observed altogether.

The dilatation characteristics are shown in Fig. 7 in the form of lateral versus axial displacement response curves. Again the lateral expansion diminishes rapidly with increasing confinement pressure. This indicates that volumetric dilatation accompanies strain-softening and that the transition from brittle to ductile fracture is related to the transition from volume dilation to volume compaction.

If the axial and radial displacements in Fig. 7 were converted into nominal strains their ratio would remain fairly constant in the softening regime and would decrease rapidly with increasing confinement. It was therefore felt that the inelastic dilatancy ratio $\alpha = \dot{\varepsilon}_r^f / \dot{\varepsilon}_z^f$ could provide a proper fracture characteristics which would, however, depend on the confining stress. The post-peak response at low confinement is accompanied by large inelastic volume dilation which decreases rapidly under increasing confining stress and results in inelastic compaction rather than dilation.

The triaxial strength results are summarized in Fig. 8 with a plot of the test data in the Rendulic plane where the data are shown on the compressive meridian. The diagram depicts the maximum strength envelope in conjunction with the residual strength data. The residual strength diminishes to zero at zero confinement and approaches rapidly the maximum strength envelope with increasing confinement at the transition point from brittle to ductile fracture when softening is suppressed altogether. Since the entire test program was focused on the softening behavior under low confinement no attempt was made to extract the hardening behavior which had been explored in a separate research effort by Stankowski and Gerstle [17].

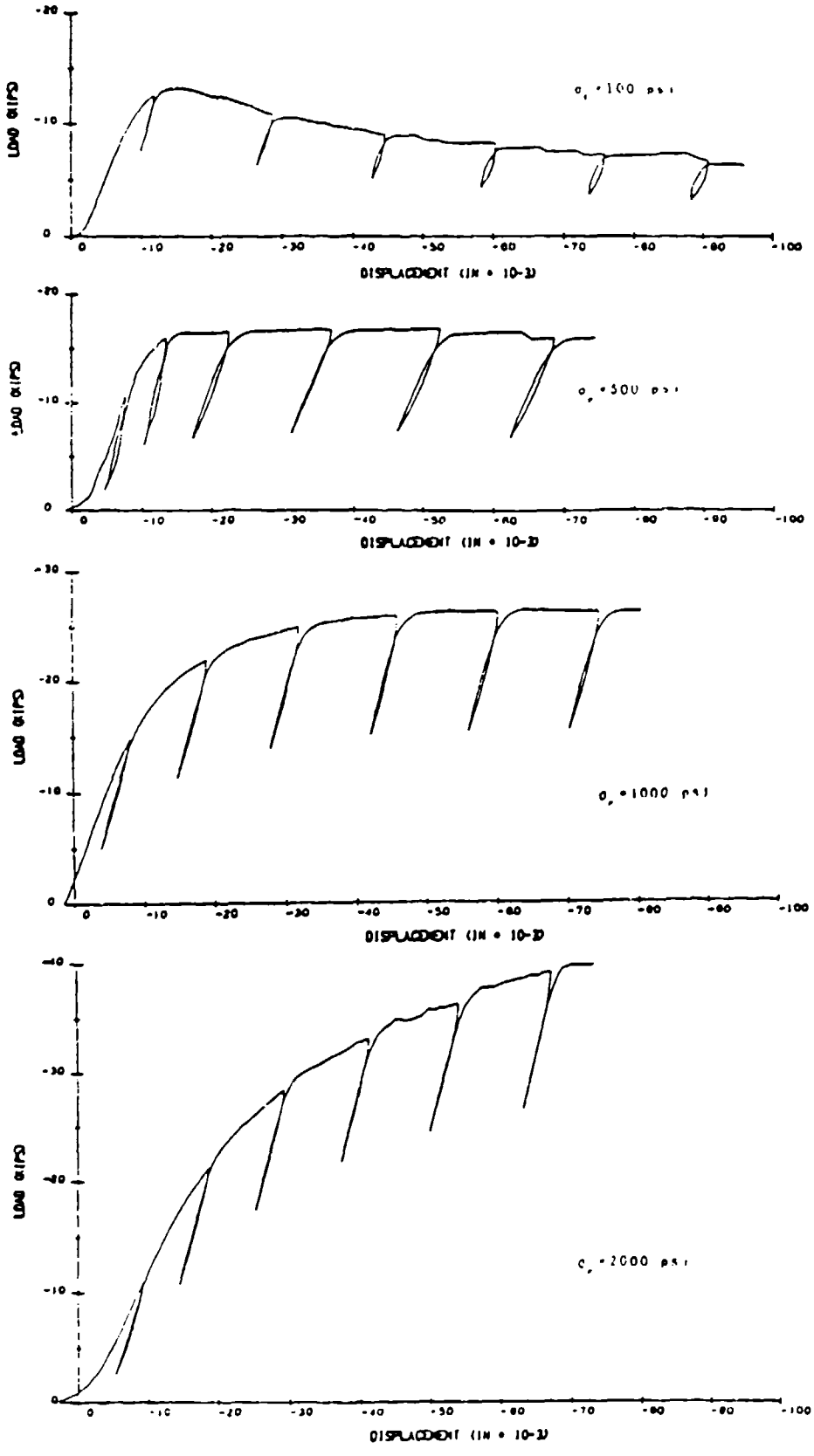

Figure 6 Conventional Triaxial Compression Tests with Partial Unloading

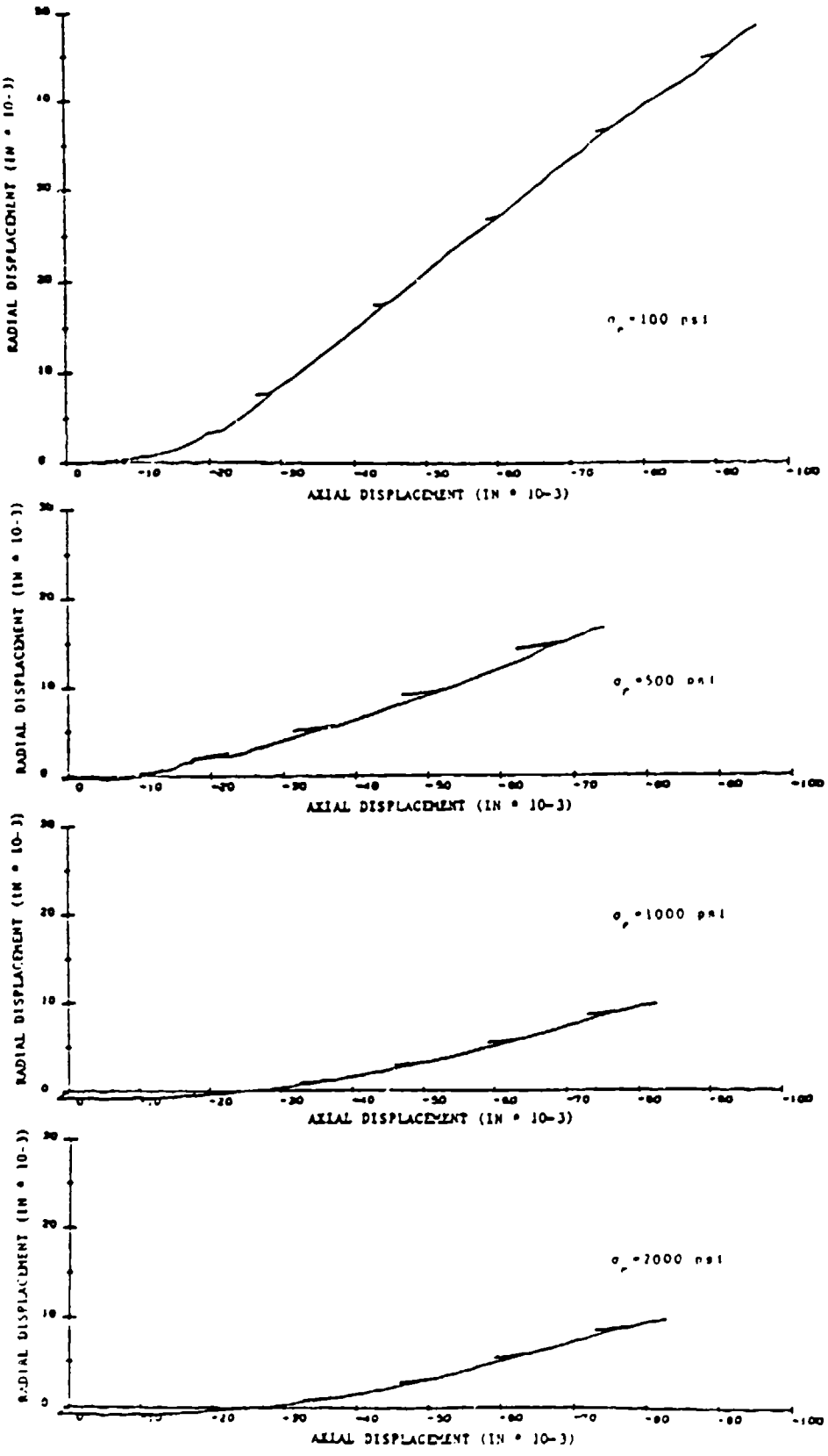

Figure 7 Dilatation Response of Conventional Triaxial Compression Tests with Partial Unloading

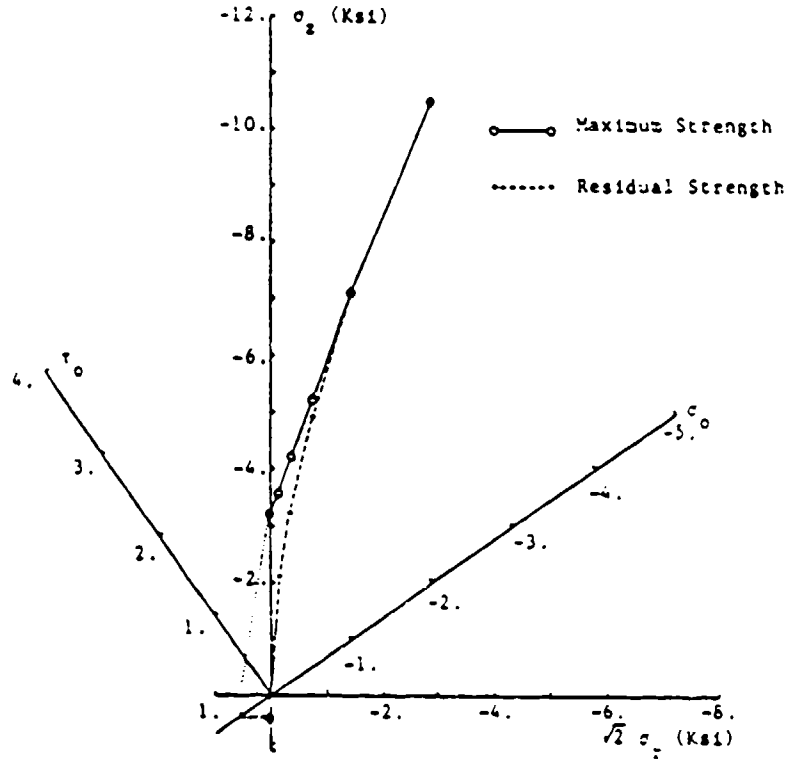

Figure 8 Strength Envelopes in the Rendulic Plane

COMPOSITE FRACTURE MODEL

Up to now the test results were intentionally described in terms of overall load-displacement diagrams because of the strain localization during progressive fracturing in the softening regime. Therefore, we have to ask ourselves whether or not useful information can be extracted from the softening data which is not only generic to the particular test specimen but which can also be used in the analysis of actual structures. In order to clarify the underlying issues let us consider the "simple" configuration of the direct tension experiment. In this case the elementary study of an axial tension specimen yields some surprising results with far-reaching conclusions.

Consider a uniaxial tension specimen of height H and cross-section A with the uniaxial tensile strength σ_t. The incremental stiffness relation follows the elementary axial force-deformation relation

$$\dot{\sigma}_z = \frac{\dot{P}}{A} = \frac{E_T}{H}\,\dot{u}_z \qquad (1)$$

where E_T denotes the tangent modulus, $\dot{\sigma}_z$ the nominal stress rate and $\dot{u}_z$ the axial rate of extension. If we assume a simple bilinear material law with $E_T = E$ for hardening and $E_T = -E$ for softening, uniform degradation of strength without localization will result in the bilinear response depicted in the left plot of Fig. 9 for monotonically increasing extension. Moreover, the total strain energy dissipation for tensile fracture is

$$U_f = \frac{\sigma_t^2}{E} AH \tag{2}$$

which is thus proportional to the height H of the uniaxial tension specimen. This implies that in the limit the energy dissipation would diminish to zero as the height of the specimen were reduced to zero, a fact which has been rightly criticized by Bazant et al. at several occasions [1,2,3]. On the other hand, if we would adopt the notion of a constant fracture energy release rate for the formation of a single crack, then the energy expended for generating a crack of unit area is

$$G_f^I = \frac{dU_f}{dA} = \frac{\sigma_t^2}{E} H \tag{3}$$

which should remain constant irrespective of the size of the specimen. This could be simply accomplished by adjusting the softening slope according to the size of the softening zone, i.e. $E_T = -E/3$ for half the specimen height, in order to maintain a constant fracture energy release rate as indicated in the right plot of Fig. 9.

In order to probe this notion of constant versus variable fracture energies involved, let us compare the two direct tension experiments illustrated in Figs. 2 and 4. Converting the axial load into nominal axial stress, the area under the σ_t-u_f diagram can be readily evaluated, and yields the following average values for the full and the half size NX- specimens:

$$\left.G_f^I\right|_1 = 0.322 \text{ lbf/in} = 56 \text{ N/m} \qquad \text{for} \quad H = 4.25 \text{ in} = 108 \text{ mm}$$

$$\left.G_f^I\right|_{1/2} = 0.354 \text{ lbf/in} = 62 \text{ N/m} \qquad \text{for} \quad H = 2.125 \text{ in} = 54 \text{ mm} \tag{4}$$

The fracture energy release rate slightly increases rather than decreases with decreasing specimen height. Therefore, the direct tension experiments fully support the fracture energy release rate concept. This is not surprising since the specimen ultimately fails in the form of a single localized macrodefect and not in the form of continuous debonding of microdefects which are uniformly distributed over the entire length of the specimen.

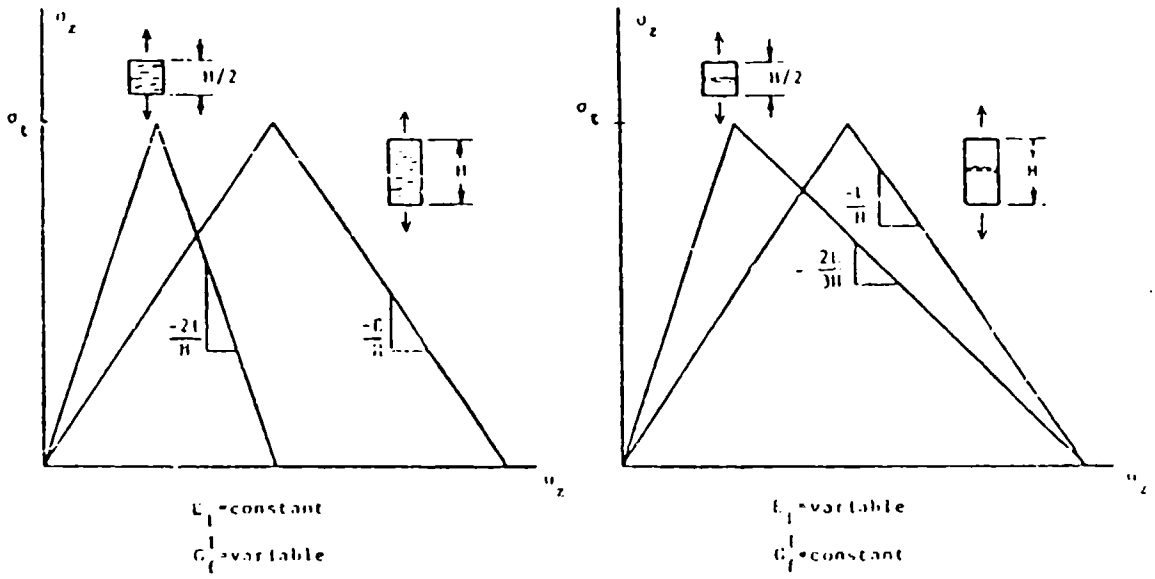

Figure 9 Fracture Energy for Different Specimen Heights

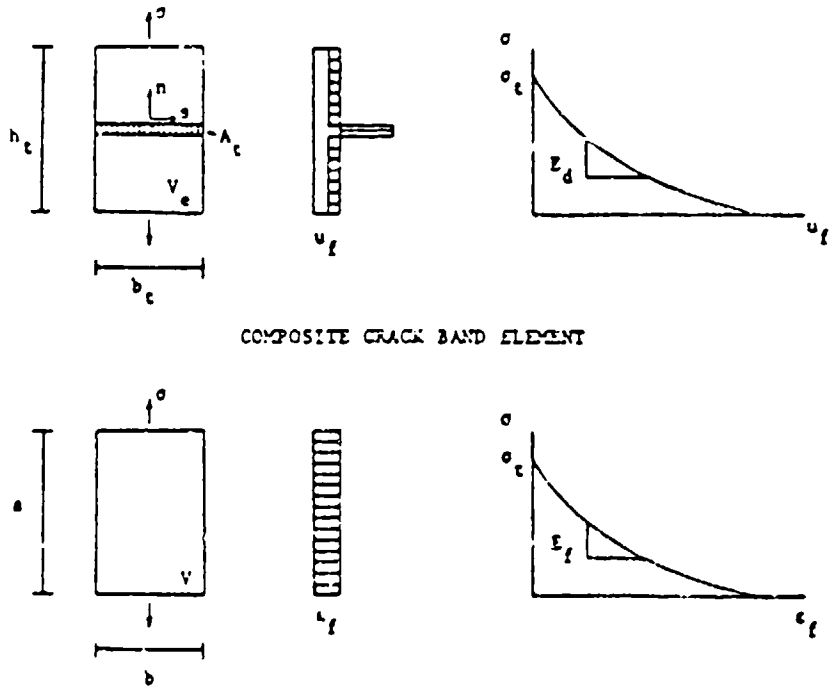

Figure 10 Composite Fracture Model for Tensile Cracking

In the following discussion we will adopt this rationale to develop a strain-softening plasticity model which accounts for the localization of fracture and which monitors constant fracture energy release rates in tension and shear. Conceptually, this approach corresponds to the modification of the softening modulus according to the geometry very much along the line of the elementary example above.

Fracture Based Strain-Softening Model for Tension

The composite fracture formulation is in essence an attempt to incorporate constant fracture energy release rate in the strain-softening formulation of an equivalent elastic-plastic continuum.

For simplicity let us consider the elementary volume V = abt which is subjected to the tensile state of stress depicted in Fig. 10. The maximum stress criterion results in the localized crack band $A_t = b_t t$ which is oriented normal to the direction of major principal stress "n". Incipient cracking is controlled by the initially isotropic fracture condition

$$F(\sigma,k) = \sigma_n - \sigma_t = 0 \qquad \text{where } \sigma_n = \sigma_1 \text{ with } \sigma_1 \geq \sigma_2 \geq \sigma_3 \qquad (5)$$

$$\text{and} \quad \sigma_t = \sigma_t(k)$$

For the first active crack the normal tensile stress coincides with the major principal stress $\sigma_n = \sigma_1$. The tensile strength σ_t describes the degradation of bond stresses across the crack band as a function of the tensile crack opening u_f in analogy to the fictitious crack band model of Hillerborg, Modeer and Peterson [7].

Restricting our attention to Mode I type cracking the fracture potential $Q(\sigma)$ coincides with the fracture condition $F(\sigma,k)$ along the line of an associated flow rule and degenerates in the case of primary crack initiation to the unit vector in three space. The associated fracture rule

$$\dot{\varepsilon}_f = \dot{\lambda}\, m \quad \text{where } m = \frac{\partial Q}{\partial \sigma} = \begin{bmatrix} \frac{\partial Q}{\partial \sigma_1} \\ \frac{\partial Q}{\partial \sigma_2} \\ \frac{\partial Q}{\partial \sigma_3} \end{bmatrix} = \begin{bmatrix} 1 \\ 0 \\ 0 \end{bmatrix} \qquad (6)$$

defines direction and magnitude of the tensile strain-softening response in accordance to the flow rule of traditional plasticity theory. In view of the strain-space setting of the computational algorithm, the consistency condition

$$\dot{F} = \frac{\partial F}{\partial \sigma}^t \mathbb{E}(\dot{\varepsilon} - \dot{\lambda} n) - \left(\frac{\partial F}{\partial k} \frac{\partial k}{\partial \varepsilon_f}\right)^t \dot{\lambda}\, n = 0$$

leads to the tensile fracture parameter $\dot{\lambda}$,

$$\text{where} \quad \dot{\lambda} = \frac{n^t \mathbb{E}\, \dot{\varepsilon}}{E_f + n^t \mathbb{E}\, n} \qquad \text{for } n^t \mathbb{E} \dot{\varepsilon} > 0 \quad \text{Progressive Cracking}$$

$$\text{and} \quad \dot{\lambda} = 0 \qquad \text{for } n^t \mathbb{E} \dot{\varepsilon} \leq 0 \quad \text{Elastic Behavior} \tag{8}$$

where the additive decomposition of strain rate $\dot{\varepsilon} = \dot{\varepsilon}_e + \dot{\varepsilon}_f$ has been inferred and where $\mathbb{E}$ denotes the elastic material law in three space. Let us now consider the hardening or rather the softening modulus E_f which provides the key to incorporate the fracture energy concept within the framework of strain- softening plasticity. Formally, the softening modulus E_f in Eq. 8 is defined by

$$E_f = \left(\frac{\partial \sigma_t}{\partial k} \frac{\partial k}{\partial \varepsilon_f}\right)^t n \tag{9}$$

In order to control the fracture energy release rate via the strain-softening modulus E_f we will pursue the following approach: Consider the invariance of the softening branch for different specimen heights in the σ_t-u_f space and the inherent definition of fracture energy in terms of

$$G_f^I = \int_0^{u_r} \sigma_t \, du_f \tag{10}$$

Then it is only natural to monitor softening directly in terms of the fracture modulus E_d which denotes the slope of σ_t-u_f in Figure 10. The mapping between the crack opening displacement du_f and the equivalent tensile fracture strain $dk = d\varepsilon_f$ leads to the following definition of the fracture energy based strain-softening modulus

$$E_f = \left(\frac{\partial \sigma_t}{\partial u_f} \frac{\partial u_f}{\partial \varepsilon_f} \frac{\partial \varepsilon_f}{\partial \varepsilon_f}\right)^t n \quad \text{where} \quad \dot{\varepsilon}_f = \langle \dot{\varepsilon}_f^t \, \dot{\varepsilon}_f \rangle_+^{1/2} = \sqrt{\langle \dot{\varepsilon}_1 \rangle_f^2 + \langle \dot{\varepsilon}_2 \rangle_f^2 + \langle \dot{\varepsilon}_3 \rangle_f^2} \tag{11}$$

In Eq. 11 the MacCauley brackets extract the tensile components of the fracture strain rate $\dot{\varepsilon}_f$. This provides the key for the homogenization of the localized crack discontinuity over the elementary volume of size $V = abt$. In fact, if we denote by h_t the height of the elementary volume normal to the crack band $A_t = b_t t$, then the projection along the normal vector "n" yields the geometric "gage length" h_t for the evaluation of the softening modulus for cracking in direction "1"

$$E_f = E_d \, h_t \qquad \text{where } E_d = \frac{\partial \sigma_t}{\partial u_f}\,; \; h_t = \frac{\partial u_f}{\partial \varepsilon_f}\,; \quad \left(\frac{\partial \varepsilon_f}{\partial \varepsilon_f}\right)^t n = 1 \tag{12}$$

As a consequence of this definition of the strain-softening modulus E_f the resulting tangential material law

$$\boxed{\dot{\sigma} = \mathbb{E}_T \dot{\epsilon}} \qquad \text{where } \mathbb{E}_T = \mathbb{E} - \frac{\mathbb{E}\, n\, n^t \mathbb{E}}{E_f + n^t \mathbb{E}\, n} \tag{13}$$

will depend on the mesh size through the geometry of the elementary volume similar to non-local continuum theories.

The composite fracture theory is based on the equivalence of the fracture energy in the crackband A_t in the composite element with that of the equivalent continuum element V. This energy equivalence was previously utilized by the authors [19] in order to express the surface dominated fracture process in terms of an equivalent volume dominated failure phenomenon

$$\int_{A_t} \sigma_t du_f dA = \int_V \sigma^t d\epsilon_f dV \tag{14}$$

where the individual terms are defined in Fig. 10. Assuming linear softening to simplify the algebra the tensile energy release for the formation of a single crack band ΔA_t within the composite element is simply

$$\Delta U_t^{CE} = -G_f^I \Delta A_t = \frac{1}{2} \frac{\sigma_t^2}{E_d} b_t t \qquad \text{where} \quad E_d = \frac{d\sigma_t}{du_f} = -\frac{1}{2} \frac{\sigma_t^2}{G_f^I} \tag{15}$$

The energy release characteristic of the equivalent continuum element is defined by the energy dissipated during softening up to rupture

$$\Delta U_t^{EQ} = \frac{1}{2} \frac{\sigma_t^2}{E_f} V = \frac{1}{2} \frac{\sigma_t^2}{E_f} abt \qquad \text{where} \quad E_f = \frac{d\sigma_t}{d\epsilon_f} \tag{16}$$

From the equivalence of the energy release during the formation of the crack band, $\Delta U_t^{CE} = \Delta U_t^{EQ}$, the governing strain-softening modulus E_f in the homogenized continuum can be expressed in terms of the fracture modulus E_d or the equivalent fracture energy release rate G_f^I

$$E_f = E_d \frac{V}{A_t} = -\frac{\sigma_t^2}{2G_f^I} \frac{V}{A_t} \tag{17}$$

In the case of uniaxial tension in the axial direction the geometric properties of the crack band are readily expressed in terms of those of the elementary volume, i.e. $A_t = b_t t$ and $h_t = a$, thus

$$E_f = E_d h_t \quad \text{where } h_t = \frac{V}{A_t} \tag{18}$$

We observe that this expression is identical with the definition of the strain-softening modulus E_f developed previously in Eq. 12. This

result clearly demonstrates that strain-softening in the equivalent continuum element depends on the geometry of the elementary volume and thus exhibits a pronounced size effect. In other words, the fracture modulus E_f has to be adjusted to the mesh size of the particular finite element idealization if the fracture energy release rate G_f^I should remain constant. As a result the fracture mechanics concept leads to a non-local format of the governing softening properties which is fundamentally different from the local (geometry independent) format of strain-softening plasticity and progressive fracture theories.

In conclusion let us consider the particular concrete tested in the direct tension experiment. For linear softening the fracture modulus is readily evaluated from the nominal uniaxial tensile strength σ_t = 400 psi (2.76 MPa) and the fracture energy release rate for Mode I type cracking, G_f^I = 0.322 lb/in. (56 N/m).

$$E_d = \frac{d\sigma_t}{du_f} = -\frac{\sigma_t^2}{2G_f^I} = -248.45 \ \frac{kip}{in^3} = -67.44 \ \frac{N}{mm^3} \qquad (19)$$

The characteristic crack length which defines the range of debonding within an elastic perfectly brittle comparison solid is in this case

$$\ell_t = \frac{G_f^I E}{\sigma_t^2} = 5.63 \text{ in} = 143 \text{ mm} \quad \text{where } E = 2800 \text{ ksi} = 19305 \text{ MPa}. \qquad (20)$$

Since the characteristic length is larger than the specimen height, linear elastic fracture mechanics does hardly apply. Along the same vein, previous suggestions by Bazant et al [1] of three times the aggregate size for the width of the crack band are also open to question.

The numerical stability of strain-softening computations imposes definite restrictions on the localization of fracture within a given finite element mesh which were recently discussed by the authors [20]. We recall that the softening formulation infers unstable material behavior with a corresponding energy release. As long as these material instabilities are localized and contained within the overall structure, stability in the large can be monitored by displacement control since the structural stiffness remains positive definite. On the other hand, since stability in the small is violated by the loss of positive definiteness of the tangent material law E_T in Eq. 13, we can examine the limiting condition when $E_T \to -\infty$, which corresponds to perfectly brittle behavior. In the case of tensile softening this takes place when the denominator in the fracture correction of the elastic material stiffness vanishes, i.e. when the following condition holds

$$E_f + n^t E n = 0 \qquad (21)$$

Let us consider for definiteness the case of plane strain and the normality vector n in Eq. 6. Then the limiting condition for the softening modulus reduces to

$$- E_f \leq E \frac{1-\nu}{(1+\nu)(1-2\nu)} \qquad \text{where } E_f = E_d \, h_t \tag{22}$$

In other words the mesh size "h" must be such that the following constitutive constraint is satisfied

$$- h \leq \frac{E}{E_d} \frac{1-\nu}{(1+\nu)(1-2\nu)} \tag{23}$$

For the concrete properties above and $\nu = 0.2$ this constraint results in the maximum height of the elementary volume

$$h \leq \frac{2800}{248.45} \frac{0.8}{1.2 * 0.6} = 12.52 \text{ in} = 318.06 \text{ mm} \tag{24}$$

for which stable post-critical strain control may be maintained. We observe that this mesh size constraint is quite restrictive if large scale massive concrete structures such as dams or pressure vessels are considered. It is a direct consequence of the fracture energy basis of the equivalent strain-softening model which increases the ductility with decreasing mesh size and, vice versa, increases the brittleness with increasing mesh sizes.

Strain-Softening Regime and Transition of Brittle-Ductile Failure

In the following let us probe whether the concept of a composite fracture model for Mode I type tensile cracking could be extended to the Mode II type shear fracture in order to capture the pronounced softening response in low confined compression. In the previous approach Day [4] and the authors [19] utilized the Mohr-Coulomb condition as point of departure augmented by an independent tension cut-off. In that case tensile debonding was controlled by the fracture energy release rate G_f^I for Mode I type cracking similar to the strain-softening formulation for crack bands delineated above. On the other hand, decohesion due to frictional slip was monitored by the fracture energy release rate G_f^{II} for Mode II type fracture governing the formation of shear bands. Because of the tenfold increase of uniaxial compressive versus tensile strength, the value of G_f^{II} was approximately 50 times larger than G_f^I when faulting along a single shear plane was considered along the line of the Mohr-Coulomb failure hypothesis. At this stage it was noted that mixed mode shear fracture is actually initiated by tensile splitting and the formation of a single shear band is thus the result of coalescing crack feathers along an inclined slip plane. Therefore, the postulate of an independent faulting mechanism is really the consequence of the limited resolution of current tools to trace each individual tensile crack preceding the formation of a single shear band.

Since tensile cracking and shear faulting are clearly interrelated we resort here to a continuous failure condition which comprises both tensile as well as shear fracture within a single criterion according to Hoek and Brown [8]. This empirical criterion was originally developed to characterize the triaxial strength of rock specimens which were failed in the conventional triaxial compression experiment. The three parameter failure model neglects the influence of the intermediate principal stress and can be viewed as a combination of the Mohr-Coulomb criterion with the tension cut-off condition very much along the line of the parabolic failure envelope originally proposed in 1933 by Leon for concrete [16].

$$F(\sigma, k) = \sigma_1 - \sigma_3 - (c\sigma_c^2 - m\sigma_c\sigma_1)^{1/2} = 0 \qquad (25)$$

σ_c denotes the uniaxial compressive strength and m and c define the frictional and cohesive strength material parameters to be calibrated from the uniaxial tension experiment and a third condition when "cohesive" damage is considered with $c<1$. Neglecting hardening behavior before the peak strength is reached the uniaxial compression experiment yields with $\sigma_1 = 0$ and $c = 1$

$$-\sigma_3 = (c\,\sigma_c^2)^{1/2} \qquad \text{where } \sigma_c = f_c' = 3.2 \text{ ksi} = 22.06 \text{ MPa} \qquad (26)$$

Thus under uniaxial compression $\sigma_3 = -3.2$ ksi as long as intact cohesive behavior prevails with $c = 1$. The uniaxial tension experiment on the other hand leads to calibration of m via solution of the quadratic equation Eq. 25 with $\sigma_1 = \sigma_t$ and $\sigma_3 = 0$

$$m = \frac{c\sigma_c^2 - \sigma_t^2}{\sigma_c\sigma_t} \qquad \text{where } \sigma_t = f_t' = 0.4 \text{ ksi} = 2.76 \text{ MPa} \qquad (27)$$

This condition yields $m = 7.9$ for the frictional strength parameter at peak strength. Fig. 11 illustrates the fit of the failure envelope with the experimental strength values in terms of the Mohr diagram depicting the normalized shear strength versus effective normal stress, τ_n-σ_n.

Let us now examine whether the triaxial strength envelope could be used to describe softening behavior in tension and shear, whereby both the uniaxial tensile strength and the uniaxial compressive strength diminish to zero in the post-peak regime. Fig. 12 delimits the strain-softening regime in terms of the maximum strength and the residual strength envelopes which coalesce at the transition point P of brittle-ductile failure. The direction of inelastic fracture strain rates has been superimposed on a separate diagram in order to illustrate normality and feasible formats of the corresponding plastic potential.

If we rewrite the failure condition Eq. 25 then strain-hardening/softening can be accommodated by the variation of the two parameters m and c.

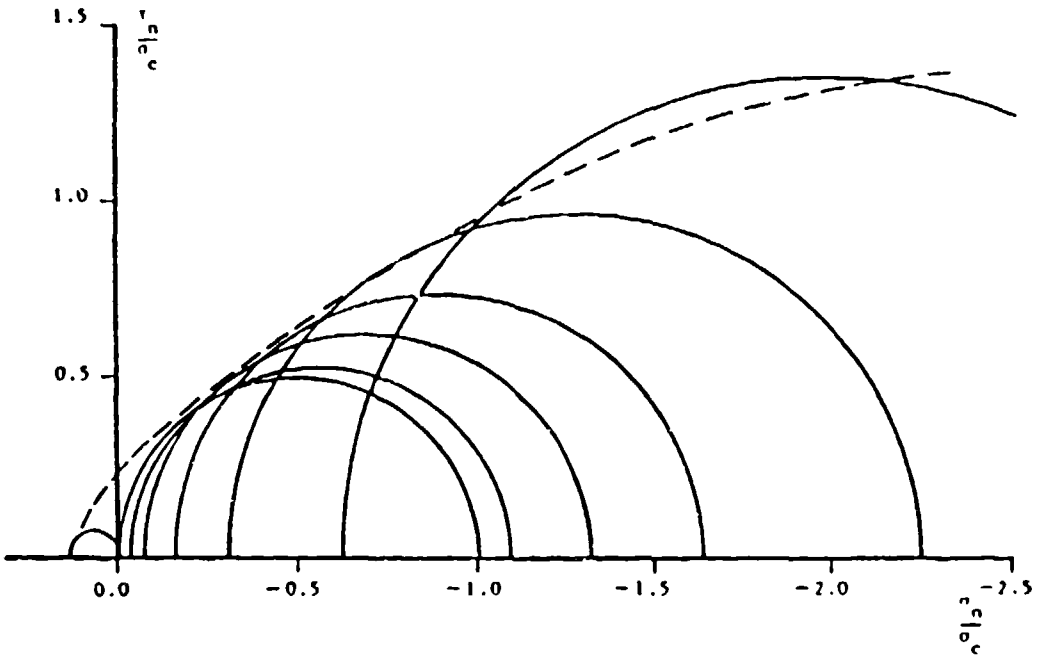

Figure 11 Mohr's Diagram of Triaxial Strength Data

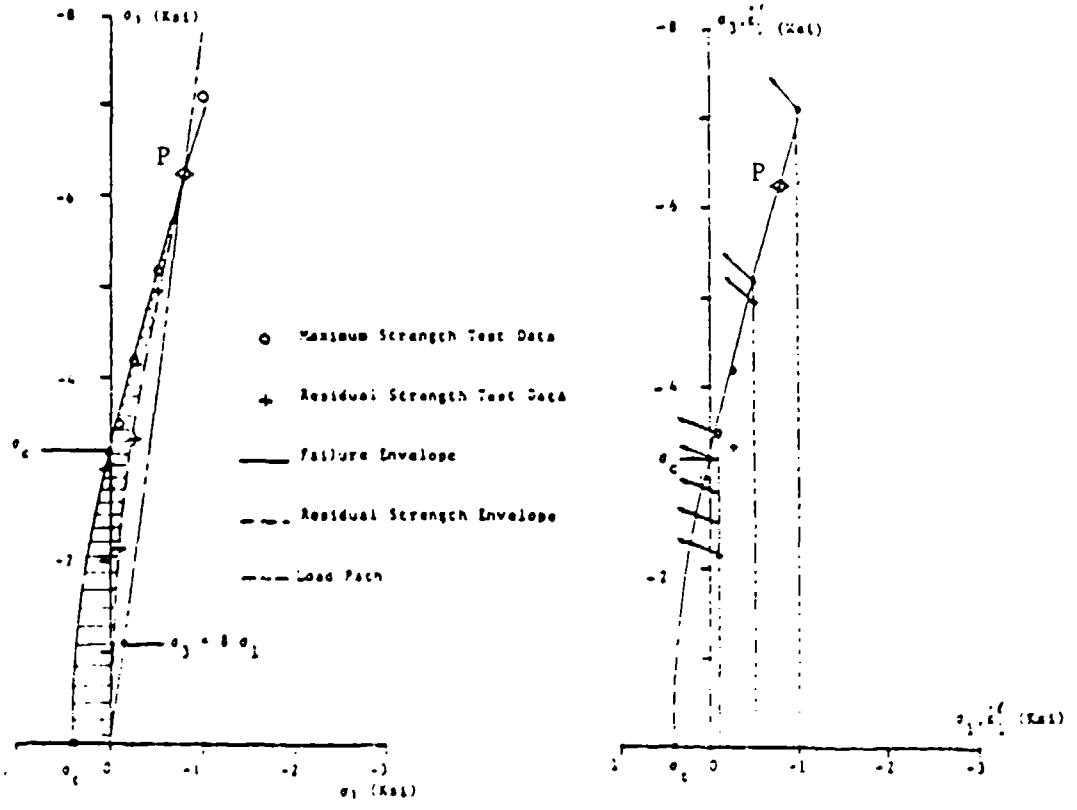

Figure 12 Brittle-Ductile Transition Point and Inelastic Dilatancy

$$F(\sigma,k) = \tau - (c - m\sigma)^{1/2} = 0 \qquad \text{where } \tau = \left|\sigma_1-\sigma_3\right|/\sigma_c \text{ and } \sigma = \sigma_1/\sigma_c \qquad (28)$$

$$\text{with} \quad m_o = 7.9 \text{ and } c_o = 1$$

We recognize that $m = m(k)$ describes the variation of the frictional and $c = c(k)$ that of the cohesive resistance. A possible interpretation considered previously in [4] assumes that softening is a purely decohesive mechanism where $c(k) \to 0$. This corresponds to a vertical shift of the failure surface to pass ultimately through the origin. This would however imply that the triaxial strength under high confinement would also degrade while Fig. 6 clearly demonstrates that the opposite is true. In fact Fig. 8 illustrates that there is a clear transition from brittle to ductile fracture between $-0.5 \leq \sigma_r \leq -1.0$ ksi (-3.45 to -6.89 MPa) confining stress beyond which continuous plastic flow and increasing hardening tendencies prevail. Therefore, decohesion should be accompanied by simultaneous frictional hardening as proposed by Vermeer and de Borst [18] such that the two mechanisms compensate each other at the brittle-ductile transition point P.

It has been noted previously by Mazars [12] and others that fracture is really induced by tensile strain rather than stress. Thus the location of the transition point P should roughly correspond to a vanishing elastic tensile strain in the radial direction if the cylindrical specimen is considered

$$\varepsilon_r^e = \frac{1}{E}\left(\sigma_r - \nu\left(\sigma_\theta + \sigma_z\right)\right) \qquad (29)$$

This yields the following condition for $\varepsilon_r^e = 0$ and $\sigma_r = \sigma_\theta$:

$$\sigma_r = \frac{\nu}{1-\nu}\sigma_z \text{ and} \quad \sigma_3 = 8\ \sigma_1 \quad \text{for } \nu = 0.111 \qquad (30)$$

The tensile strain condition plots in Fig. 12 as a straight line through the origin. For a Poisson's ratio of $\nu = 0.2$ the tensile strain cut-off corresponding to $\sigma_3 = 4\sigma_1$ does hardly intersect the maximum strength envelope. However, the value $\nu = 0.111$ corresponds to the maximum strain criterion with $\sigma_3 = -\sigma_c + 8\sigma_1$ where the ratio of the uniaxial compressive to uniaxial tensile strength $\sigma_c/\sigma_t = 8$ coincides with the biaxial Griffith criterion, see e.g. [16]. In this case the zero tensile strain condition in Eq. 30 does intersect the maximum strength envelope very near the experimental transition point P for brittle and ductile fracture which separates softening from hardening response regimes. Therefore we could regard the tensile cap beyond the residual strength envelope as a transient strength regime which ultimately collapses to the residual strength level upon continuous tensile straining. In fact the trace of the residual strength envelope is captured fairly well by the following modification of Eq. 28 for purely frictional resistance

$$F_r(\sigma,k) = \tau - (-m_r\sigma)^{1/2} = 0 \qquad \text{where } m_r = 11.96 \text{ and } c_r = 0 \qquad (31)$$

From the directions of the inelastic strain rates in Fig. 12 we observe that the trace of the maximum strength envelope furnishes an acceptable format for the inelastic potential $Q(\sigma)$ to be used as fracture rule for strain-softening under mixed mode fracture processes.

Fracture Based Strain-Softening Model for Mixed Mode Fracture

Considering the strain softening formulation for Mode I type fracture in the previous section, let us examine the pertinent generalization to mixed mode fracture along the line of the combined softening model for tension and shear.

Starting from the maximum strength condition Eq. 28 we recognize that decohesion is accompanied by frictional hardening. During failure the fracture rule defines the direction and magnitude of inelastic fracture strains in the homogenized continuum.

$$\dot{\varepsilon}_f = \dot{\lambda}_f \, n \qquad \text{where} \qquad n = \frac{\partial Q}{\partial \sigma} \tag{32}$$

From Fig. 12 we recognize that the direction of inelastic strain rate is fairly well defined by normality to maximum strength envelope. Therefore, the fracture potential is in this case described by Eq. 28 with $m = m_o$ and $c = c_o$

$$Q(\sigma) = \tau - (c_o - m_o \sigma)^{1/2} = 0 \qquad \text{where } m_o = 7.9 \quad \text{and} \quad c_o = 1 \tag{33}$$

The gradient of the fracture potential defines the direction and thus the inelastic dilatation in principal stress space

$$n = \frac{\partial Q}{\partial \sigma} = \begin{bmatrix} \frac{\partial Q}{\partial \sigma_1} \\ \frac{\partial Q}{\partial \sigma_2} \\ \frac{\partial Q}{\partial \sigma_3} \end{bmatrix} = \frac{1}{\sigma_c} \begin{bmatrix} 1 + \frac{1}{2} \frac{m_o}{(c^* - m_o \sigma)^{1/2}} \\ 0 \\ -1 \end{bmatrix} \tag{34}$$

Similar to the Mohr-Coulomb condition there is no inelastic component in the direction of intermediate principal stress. We also note that the fracture component in the minor direction does not depend on the frictional resistance m because the normal stress σ in Eq. 28 is defined only in terms of the major principal stress σ_1 and not in terms of the average value of the major and minor normal stress used in the Mohr-Coulomb condition. For computational reasons the fictitious cohesion $c^* = \tau^2 + m_o \sigma$ has been introduced in order to accommodate

"elastic" trial stress states beyond the failure condition which are restricted to major principal stress values $\sigma_1 < c_o\sigma_c/m_o$.

The fracture parameter $\dot{\lambda}_f$ determines the magnitude of inelastic straining during mixed mode fracture. With the aid of the consistency condition $\dot{F} = 0$ the fracture parameter $\dot{\lambda}_f$ reads in the case of a non-associated flow rule where $F \neq Q$

$$\dot{\lambda}_f = \frac{\mathbf{m}^t \mathbb{E}\, \dot{\boldsymbol{\varepsilon}}}{F_f + \mathbf{m}^t \mathbb{E}\, \mathbf{n}} \qquad \text{for } \mathbf{m}^t \mathbb{E}\, \dot{\boldsymbol{\varepsilon}} > 0$$

$$\dot{\lambda}_f = 0 \qquad \text{for } \mathbf{m}^t \mathbb{E} \dot{\boldsymbol{\varepsilon}} \leq 0 \tag{35}$$

In this case the vectors $\mathbf{m}$ and $\mathbf{n}$ denote the gradients of the current loading surface $F(\sigma,k)$ and the fracture potential $Q(\sigma)$, the latter of which was previously developed in terms of principal stresses. In analogy to Eq. 34 we find with $c^* = \tau^2 + m\sigma$

$$\mathbf{m} = \frac{\partial F}{\partial \boldsymbol{\sigma}} = \begin{bmatrix} \frac{\partial F}{\partial \sigma_1} \\ \frac{\partial F}{\partial \sigma_2} \\ \frac{\partial F}{\partial \sigma_3} \end{bmatrix} = \frac{1}{\sigma_c} \begin{bmatrix} 1 + \frac{1}{2} \frac{m}{(c^* - m\sigma)^{1/2}} \\ 0 \\ -1 \end{bmatrix} \tag{36}$$

The principal issue of the non-associated softening formulation revolves around the proper definition of E_f. Formally we obtain from the consistency condition $F = 0$ the following expression for the instantaneous strain-softening modulus

$$E_f = -\left(\frac{\partial F}{\partial k} \frac{\partial k}{\partial \varepsilon_f}\right)^t \frac{\partial Q}{\partial \boldsymbol{\sigma}} \quad \text{where } k = k(\varepsilon_f) \tag{37}$$

We recall that decohesion is accompanied by frictional hardening both of which are mobilized by tensile straining during compressive splitting in the brittle failure regime. Therefore it is natural to adopt again the definition of equivalent tensile fracture strain $\dot{\varepsilon}_f$ in Eq. 11 which played the role of the kinematic damage metric of the homogenized continuum subjected to tensile cracking.

$$dk = d\varepsilon_f \text{ where } \dot{\varepsilon}_f = \langle \dot{\boldsymbol{\varepsilon}}_f^t \dot{\boldsymbol{\varepsilon}}_f \rangle_+^{1/2} = \sqrt{\langle \dot{\varepsilon}_1 \rangle_f^2 + \langle \dot{\varepsilon}_2 \rangle_f^2 + \langle \dot{\varepsilon}_3 \rangle_f^2} \tag{38}$$

We note that the MacCauley brackets only extract the positive, i.e. the tensile fracture strain rates from the inelastic strain rate tensor $\dot{\boldsymbol{\varepsilon}}_f$.

In case of compressive splitting the chain rule of differentiation leads to the following definition of the strain-softening modulus in terms of the tensile fracture behavior

$$E_f = - \frac{\partial F}{\partial c} \frac{\partial c}{\partial \sigma_t} \frac{\partial \sigma_t}{\partial u_f} \frac{\partial u_f}{\partial \varepsilon_f} \left(\frac{\partial \varepsilon_f}{\partial \epsilon_f}\right)^t \frac{\partial Q}{\partial \sigma} \tag{39}$$

Recollecting that tensile splitting in compression as well as shear faulting is preceded by distributed microcracking and that the actual crack surface is in this case a multiple of that in the direct tension experiment, we resort to the fundamental definition of Mode I type cracking. For the current concrete this fracture property is characterized by $G_f^I = 0.322$ lbf/in. (56 N/m) which corresponds to the area under the tensile softening law in Fig. 13.

The individual terms in Eq. 39 are defined as follows

$$\frac{\partial F}{\partial c} = \frac{-1}{2(c - m\sigma)^{1/2}} \qquad \text{with } dm = -4.06\ dc \tag{40}$$

The interdependence between the cohesive strength parameter and the tensile strength results in our case to

$$\frac{\partial c}{\partial \sigma_t} = 2.5 \qquad \text{where } \sigma_t = 0.4 \text{ ksi} = 2.76 \text{ MPa} \tag{41}$$

The relationship between the degrading tensile strength σ_t and the crack opening displacement u_f was previously characterized by the fracture modulus of the uniaxial tension experiment, see Fig. 10.

$$E_d = \frac{d\sigma_t}{du_f} = \frac{d^2 G_f^I}{du_f^2} \tag{42}$$

An exponential fit of the normalized test data is shown in Fig. 13 which leads to the following decaying softening function

$$E_d = -\sigma_t \left(\frac{5}{u_r}\right) e^{-5 \frac{u_f}{u_r}} \tag{43}$$

where σ_t denotes the uniaxial tensile strength and u_r the crack opening displacement at rupture when the interfacial bond stresses have diminished to zero (in our case $u_r = 0.002$ in. = 0.05 mm, from Fig. 2).

It remains to relate the crack opening displacement u_f to the tensile fracture strain ε_f of the equivalent continuum. In Fig. 7 we have seen that the lateral extension is over ten times larger than the axial extension in the direct tension experiment shown in Fig. 2. This

should be of no surprise since the splitting compression mode of failure is far more distributed which is in turn responsible for the eight to tenfold increase of the uniaxial compressive over the tensile strength values.

A fracture energy argument similar to that developed for tensile cracking leads the following relationship between the crack opening displacement and the equivalent tensile fracture strain in compression

$$\frac{du_f}{d\varepsilon_f} = \frac{V}{A_c} \approx h_c \tag{44}$$

where the volume fraction A_c/V represents the microcrack density in compression. We observe that Eq. 44 plays the fundamental role of the geometric "gage length" and has the simple physical interpretation of the crack spacing h_c in the case of splitting compression. From the global observations it may be evaluated approximately in terms of the ratio between the fracture energy release rate in tension G_f^I and that in shear G_f^{II}. Thereby it is understood that the second quantity by itself is already the result of homogenizing distributed tensile cracks into a single shear band with the surface area A_s which has the same order of magnitude as the crack surface in direction tension, i.e. $A_t \approx A_s$. From the equivalence of fracture energy

$$G_f^I \, \Delta A_c = G_f^{II} \, \Delta A_t \tag{45}$$

we can find the unknown fracture surface under splitting compression from

$$\Delta A_c = \frac{G_f^{II}}{G_f^I} \Delta A_t \tag{46}$$

This yields in the case of the uniaxial compression test with $G_f^{II} = 27.2$ lbf/in (4763 N/m) the following measure of longitudinal crack spacing

$$h_c \approx \frac{V}{A_c} = \frac{G_f^I}{G_f^{II}} \frac{V}{A_t} = 0.05 \text{ in} = 1.28 \text{ mm} \tag{47}$$

which should be compared with the characteristic length $\ell_t = 5.63$ in. (143 mm) in the case of Mode I type cracking. The ratio G_f^{II}/G_f^I represents the magnification of tensile crack surface when compared with that of direct tension test. This ratio increases with increasing confining pressure in order to simulate the diffuse damage mechanism around and beyond the brittle-ductile transition point. Using the experimental data described earlier, a first order approximation yields the following expression for the fracture energy ratio as a function of the minor principal stress σ_3

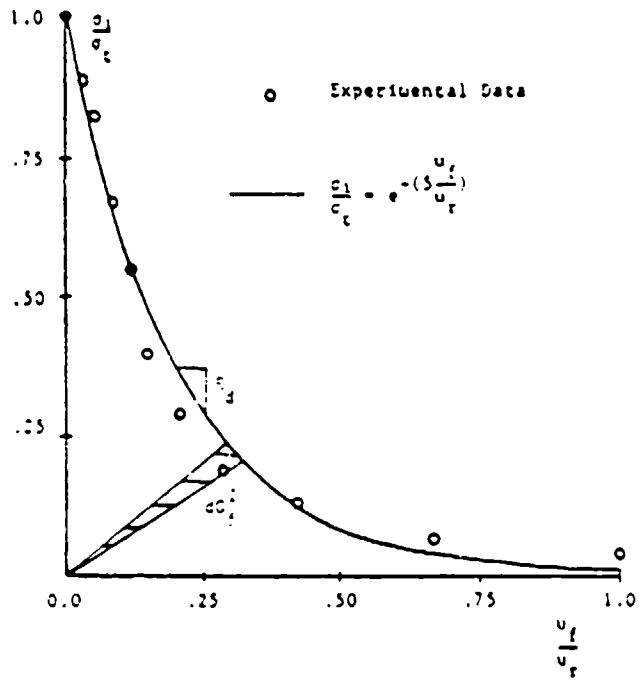

Figure 13 Experimental Softening Model

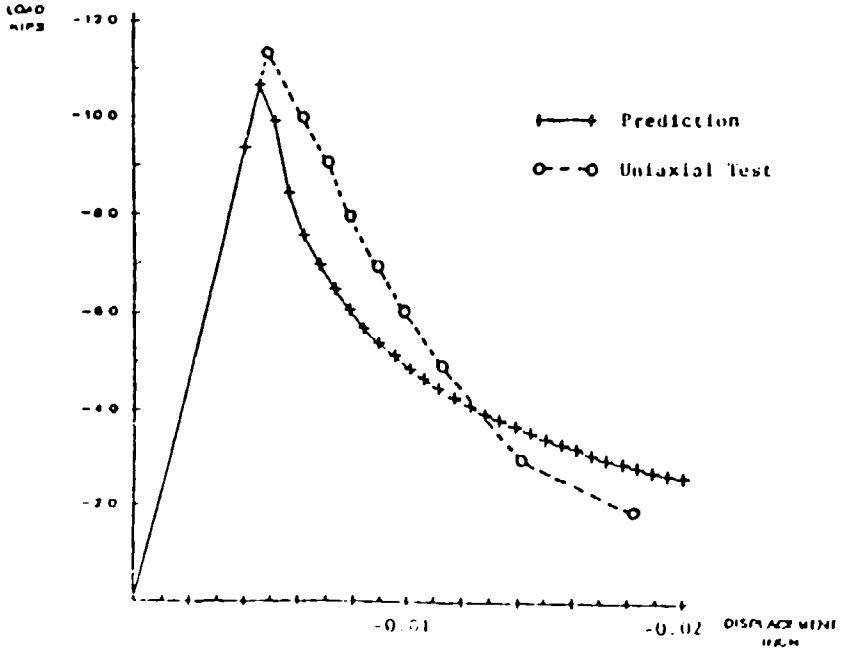

Figure 14 Softening Response in Uniaxial Compression

$$\frac{G_f^{II}}{G_f^I} = 1.0 - 84 \left(\frac{\langle \sigma_3 \rangle_-}{f'_c} \right)^5 \qquad (48)$$

This ratio reduces to one in the case of triaxial tension when $\langle \sigma_3 \rangle_- = 0$. It increases rapidly with increasing confinement $\sigma_3 < 0$ and reduces the strain-softening modulus to $E_f \to 0$ as $h_c \to 0$ which corresponds to perfectly plastic behavior when $\sigma_3 \ll 0$.

In conclusion let us summarize the tangential material law for frictional hardening and non-associated decohesion

$$\boxed{\dot{\sigma} = \mathbb{E}_T \, \dot{\varepsilon}} \quad \text{where} \quad \mathbb{E}_T = \mathbb{E} - \frac{\mathbb{E}\, n\, m^t\, \mathbb{E}}{E_f + m^t \mathbb{E}\, n} \qquad (49)$$

$$\text{and} \quad E_f = \frac{2.5}{2(c - m\sigma)^{1/2}} E_d \frac{V}{A_c} \frac{\partial \varepsilon_f}{\partial \varepsilon_f}^t \frac{\partial Q}{\partial \sigma}$$

The strain-softening formulation above is based on the fracture energy release rate G_f^I and the concomitant exponential decay function for E_d using energy equivalence concepts to homogenize the underlying failure phenomena. Fig. 14 illustrates the performance of the fracture energy based strain-softening plasticity model when the post-peak response of the uniaxial compression test is considered. In this case only the exponential softening law for tensile cracking in Fig. 13 was utilized, in order to predict the softening response under compression.

CONCLUDING REMARKS

A strain-softening elastic-plastic formulation has been presented for the description of the fracture mechanisms in concrete which range from brittle Mode I type cracking in tension to ductile mixed mode fracture in compression. The composite fracture theory is based on the fracture energy content of the homogenized continuum which is subjected to equivalent strain softening mechanisms in tension and shear.

We conclude that the combined mechanism of cohesive softening and frictional hardening covers the entire failure spectrum of concrete which is monitored solely by the fracture modulus E_d of the underlying Mode I type cracking. We note that an overall constitutive formulation for triaxial concrete behavior should include a hardening cap in compression in addition to the tensile strain-softening mechanism for brittle failure in tension and shear.

ACKNOWLEDGEMENT

This investigation was supported by the U.S. Air Force Office of Scientific Research Contract AFOSR 82-0273 with the University of Colorado, Boulder under liaison of Lt. Col. Lawrence Hokanson, which is gratefully acknowledged.

APPENDIX I - REFERENCES

[1] Bažant, Z.P. and Cedolin, L., "Blunt Crack Band Propagation in Finite Element Analysis," Trans. American Society of Civil Engineers, EMD Vol. 105, No. EM2 (1979), pp. 297-315.

[2] Bažant, Z.P. and Belytschko, T.B., "Continuum Theory for Strain-Softening," Trans. American Society of Civil Engineers, EMD Vol. 110, No. 12 (1984), pp. 1666-1692.

[3] Belytschko, T. and Bažant, Z., "Strain-Softening Materials and Finite Element Solutions," ASME/WAM'84, New Orleans, Symposium on Constitutive Equations, Macro and Computational Aspects, ASME Vol. G00274, (K. Willam, ed.), New York (1984), pp. 253-277.

[4] Day, S.E., "A Softening Plasticity Model for Concrete," M.S. Thesis, CEAE Department, University of Colorado, Boulder, Colorado, 1985.

[5] Dougill, J.W., "On Stable Progressively Fracturing Solids," J. Appl. Math. Physics, ZAMP, Vol. 27 (1976), pp. 423-436.

[6] Gopalaratnam, V.S. and Shah, S.P., "Softening Response of Concrete in Direct Tension," Technological Institute, Report, Northwestern University, Evanston, 1984.

[7] Hillerborg, A., Modéer, H. and Petersson, P.E., "Analysis of Crack Formation and Crack Growth in Concrete by Means of Fracture Mechanics and Finite Elements," Cement and Concrete Research, Vol. 6 (1976), pp. 773-781.

[8] Hoek, E. and Brown, E.T., "Underground Excavation in Rock," The Institution of Mining and Metallurgy, London, 1980.

[9] Hurlbut, B., "Experimental and Computational Investigation of Strain-Softening in Concrete," M.S. Thesis, CEAE Department, University of Colorado, Boulder, Colorado, 1985.

[10] Janson, J. and Hult, J., "Fracture Mechanics and Damage Mechanics, a Combined Approach," J. de Mechanique Appliquee, Vol. 1 (1977), pp. 69-84.

[11] Krajinovic, D. and Fonseka, G.U., "The Continuous Damage Theory of Brittle Materials, - Part I: General Theory," ASME J. Appl. Mech. Vol. 48 (1981), pp. 809-815.

[12] Mazars, J., "Application de la Mecanique de l'Endommagement au Comportment Non Lineaire et a la Rupture du Beton de Structure," Ph.D. Dissertation, Université Pierre et Marie Curie, Paris, 1984.

[13] van Mier, J.G.M., "Strain-Softening of Concrete under Multiaxial Loading Conditions," Ph.D. Dissertation, University of Technology, Eindhoven, 1984.

[14] Ortiz, M., "A Constitutive Theory for the Inelastic Behavior of Concrete," Division of Engineering Research Report, Brown University, Providence, Rhode Island, 1984.

[15] Reinhardt, H.W., "Fracture Mechanics of an Elastic Softening Material like Concrete," Heron Publ. Vol. 29, No. 2, Delft, 1984.

[16] Romano, M., "On Leon's Criterion", Meccanica (1969), pp. 48-66.

[17] Stankowski, T. and Gerstle, K.H., "Simple Formulation of Concrete Behavior Under Multiaxial Load Histories," J. ACI. Vol. 82, No. 2, 1985, pp. 213 - 221.

[18] Vermeer, P.A. and De Borst, R., "Non-Associated Plasticity for Soils, Concrete and Rock," Heron Publ. Vol. 29, No. 3, Delft, 1984.

[19] Willam, K.J., Bićanić, N., and Sture, S., "Constitutive and Computational Aspects of Strain-Softening and Localization in Solids," ASME/WAM '84 Meeting, New Orleans, Symposium on Constitutive Equations, Macro and Computational Aspects, ASME Vol. G00274, (K. Willam ed.), New York (1984), pp. 233-252.

[20] Willam, K., Pramono, E. and Sture, S., "Stability and Uniqueness of Strain-Softening Computations", Europe-U.S. Symposium on Finite Element Methods for Nonlinear Problems, NIT Trondheim, Norway, Aug. 12-16, 1985. Structures Research Series 8503, University of Colorado, Boulder, Colorado, 1985.

APPENDIX C

APPENDIX C

"Stability and Uniqueness of Strain-Softening Comutations"

by

Kaspar Willam, Eddy Pramono and Stein Sture

Paper presented at the Europe-US Symposium on

Finite Element Methods for Nonlinear Problems

NIT Trondheim, Norway, Aug. 12-16, 1985;

will be published in Conference Proceedings

by Springer Verlag, Berlin Heidelberg (1986)

STABILITY AND UNIQUENESS OF STRAIN-SOFTENING COMPUTATIONS

K.J. WILLAM, E. PRAMONO AND S. STURE

Department of Civil, Environmental and
Architectural Engineering
University of Colorado at Boulder, USA

Summary

The paper addresses computational issues of strain-softening calculations in solids. The main focus is directed towards the numerical simulation of the localization of softening within structural components with simultaneous unloading of the elastic neighborhood. The spatial aspect of the localization process requires special provisions of the incremental/iterative solution strategy in order to survive on one hand local material instabilities and capture on the other hand bifurcation of the solution path within load increments which are truly finite. The performance of several solution algorithms will be assessed with two simple model problems which illustrate the strong interaction between the numerical integration of strain-softening constitutive relations and the spatial localization of contained softening within elastic unloading zones.

Introduction

Strain-softening computations encounter puzzling phenomena during the numerical simulation of distributed damage and localized fracture which transcend previous experience with the inelastic analysis of "stable" materials. In fact these numerical difficulties are exacerbated by the loss of "normality" and the dominance of shear dilatancy under mixed mode fracture which results in predominant straining orthogonal to the loading direction. On one side the failure analysis of brittle solids and structures is very susceptible to the formulation of strain-softening constitutive relations which are equivalent in the sense of strength, stiffness as well as fracture energy to the actual discontinuous failure process. On the other side, the numerical implementation of strain-softening models is far from successful if accepted and conventional numerical tools for strain-hardening plasticity are simply extended into the softening regime. In fact it is the localization phenomenon which leads to simultaneous loading and unloading in adjacent elements which has to be monitored properly. Therefore many numerical algorithms which perform very well in the case of weak continuous nonlinearities are not successful at all when a hard discontinuity takes place within a contiguous material in a finite load interval which draws the demarcation between the localized strain-softening regime and the elastically unloading surrounding.

The intent of this paper is to clarify the computational issues of strain-softening calculations. To this end the composite fracture model for strain-softening will be reviewed together with local and global uniqueness conditions for non-associated hardening/softening solids in order to delineate guidelines for successful strain-softening computations. Subsequently three incremental/iterative solution methods will be scrutinized with regard to their ability to capture strain localization. Two simple model problems will be adopted in order to illustrate the respective performance of initial load and tangential stiffness methods when applied to strain-softening elastic-plastic computations. In conclusion the constant arc length method will be examined for stabilizing the post-critical response calculations beyond the range of direct displacement control.

Composite Fracture Model for Strain-Softening

Strain-softening or rather the degradation of strength is normally attributed to the change of internal microstructure of the material. Two philosophies have recently emerged for the interpretation of the post-critical response regimes of stroke-controlled experiments.

(i) The progressive fracture [1] and continuous damage theories [2] start from the notion of distributed microdefects which coalesce continuously during progressive failure. The simultaneous decrease of strength and stiffness essentially results in a secant-type material formulation where no permanent deformations accompany the failure process during loading-unloading cycles. This concept corresponds to a parallel arrangement of elastic-perfectly brittle elements which fail progressively under increased deformation.

(ii) The blunt crack approach [3] and the composite fracture model [4] on the other hand start from the notion of a constant energy release rate which accompanies the progressive failure process in the form of a contained crack band. The simultaneous decrease of strength and the increase in irreversible fracture deformations essentially result in a tangent-type material formulation where no degradation of stiffness takes place as long as the elastic recovery process remains uncoupled from the progressive failure process. This concept corresponds to a series arrangement of intact elastic and strain-softening failure zones very much along the line of strain-softening plasticity which is based on the additive decomposition of deformation rates into elastic and plastic components.

In view of recent post-critical experiments on concrete [5] the composite fracture model will be adopted which collapses to previous strain-softening formulations of elastic-plastic solids [6,7] when the fracture

energy release concept is abandoned. For simplicity we will focus on tensile softening, i.e. the composite fracture formulation of an equivalent strain-softening continuum which maintains constant fracture energy release rate during Mode I type cracking. For the extension to general three-dimensional conditions with Mode II and mixed mode failure the reader is referred to Ref. [5].

In the case of tensile cracking, fracture initiation is defined by the maximum tensile stress criterion

$$F(\boldsymbol{\sigma},\mathbf{q}) = \sigma_n - \sigma_t = 0; \quad \text{where } \sigma_n = \sigma_1 \text{ and } \sigma_1 \geq \sigma_2 \geq \sigma_3$$

$$\text{and } \sigma_t = \sigma_t(\mathbf{q}) \tag{1}$$

For initially isotropic conditions the normal tensile stress σ_n in an active crack coincides with the major principal stress, i.e. $\sigma_n = \sigma_1$. The tensile strength σ_t describes the degradation of bond stresses in terms of the internal variables $\mathbf{q}$ which characterize the change of the internal microstructure during softening. In the case of single localized macrodefects the fracture energy release rate G_f^I will provide the missing link between the macroscopic measure of strength and the internal fracture state. The consistency condition

$$\dot{F} = \frac{\partial F^t}{\partial \boldsymbol{\sigma}} \dot{\boldsymbol{\sigma}} + \frac{\partial F}{\partial \mathbf{q}} \dot{\mathbf{q}} = \mathbf{n}^t \mathbf{E}(\dot{\boldsymbol{\epsilon}} - \dot{\boldsymbol{\epsilon}}_f) + \mathbf{p}^t \dot{\mathbf{q}} = 0 \tag{2}$$

leads to the following strain-based loading conditions for progressive cracking

$$\text{for} \qquad \mathbf{n}^t \mathbf{E}\, \dot{\boldsymbol{\epsilon}} \geq 0 \qquad \text{then } \dot{\boldsymbol{\epsilon}}_f \neq 0 \tag{3}$$

$$\text{and } \dot{\mathbf{q}} \neq 0$$

Fig. 1 illustrates the progressive degradation of tensile strength σ_t when the elastic trial stress rate $\dot{\boldsymbol{\sigma}}_T = \mathbf{E}\dot{\boldsymbol{\epsilon}}$ has a positive component in the direction of the gradient $\mathbf{n} = \partial F/\partial \boldsymbol{\sigma}$. The constitutive behavior is characterized by the following evolution laws:

$$\begin{aligned} &\text{Elastic:} && \dot{\boldsymbol{\sigma}} = \mathbf{E}(\dot{\boldsymbol{\epsilon}} - \dot{\boldsymbol{\epsilon}}_f) \\ &\text{Fracture:} && \dot{\boldsymbol{\epsilon}}_f = \dot{\lambda}_f \mathbf{m} \quad \text{where } \mathbf{m} = \frac{\partial Q}{\partial \boldsymbol{\sigma}} \\ &\text{Internal State:} && \dot{\mathbf{q}} = \mathbf{G}\, \dot{\boldsymbol{\epsilon}}_f \end{aligned} \tag{4}$$

When the elastic response behavior is not affected by the progressive fracturing process the elasticity tensor remains invariant, $\mathbf{E}=\text{const}$, and

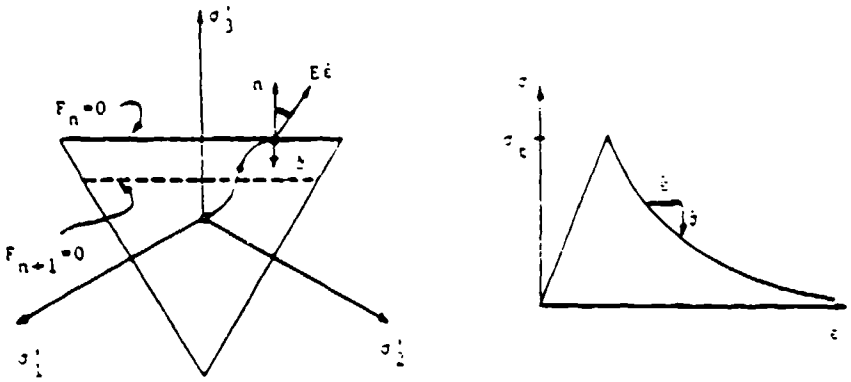

FIG. 1 STRAIN - SOFTENING MODEL FOR TENSION

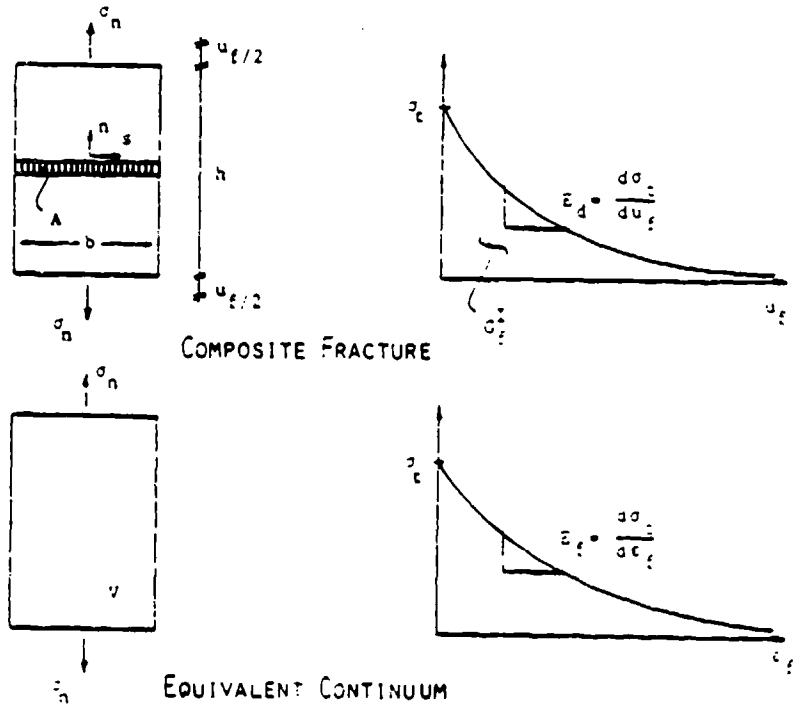

FIG. 2 COMPOSITE FRACTURE MODEL FOR TENSILE CRACKING

does not depend on the internal variable q. In this simple case the elastic stiffness and the degradation of strength during the progressive fracture process are decoupled entirely which is partly supported by the experimental evidence reported in Ref. [5].

The evolution of fracture strains $\boldsymbol{\varepsilon}_f$ is characterized by the fracture rule $\dot{\boldsymbol{\varepsilon}}_f = \dot{\lambda}_f \mathbf{m}$ which defines direction and magnitude of the macroscopic strain-softening response via the gradient of the fracture potential $Q = Q(\boldsymbol{\sigma})$ and the fracture parameter λ_f. In the case of Mode I type cracking in the direction of the major principal stress the associated fracture rule with $\mathbf{m} = \mathbf{n}$ degenerates to the unit vector in three space

$$\mathbf{m} = \mathbf{n} = \begin{bmatrix} \frac{\partial Q}{\partial \sigma_1} \\ \frac{\partial Q}{\partial \sigma_2} \\ \frac{\partial Q}{\partial \sigma_3} \end{bmatrix} = \begin{bmatrix} 1 \\ 0 \\ 0 \end{bmatrix} \tag{5}$$

The general setting for the internal state variable $\mathbf{q}$ follows the early proposal by Kröner [8] who introduced the material tensor $\mathbf{G}$ in order to map changes of the microstructure, i.e. the moments of dislocation pile-ups in metals onto the macrostructure. In our case of tensile cracking we will resort to this generalization of the traditional definitions of strain/and work hardening in order to incorporate the concept of a constant fracture energy release rate.

To this end let us consider the elementary volume V=hbt which is composed of an intact elastic portion and a contained crack band of the area A=bt where t denotes the thickness. Fig. 2 illustrates the composite fracture element and the equivalent continuum element which dissipate the same fracture energy when the tensile strength diminishes to zero residual level during increased straining. In the post-critical response regime the tensile softening localizes into a single tensile crack band, the formation of which requires the following supply of separation energy

$$G_f^I = \int_0^{u_r} \sigma_t \, du_f \tag{6}$$

Note that this expression is a first approximation for the extraction of the critical fracture energy release rate from direct tension experiments, whereby the inelastic dissipation mechanisms which accompany the coalescence of distributed microdefects into a single macrodefect have been neglected. If we adopt the basic postulate of fragmentation theory where

the surface area generated during fracture is proportional to the energy expended [9]

$$G_f = -\frac{\partial \Pi}{\partial A} = \text{const.} \tag{7}$$

then strain-softening may be monitored directly in terms of the raw experimental data involving the nominal tensile strength σ_t and the overall extension u_f. Because of the localized character of the tensile crack and the elastic unloading process of the remaining region, the overall extension u_f is really the crack opening displacement in the final stage of separation.

The question remains how can this relative displacement measure be converted into an equivalent strain in order to be amenable to strain rather than displacement-softening computations? To achieve this we resort to the notion of an equivalent continuum element which dissipates the same amount of fracture energy in the σ_t-ε_f space as does the composite fracture model in the σ_t-u_f space. An elementary energy consideration leads to the following relationship between the softening modulus E_f and the fracture modulus E_d

$$E_f = E_d \frac{V}{A} = E_d h \qquad \text{where } E_d = \frac{d\sigma_t}{du_f} = \frac{d^2 G_f^I}{du_f^2} \tag{8}$$

Clearly in the case of the direct tension test the gage length $V/A=h$ corresponds to the height of the specimen and thus to the crack spacing which converts the overall extension into a nominal strain, $du_f = h d\varepsilon_f$. Therefore, spatial discretization with a finite element mesh size of that particular height would yield the correct fracture energy, while a finer mesh resolution would yield far more brittle response predictions, if the fracture modulus E_f were not adjusted to facilitate the corresponding element height. On the other hand if an elemental philosophy were adopted in which h corresponds to the height or rather the governing element size in the direction of the major principal stress then we have to ascertain that localized cracking is contained to a single element at a time. In this sense the fictitious crack approach by Hillerborg et al. [10] and the blunt crack approach by Bazant et al. [3] solve the spatial problem by following a particular fracture topology similar to the discrete fracture model of Ingraffea and Saouma [11]. In contradiction the current composite fracture model does not involve remeshing but requires a solution strategy for the numerical integration of the strain-softening relations which captures the strain localization within a single element in order to monitor the proper fracture energy release rate.

For the construction of a general fracture-based strain-softening theory we have to map the crack opening displacement du_f and the equivalent tensile fracture strain $d\varepsilon_f$ into three dimensions. To this end let us return to the general formulation outlined in Eqs. 1-5. Introducing the evolution laws in Eq. 4 into the consistency condition in Eq. 2, we obtain the missing expression for the fracture parameter

$$\dot{\lambda}_f = \frac{\langle n^t \mathbf{E}\, \dot{\varepsilon} \rangle}{E_f + n^t \mathbf{E}\, m} \qquad \text{where } E_f = -p^t G\, m \tag{9}$$

If we resort to a strain definition of the internal state variable $dq = d\varepsilon_f$ with $G = I$ then the metric of tensile deformation is defined by the equivalent tensile fracture strain

$$\dot{\varepsilon}_f = \langle \dot{\varepsilon}_f^t\, \dot{\varepsilon}_f \rangle^{1/2} = \sqrt{\langle \dot{\varepsilon}_1 \rangle_f^2 + \langle \dot{\varepsilon}_2 \rangle_f^2 + \langle \dot{\varepsilon}_3 \rangle_f^2} \tag{10}$$

which extracts from the strain tensor only the positive tensile components. The fracture modulus E_f in Eq. 9 characterizes the strain-softening behavior of the equivalent continuum as follows

$$E_f = -\frac{\partial F^t}{\partial \varepsilon_f}\,\frac{\partial Q}{\partial \sigma} = \left(\frac{\partial \sigma_t}{\partial u_f}\,\frac{\partial u_f}{\partial \varepsilon_f}\,\frac{\partial \varepsilon_f}{\partial \varepsilon_f}\right)^t m \tag{11}$$

$$\text{where} \quad \frac{\partial \sigma_t}{\partial u_f} = E_d \quad \text{and} \quad \frac{\partial u_f}{\partial \varepsilon_f} = \frac{V}{A}$$

For uniaxial tension this expression reduces to the relationship in Eq. 8, i.e. $E_f = E_d h$, where h defines the characteristic dimension of the elementary volume in the direction of major tensile straining. Note that this geometric quantity lends itself to a more fundamental micromechanical interpretation since $h = V/A$ is nothing but the reciprocal value of the microcrack density, i.e. the crack surface per unit volume within the solid.

Combining the evolution laws for the elastic and inelastic fracture behavior we arrive at the tangential constitutive relation to be compared with non-associated elastic-strain softening formulations

$$\dot{\sigma} = \mathbf{E}_T \dot{\varepsilon} \qquad \text{where } \mathbf{E}_T = \mathbf{E} - \frac{\mathbf{E}\, m\, n^t \mathbf{E}}{E_f + n^t \mathbf{E} m} \tag{12}$$

The principal difference is the definition of the strain-softening modulus E_f in Eq. 11 which monitors directly the fracture energy release rate via E_d

$$E_f = E_d \frac{V}{A} \left(\frac{\partial \epsilon_f}{\partial \epsilon_f}\right)^t \mathbf{m} \qquad \text{where} \quad E_d = \frac{d^2 G_f^I}{du_\xi^2} \tag{13}$$

On the other hand the fracture-based formulation reproduces the traditional strain-softening models which describe the degradation of strength directly in strain rather than displacement space.

Uniqueness

Let us consider for a moment local and global uniqueness conditions of the elastic plastic strain-softening solution. In the past considerable discussion has revolved around the well-posedness of strain-softening computations with repeated reference to Hadamard [12]. The argument relates to wave propagation in elastic solids whereby the hyperbolic nature of the characteristic equation and the concomitant speed of wave propagation is limited by the positive definiteness of the tangential material law, i.e.

$$\mathbf{x}^t \mathbf{E}_T \mathbf{x} > c\, \mathbf{x}^t \mathbf{x} \qquad \text{with } c > 0 \tag{14}$$

The local stability postulate of Drucker [13] leads to a similar conclusion, since the condition

$$\dot{\boldsymbol{\sigma}}^t \dot{\boldsymbol{\epsilon}} > 0 \tag{15}$$

is synonymous with the positive definiteness of E_T according to Eq. (14). Clearly this stringent requirement leads to severe restrictions of the material model to positive behavior with unlimited ductility. Therefore, if we intend to capture the degradation of strength by strain-softening material models we have to resort to contiguous uniqueness arguments which are considerably less restrictive. In this context we recall the original work of Melan [14] who studied uniqueness of strain-hardening elastic-plastic solutions. The classical approach revolves around the solution of an auxiliary problem in which we examine the condition under which two different solutions may exist at the time t_{n+1} when a unique solution exists at the time t_n. For quasistatic conditions the proof of uniqueness of the solution of the initial value problem results in the question whether the following relation can vanish for $\dot{\boldsymbol{\sigma}}_1 \neq \dot{\boldsymbol{\sigma}}_2$ and/or $\dot{\boldsymbol{\epsilon}}_1 \neq \dot{\boldsymbol{\epsilon}}_2$

$$\int_V (\dot{\boldsymbol{\sigma}}_2 - \dot{\boldsymbol{\sigma}}_1)^t (\dot{\boldsymbol{\epsilon}}_2 - \dot{\boldsymbol{\epsilon}}_1) dV = \int_V \Delta\dot{\boldsymbol{\sigma}}^t \Delta\dot{\boldsymbol{\epsilon}}\, dV = 0 \tag{16}$$

Local uniqueness is therefore assured whenever the governing tangential material law is positive definite i.e. when

$$x^T E_T x > 0 \quad \text{where} \quad x = \Delta\dot{\epsilon} = (\dot{\epsilon}_2 - \dot{\epsilon}_1) \tag{17}$$

In the case of the non-associated strain-softening law in Eq. 12 this constraint leads to the following limiting inequality examined originally by Mroz [15]

$$E_f + n^t E m > \frac{(x^t E m)(n^t E x)}{x^t E x} \tag{18}$$

This leads in the worst case to the "hard" restriction on the strain-softening modulus [16] that

$$2E_f > (m^t E m)^{1/2}(n^t E n)^{1/2} - n^t E m \tag{19}$$

Clearly, for associated behavior with $n = m$ we recover the classic statement of Melan [14] that uniqueness is guaranteed for strain-hardening behavior with $E_f > 0$.

On the other hand, when the strain rate satisfies either orthogonality condition

$$x^t E m = 0 \tag{20}$$
$$\text{or} \quad x^t E n = 0$$

then we recover the far less restrictive uniqueness condition for the strain-softening modulus E_f

$$-E_f < n^t E m \tag{21}$$

Therefore in the most fortuitous case of orthogonality between the elastic stress rate $E\Delta\dot{\epsilon}$ and the gradients n, m uniqueness is assured as long as the softening modulus $-E_f$ is smaller than $n^t E m$, see also Ref. [7]. In the case of uniaxial tension this condition implies that the softening slope must be less than the elastic modulus, i.e.

$$-E_f < E \tag{22}$$

As a result the choice of softening modulus is quite restrictive. Recalling that the fracture based softening formulation introduces with h a characteristic dimension into the definition of $E_f = E_f h$ such that the restriction in Eq. 22 results in a following limitation of the mesh size h

$$h < h_c = \frac{E}{-E_d} \tag{23}$$

This last expression clearly illustrates the interrelationship between the fracture-based strain-softening formulation and the element size in which fracture energy is released. In fact the ratio between the elastic and the fracture moduli governs the maximum mesh size h_c for which weak uniqueness is ascertained.

In this context Valanis [17] demonstrated very recently that rate dependent constitutive relations for strain-softening viscoelastic and viscoplastic solids satisfy the local uniqueness condition as long as the elastic component remains positive.

Since the pivotal uniqueness condition in Eq. 16 involves the volume integral over the entire domain, let us examine the implication related to global uniqueness, see also Ref. [6]. To achieve this we subdivide the domain into a zone $V-V_f$ in which the positive material operator assures local uniqueness in the strong sense and into a zone V_f in which the non-positive material operator may lead to the loss of uniqueness.

$$\int_{V-V_f} \Delta\dot{\sigma}^t \, \Delta\dot{\varepsilon} \, dv + \int_{V_f} \Delta\dot{\sigma}^t \, \Delta\dot{\varepsilon} \, dv = 0 \tag{24}$$

Clearly, the concomitant finite element discretization results in the question, if the tangent stiffness remains positive definite, i.e.

$$\Delta\dot{r}^t \, \mathbb{K}_T \, \Delta\dot{r} > 0 \quad \text{where } \mathbb{K}_T = \mathbb{K} - \mathbb{K}_f$$

$$\text{with } \mathbb{K} = \int_V \mathbb{B}^t \, \mathbb{E} \, \mathbb{B} \, dv \tag{25}$$

$$\text{and } \mathbb{K}_f = \int_{V_f} \mathbb{B}^t \, \mathbb{E}_f \, \mathbb{B} \, dv$$

In the case of contained strain-softening computations the splitting of the tangential stiffness operator into a positive elastic component $\mathbb{K}$ and into an non-positive contribution $\mathbb{K}_f$ leads to the question: Under which circumstances will the softening material operator contaminate the overall stiffness and lead to a loss of positiveness of $\mathbb{K}_T$? Clearly, there is no general answer to this problem, because the topology and boundary conditions determine the extent of the localized strain-softening region V_f for a given load history. As a guideline one might speculate that sharp localization of the softening zone will enhance the confinement and will thus retard the loss of positiveness. Therefore, the numerical

integration of the differential constitutive relations has to capture the spatial localization of strain-softening as well as contiguous elastic unloading of the neighborhood.

In conclusion let us consider global stability which corresponds to the local statement in Eq. 15. In this case the change of stress leads to the following exchange of internal and external energy

$$\frac{1}{2}\int_{V-V_f} \dot{\sigma}^t \dot{\epsilon}\, dV + \frac{1}{2}\int_{V_f} \dot{\sigma}^t \dot{\epsilon}\, dV = \frac{1}{2}\int_{S_\sigma} \dot{p}_s^t \dot{u}\, dS + \frac{1}{2}\int_{S_u} \dot{p}^t \dot{u}_s\, ds \qquad (26)$$

Adsorption Release Positive Positive/Negative

where body forces are neglected and a small displacement gradient theory is presumed. The softening in region V_f results in a release of energy which is monitored by the fracture-based softening law in Eq. 12. On the other hand the rate of external work by the prescribed surface tractions p_s is always positive, while that of prescribed surface displacements u_s can be positive or negative. This clearly demonstrates the stabilizing influence of displacement control which provides the computational tool for tracing the post-critical response behavior. On the finite element level Eq. 26 reduces to the incremental equilibrium relation

$$(K - K_f)\,\dot{r} = \dot{R}_p + \dot{R}_u \qquad (27)$$

If we transform the non-positive softening stiffness K_f into an equivalent force contribution on the right hand side we obtain

$$K\,\dot{r} = \dot{R}_f + \dot{R}_p + \dot{R}_u \qquad (28)$$

where $\dot{R}_f$ denotes the crack driving force defined as

$$\dot{R}_f = K_f \dot{r} = \int_{V_f} B^t E\, \dot{\epsilon}_f\, dV \qquad (29)$$

Note that the fracture strain rate $\dot{\epsilon}_f$ monitors crack extension via the fracture energy release rate embedded in Eqs. 9 and 11. We recognize that $\dot{v}_f = E\,\dot{\epsilon}_f$ in expression Eq. 29 corresponds to the crack extension stress in fracture mechanics which monitors the separation of nodes between contiguous elements when a discrete fracture approach is adopted [10,11]. The principal difference between this scheme and the discrete fracture approach is that equivalent strain-softening takes place within an element rather than at the interface between adjacent elements. This fracture

energy equivalence is assured as long as strain-softening is localized in a single element and does not spill over into contiguous elements.

Model Problems

In conclusion we examine the stability and uniqueness of the numerical solution with the two elementary model problems shown in Fig. 3. The series arrangement of two axial force members of different cross-section was selected in order to investigate the performance of three different incremental/iterative solution methods for the numerical integration of the strain-softening relations. Of particular interest was the question whether the computational strategies were able to capture the localization of fracture in the weaker element, and if a unique solution could be obtained independently of the size of the load increment. Of further interest was the overall computational efficiency and the limiting conditions for convergence in the light of the theoretical considerations delineated in the previous two sections. Particular care was exercised to implement the three algorithms in their full generality and not to bias the solution effort by taking advantage of the simple structural configuration for which hand calculations suffice to determine the reference solution.

The odd geometry and material parameters were chosen to fit the direct tension experiments on cylindrical concrete specimens reported in Ref. [5]. A linear softening model was adopted to monitor the fracture energy release rate $G_f = 0.322$ lb/in. which was required to separate the tension specimen into two competent parts. For the height $h = 2.125$ in. of each bar element the equivalent strain-softening modulus E_f is obtained as follows:

$$E_f = E_d h = \frac{1}{2} \frac{\sigma_t^2}{G_f^I} h = 0.530 \times 10^6 \text{ psi} \qquad (30)$$

with $\sigma_t = 400$ psi

and $E = 2.8 \times 10^6$ psi

Figure 4 illustrates the element deformations at three stages under the prescribed end displacement $r_p > 0$. The results clearly illustrate that beyond peak softening leads to a rapidly increasing extension of the weak element while the stronger elements contract due to elastic unloading. Therefore severe strain localization takes place during monotonically increasing loading of the structure under displacement control which results in a discontinuous strain distribution along the axis, whereby the deformation rates in the softening and the elastically unloading element have opposite directions.

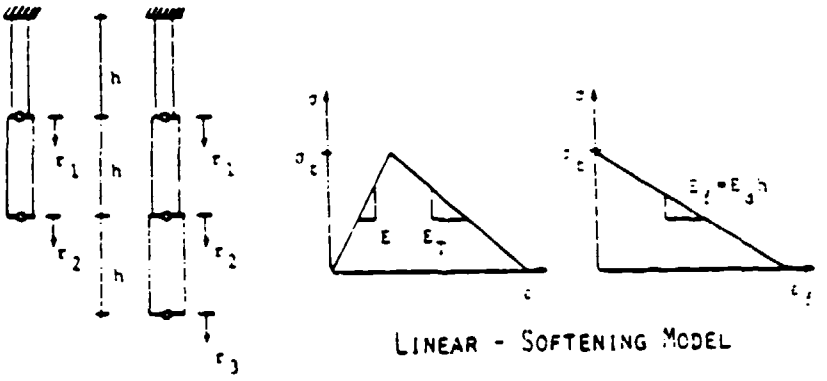

FIG. 3 LAY - OUT OF TENSILE MODEL PROBLEMS

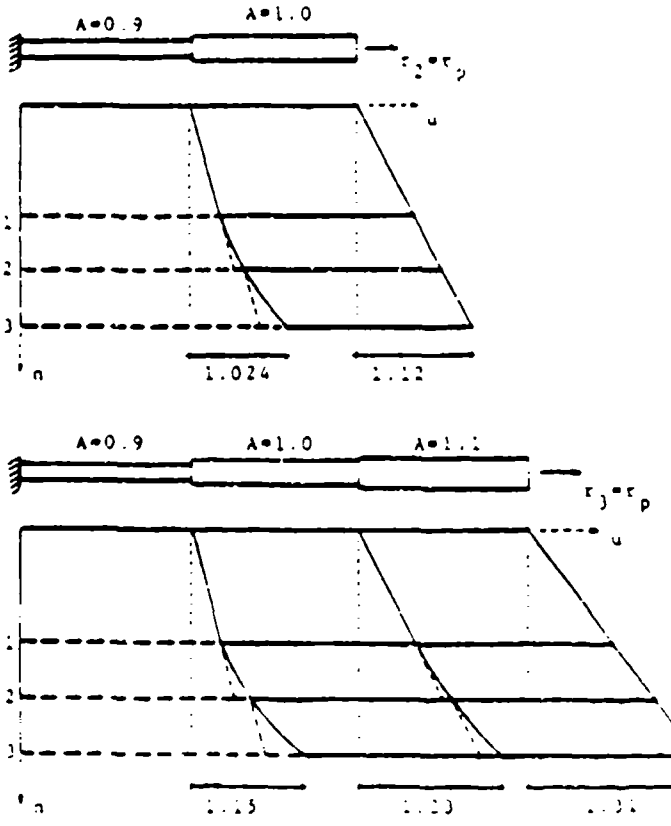

FIG. 4 LOCALIZATION OF STRAIN - SOFTENING REGIME

Figure 5 shows the representative behavior of the two bar structure when the continuation process is resolved into six relatively fine increments. The iterative refinement within each increment demonstrates rapid convergence of the strain-softening and elastic unloading deformations in the two elements. The accompanying relaxation of "real" stresses is plotted when an elastic predictor is used along the line of the initial load iteration method which dates back to the original work in Refs. [18,19]. The algorithm is summarized in the Appendix which corresponds to the elastic plastic solution strategy developed in Ref. [20]. We observe that the initial elastic predictor step at the beginning of each increment is iteratively refined until the constitutive constraint and equilibrium are satisfied simultaneously. It is intriguing that the associated inelastic flow corrections lead to a stress relaxation which is particularly pronounced in the stronger element B subjected to elastic unloading.

In the previous study the incrementation was chosen in such a way that the initial predictor step was causing strain-softening in the weaker element only. In this case all three algorithms summarized in the Appendix captured the localization of strain-softening in element A, whereby the tangent modulus-return scheme was most efficient because of its rapid convergence within two iterations. However, this conclusion only holds for the refined staging strategy in which incipient softening is traced for one element at a time. Therefore in a complex structure the continuation process would have to be subdivided into extremely fine increments in order to capture separate localization events in each softening element. This procedure corresponds to the original proposals of elastic-plastic computations at the end of the 1960's in which the load incrementation was adapted to incipient yielding of the most critical element within the mesh. In computational practice we have to resort to much bolder staging strategies which are independent of the different localization points in the continuation process. In fact the determination of the next localization point is in general quite costly particularly when arc-control is used. Therefore a more pragmatic approach resorts to the following strategy for a prescribed load increment :

(i) determine from the elastic predictor step the most critical trial stress state within the structure

(ii) monitor the structural response due to softening within this critical element, while preventing all other elements from strain localization.

This strategy was certainly successful when the present model problems were analyzed with large load increments, which might otherwise have resulted in the simultaneous softening of all elements. Because of the extensive search and sorting effort this approach is equally costly since it involves continuous exchange between structure and element oriented

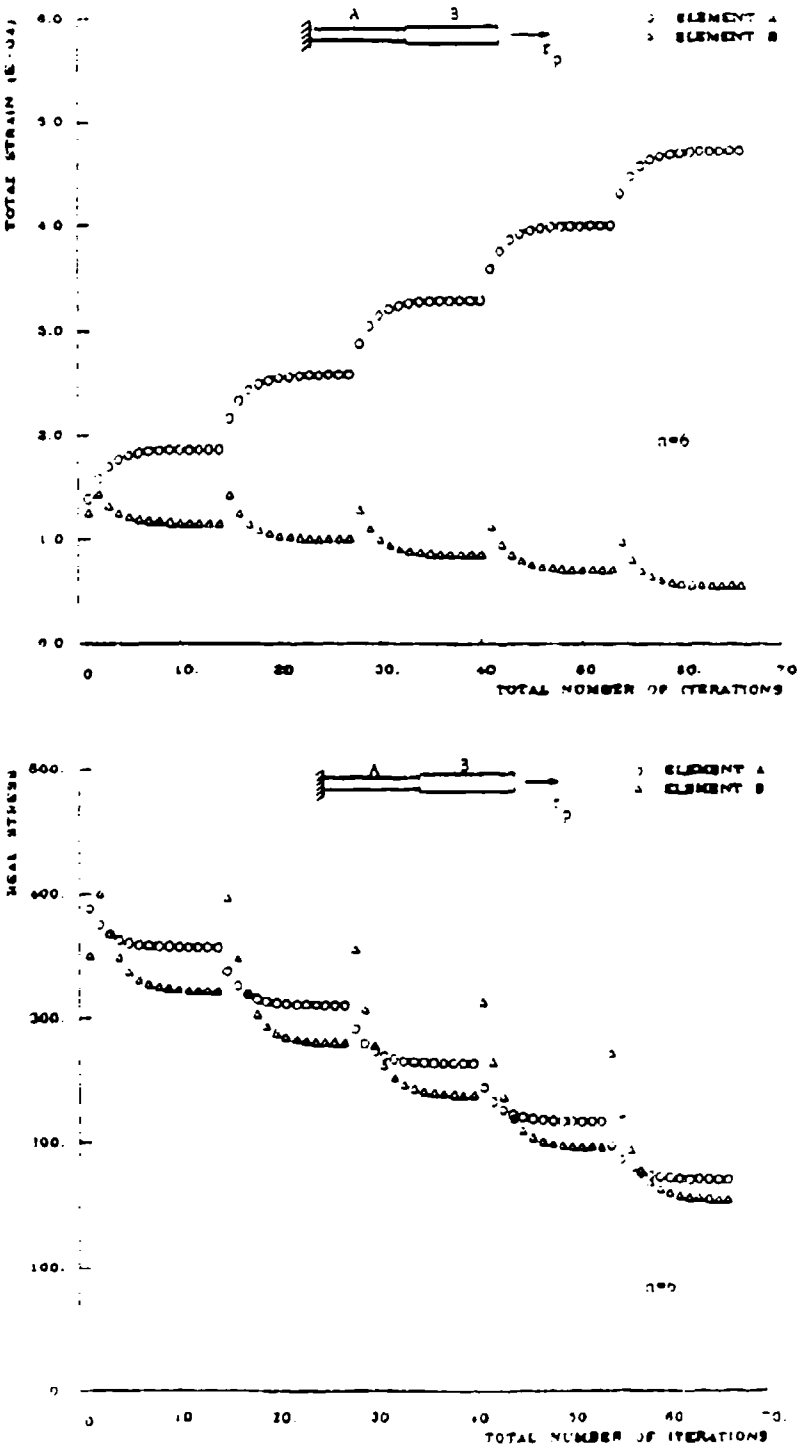

FIG. 5 RESPONSE BEHAVIOUR FOR FINE STAGING

oriented data within large scale finite element programs. Therefore it is highly desirable that the solution algorithm capture localization automatically without resorting to the artifacts above.

To this end we return to our two model problems and examine the performance of the three solution algorithms summarized in the Appendix. The load is applied in two large increments; the first is purely elastic while the second leads to simultaneous softening of all elements. Fig. 6 depicts the localization of deformations within the structure as predicted by the initial load method. Observe the snap back and the elastic recovery of the stronger elements within the second iteration of the second increment. The initial load method captures the strain localization in spite of the fact that the initial elastic predictor step mobilizes strain-softening in all elements. In fact this snap back in the stronger elements is captured by two essential ingredients of the algorithm

(i) the initial elastic stiffness is utilized throughout the analysis along the line of Eq. 28.

(ii) during elastic-inelastic transition the penetration point is located through the contact parameter, ξ.

In fact it is the latter argument which results in elastic snap back of the stronger elements because of predominant softening in the weak element. In the case of the two bar model problem the initial load method determines the increment of the free displacement degree of freedom Δr_1 according to the following iteration scheme

$$(k_A + k_B)\, \Delta r_1^{i+1} = \Delta R_f^i + \Delta R_u \tag{31}$$

where k_A and k_B denote the elastic stiffnesses of elements A and B. The crack driving force due to strain-softening in the two elements is given by

$$\Delta R_f^i = (\Delta\lambda_f^i\, AE)_A + (\Delta\lambda_f^i\, AE)_B \tag{32}$$

where the fracture parameter for uniaxial tension is

$$\Delta\lambda_f^i = (1 - \xi^i)\, \frac{E}{E_f + E}\, \Delta\varepsilon = 1.232\, (1 - \xi^i)\, \Delta\varepsilon \tag{33}$$

The contact parameter ξ locates the penetration point for elastic-inelastic transition according to linear interpolation

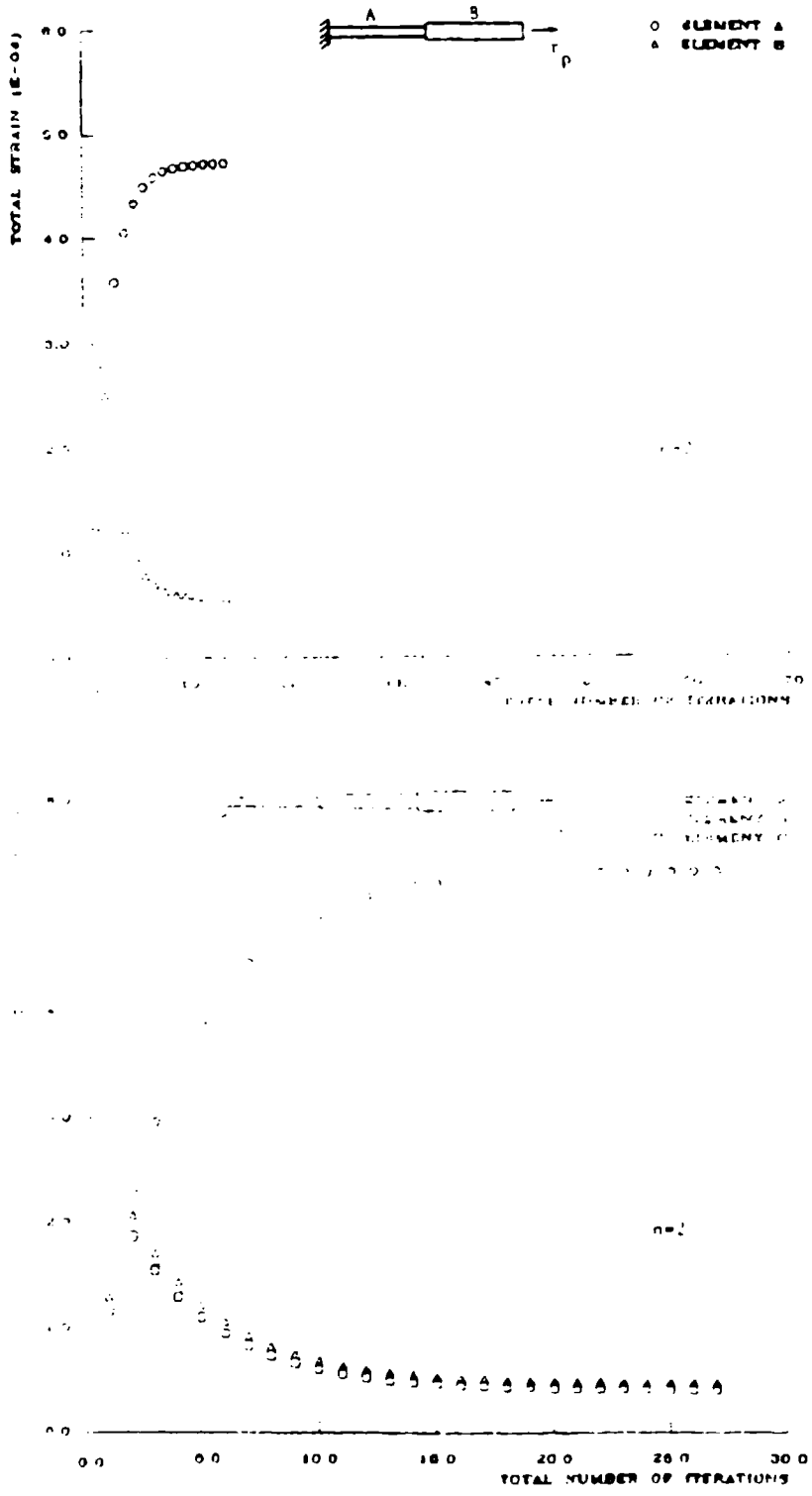

FIG. 6 STRAIN LOCALIZATION FOR COARSE STAGING

$$\xi^i = \frac{\sigma_y - \sigma_n}{\sigma^i_{n+1} - \sigma_n} \quad \text{where } 0 < \xi \leq 1 \text{ for } \sigma^i_{n+1} > \sigma_y \tag{34}$$

σ_y denotes the initial value of the tensile strength $\sigma_y = \sigma_t(\varepsilon^n_f)$ and σ_n and σ^i_{n+1} are the initial stress and the current value of the trial stress state. We observe that $\xi = 0$ for continuous loading and reduces to $\xi=1$ if $\sigma^i_{n+1} \leq \sigma_y$. The strain increment $\Delta\varepsilon$ in Eq. 33 can be expressed in terms of the displacement increment which yields for the crack extension force

$$\Delta R^i_f = 1.232\ k_A(1 - \xi^i_A)\Delta r^i_1 - 1.232\ k_B(1 - \xi^i_B)(\Delta r_p - \Delta r^i_1) \tag{35}$$

where $\Delta r_2 = \Delta r_p$ denotes the prescribed displacement increment. In the case when the weak element has arrived at the elastic limit $\xi^\circ_A = 0$ and when the sufficiently small load increment is applied such that $\xi^\circ_B = 1$ then the iterative corrector equation (Eq. 31) reduces to

$$(k_A + k_B)\ \Delta r^{i+1}_1 = 1.232\ k_A\ \Delta r^i_1 + k_B\ \Delta r_p \tag{36}$$

Convergence of the initial load iteration is assured since

$$\frac{1.232\ k_A}{k_A + k_B} = 0.58 < 1 \tag{37}$$

We observe that strain-softening results in overrelaxation of the fracture parameter $\Delta\lambda_f$ in Eq. 33 because of the magnification factor $E/(E_f + E) = 1.232 > 1$. Therefore we could ask the question what is the limiting softening modulus E^ℓ_f for which convergence breaks down when

$$\frac{E}{E^\ell_f + E}\ \frac{k_A}{k_A + k_B} = 1 \tag{38}$$

The convergence limit is reached when $E_f = E^\ell_f = -1423$ ksi. For the fracture energy release rate of G^I_f=0.322 lb/in. this limitation results in the maximum element height of

$$h_c = 5.47 \text{ in} \tag{39}$$

below which convergence can be assured. Note that this global convergence limitation is considerably more restrictive than the weak uniqueness con-

dition in Eq. 22 which was based only on the local material consideration

$$-E_f < E = 2800 \text{ ksi} \tag{40}$$

Clearly these elementary convergence observations are complicated by the general transition problem which has to be considered for large load increments, when both elements extend into the softening regime. However, from the higher stress state in the weak element A we conclude that $\xi_A < \xi_B$ which signals predominant softening in element A and results in the snap-back of the stronger element B into the elastic recovery regime according to Eq. 35.

Let us now examine the performance of the modified tangent modulus return scheme summarized in the Appendix. This particular strategy was developed by Vermeer [16] for the solution of non-associated shear dilatancy problems and it perfomed best among the numerous variations of tangential methods which were recently assessed in Ref. [21]. This strategy essentially consists of three parts an elastic predictor step and for plastic loading a subsequent plastic corrector step which is combined with the out-of-balance equilibrium step depicted in the flow chart of the Appendix. Unfortunately, many recent publications focus on a particular aspect of the algorithm such as the plastic corrector step and leave the important details of initial staging and synthesis with the out-of-balance equilibrium correction to the reader. In any case the plastic correction involves in general the solution of elastic-plastic transition problem for the contact point denoted by the subscript "c" and the tangential computation of the intermediate state "I" which is subsequently returned to the current yield surface by the plastic flow corrector. The essential step is in this case the calculation of $\Delta\lambda^I$ from the incremental format of the consistency condition using a Taylor expansion about the intermediate configuration and assuming that the total strain increment during flow correction remains constant. This yields for the plastic parameter the following expression

$$\Delta\lambda^I = \frac{< F(\sigma^I, \sigma_y) >}{E_f + m^t \mathbb{E} m} \tag{41}$$

when the intermediate trial stress state exceeds the current yield condition. In contrast to the initial load method which returns after each iteration to the initial stage "n" the state variables are now continuously updated in the spirit of the Newton-Raphson iteration strategy.

In the case of our single degree of freedom model problem the tangent modulus return scheme results in the following iterative corrector of the incremental equilibrium relation

$$(k_A + k_B)_T \, \Delta r_1^{i+1} = R - S^i + \Delta R_f^c + \Delta R_f^I \tag{42}$$

For uniaxial conditions and linear hardening/softening laws the intermediate predictor state will remain on the yield surface, thus $\Delta R_f^I = 0$. Similiarly if we monitor the load history such that only the weaker element is subjected to incipient softening $\Delta R_f^c = 0$ and the tangent stiffness is confined to element A. Since there are no external loads applied at the free degree of freedom, Eq. 42 reduces in the case of the fine staging strategy to

$$(k_{A,T} + k_B) \, \Delta r_1^{i+1} = -(A\sigma^i)_A + (A\sigma^i)_B \tag{43}$$

$$\text{where} \quad \sigma_A^i = \sigma_A + E_T \, \Delta\varepsilon_A^i - \Delta\lambda_f^i E$$

$$\text{and} \quad \sigma_B^i = \sigma_B + E \, \Delta \, \varepsilon_B^i$$

where the righthand side represents the out-of-balance force of the free degree of freedom. For the fine staging strategy the tangent modulus return scheme captures immediately softening of the weak element A and elastic unloading of the stronger element B resulting in a convergent solution after one iteration.

However, in the case of the coarse staging strategy, where both elements mobilize softening the tangent modulus return scheme results in divergent oscillations since $(k_A + k_B)_T$ is now negative definite. As a result the tangent modulus return scheme breaks down prematurely because of its inability to snap back. Only in the case of extremely careful staging of the load increments the tangent approach captures the strain localization within the structure. Ultimately failure will occur when the tangent stiffness looses positive definiteness which leads to the same restriction of the softening modulus $E_f^\ell = -1.423$ ksi as the initial load method.

The third method, the initial modulus return scheme in the Appendix is very similar to the tangent modulus return method except for the initial stiffness which is retained throughout the iteration process. The plastic flow corrector step has been discussed extensively in Ref. [22] and corresponds essentially to the flow correction from the intermediate state, Eq. 41. The performance of this algorithm is very similar to the initial load method. For fine staging convergence is obtained in approximately the same number of iterations. For coarse staging snap back is oscillatory and not as prompt as in the initial load method. However,

the same strain localization is attained in the weak element when two large load increments are used.

We conclude that the localization of strain-softening computations imposes severe restrictions on the staging strategy when tangential approaches are used. The initial stiffness methods are in this regard less restrictive and capture strain localization irrespectively of the magnitude of the load increments. All methods, however, break down when the tangent stiffness looses positive definiteness. Therefore an in-depth effort is presently on the way to explore the capabilities of the arc-length methods [23,24] to capture strain localization. Initial results for elastic softening material laws indicate very promising results when the modified constant arc length normal-projection method [23] is extended by orthogonality constraints between the initial displacement predictor and the iterative displacement corrections using the initial stiffness throughout the iteration history. In this case stable strain localization was obtained for our model problems using strain-softening moduli $E_f < -1.423$ ksi which fully contaminated the positive definiteness of the tangent stiffness operator. These results will be detailed in a forthcoming publication.

Acknowledgement

The authors would like to thank Dr. N. Bicanic for his constructive critique. The investigation was supported by the U.S. Air Force Office of Scientific Research Contract AFOSR 82-0273 with the University of Colorado, Boulder under the liaison of Lt. Col. Hokanson.

References

1. Dougill, J.W., "On Stable Progressively Fracturing Solids", J. Appl. Math. Phys., ZAMP, Vol. 27 (1976), pp. 423-436.

2. Janson, J. and Hult, J., "Fracture Mechanics and Damage Mechanics, a Combined Approach," J. De Mécanique Appliquée, Vol. 1 (1977), pp. 69-84.

3. Bažant, Z.P. and Oh, B.H., "Crack Band Theory for Fracture of Concrete", Rilem, Materiaux and Constructions, Vol. 16 (1983), pp. 155-177.

4. Willam, K.J., Bicanic, N. and Sture, S., "Constitutive and Computational Aspects of Strain Softening and Localization in Solids", ASME/WAM 1984 Symposium on Constitutive Equations Macro and Computational Aspects, (K. Willam, ed.), ASME Vol. G00274, New York (1984), pp. 233-252.

5. Willam, K.J., Hurlbut, B. and Sture, S., "Experimental Constitutive and Computational Aspects of Concrete Failure", US-Japan Joint Seminar on Finite Element Analysis of Reinforced Concrete Structures, University of Tokyo May 21-24, 1985, Proc. Vol. 1 (1985), pp. 149-171.

6. Prevost, J.-H. and Hoeg, K., "Soil Mechanics and Plasticity Analysis of Strain Softening", Geotechnique, Vol. 25 (1975), pp. 279-297.

7. Nguyen, Q.S. and Bui, H.D., "Sur les Materiaux Elastoplastiques a Ecrouissage Positif ou Négatif", J. de Mecanique, Vol. 13 (1974), pp. 321-342.

8. Kröner, E., "Plastizität und Versetzungen", Chapter 9 in Volume 2, Vorlesungen über theoretische Physik, A. Sommerfeld, Akademische Verlags gesellschaft, Leipzig (1970).

9. Von Rittinger P., "Lehrbuch der Aufbereitungskunde", Ernst und Korn, Berlin, 1867.

10. Hillerborg, A., Modéer and Peterson, P.E., "Analysis of Crack Formation and Crack Growth in Concrete by Means of Fracture Mechanics and Finite Elements", Cement and Concrete Research, Vol. 6 (1976), pp. 773-781.

11. Ingraffea, A.R. and Saouma, V., "Numerical Modeling of Discrete Crack Propagation in Reinforced and Plain Concrete", Chapter 4 in Fracture Mechanics of Concrete, M. Nijhoff Publ., Dordrecht (1985), pp. 171-225.

12. Hadamard, J.S., "Leçons sur la Propagation des Ondes", Hermann, Paris (1903).

13. Drucker D.C., "A Definition of Stable Inelastic Materials", J. Appl. Mech., Vol. 26 (1959), pp. 101-106.

14. Melan, E., "Zur Plastizität des räumlichen Kontinuums", Ing. Archiv Vol. 9, (1938), 116-126.

15. Mroz, Z., "On the Description of Anisotropic Workhardening," J. Mech. Phys. Solids, Vol. 15 (1967), pp. 163-175.

16. Vermeer, P.A., "Formulation and Analysis of Sand Deformation Problems,", Report No. 195 of the Geotechnical Laboratory, Delft University of Technology, 1978.

17. Valanis, K.C., "On the Uniqueness of Solution of the Initial Value Problem in Softening Materials", Joint ASME/ASCE Summer Mechanics Conference, June 24-26, 1985, Albuquerque, JAM, 85-APM-29 (1985), pp. 1-5.

18. Argyris, J.H. and Scharpf, D.W., "Methods of Elasto-Plastic Analysis, ISD-ISSC Symp. Stuttgart (1969), pp. 381-416; also ZAMP, Vol. 23 (1972), pp. 517-551.

19. Nayak, G.C. and Zienkiewicz, D.C., "Elasto-Plastic Stress Analysis. A Generalization for Various Constitutive Relations Including Strain-Softening", Int. J. Num. Meth. Engng., Vol. 5, (1972), pp. 113-135.

20. Balmer, H., Doltsinis, J. St. and König, M., "Elastoplastic Creep Analysis with the ASKA Program System", Comp. Meth. Appl. Mech. Eng. Vol. 3 (1974), pp. 87-104.

21. Potts, D.M. and Gens, A., "A Critical Assessment of Methods of Correcting for Drift from Yield Surface in Elasto-Plastic Finite Element Analysis", Int. J. Num. Anal. Meth. Geomech. Vol. 9 (1985), pp. 149-159.

22. Ortiz, M. and Simo, J.C., "An Analysis of New Class of Integration Algorithms for Elastoplastic Constitutive Relations", Techn. Report, Brown University, Division of Engineering, Providence (1984).

23. Ramm, E., "Strategies for Tracing Nonlinear Response Near Limit Points", Europe-US Workshop on Nonlinear Finite Element Analysis in Structural Mechanics," Proc. (Bathe, Stein, Wunderlich eds.) Springer Verlag, Berlin (1980), pp 63-89.

24. Crisfield, M.A., "A Fast Incremental/Iterative Solution Procedure that Handles Snap Through ", Computers and Structures, Vol. 13 (1981), pp. 55-62.

APPENDIX

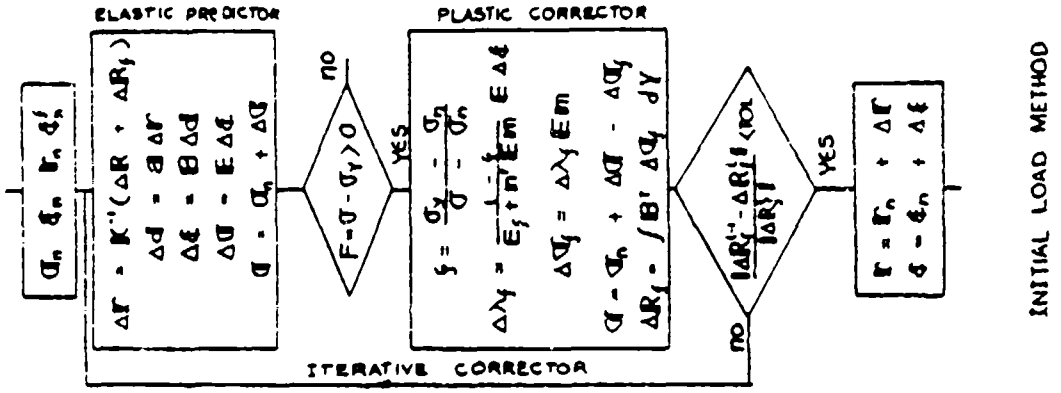
ELASTIC PREDICTOR
PLASTIC CORRECTOR
no
yes
ITERATIVE CORRECTOR
no
yes
INITIAL LOAD METHOD

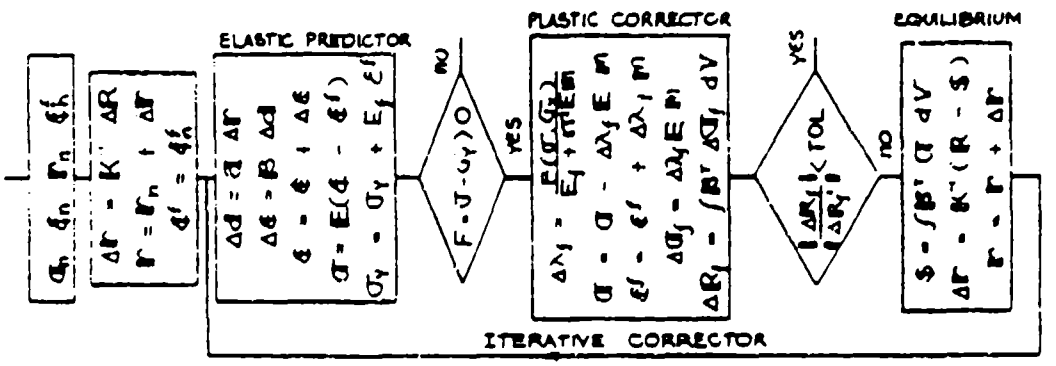
ELASTIC PREDICTOR
PLASTIC CORRECTOR
EQUILIBRIUM
no
yes
ITERATIVE CORRECTOR
INITIAL MODULUS RETURN SCHEME

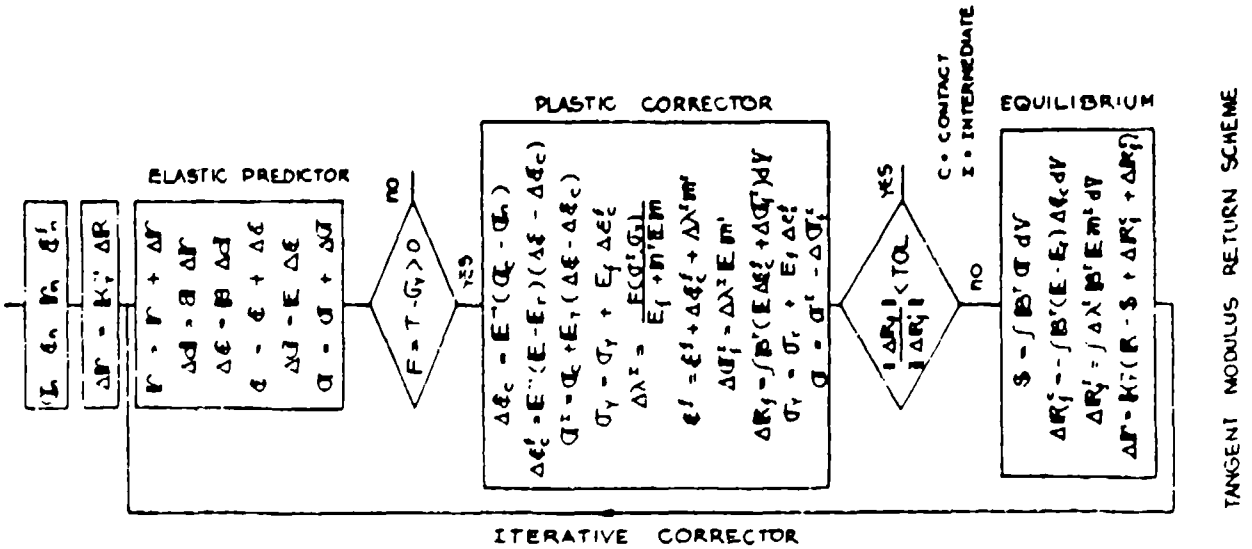
ELASTIC PREDICTOR
PLASTIC CORRECTOR
EQUILIBRIUM
C = CONTACT
I = INTERMEDIATE
no
yes
ITERATIVE CORRECTOR
TANGENT MODULUS RETURN SCHEME

APPENDIX D

APPENDIX D

"Composite Fracture Model for Strain-Softening Computations of Concrete Failure"

by

Kaspar Willam, Nenad Bicanic, Eddy Pramono and Stein Sture

Paper presented at the International Conference on Fracture Mechanics of Concrete - Fundamentals and Applications, EPF Lausanne, Switzerland Oct. 1-3, 1985; will be published in Conference Proceedings by Elsevier Publishers, Amsterdam (1986)

COMPOSITE FRACTURE MODEL FOR STRAIN SOFTENING COMPUTATIONS OF CONCRETE

K. WILLAM[1], N. BICANIC[2], E. PRAMONO[1], S.STURE[1]

[1]Dept. Civil Engineering, University of Colorado Boulder, Boulder, U.S.A.

[2]Dept. Civil Engineering, University College of Swansea, Wales, U.K.

ABSTRACT

The composite fracture model will be delineated which monitors constant fracture energy release rates in tension within an equivalent strain softening plasticity formulation. Its predictive value will be illustrated with the one-dimensional model problem of a uniaxial tension member which has been previously used to query the well-posedness of quasistatic and dynamic strain softening computations.

INTRODUCTION

It is widely accepted that post-critical experiments under stroke control are not only accompanied by changes of the internal microstructure but also by changes of the macrostructure in the form of localized fracture zones which penetrate the test specimen of finite dimension. Therefore strain softening requires homogenization of the non-uniform deformation process in order to extract ductility properties from servo-controlled experiments which do not only hold for a specific test configuration. In the case of plain concrete the underlying issue of a single macrodefect versus distributed microdefects is further complicated by the composite nature of the mortar-aggregate mixture. Clearly, the tortuous character of the macrodefects and the progressive localization of distributed microdefects cast considerable doubt on the validity of fracture mechanics on one hand and on the relevance of continuous damage mechanics on the other hand. The principal question centers around the issue if progressive failure is a surface or a volume dominated process. In direct tension there is little argument that the formation of a discrete macrocrack poses a fracture mechanics problem in which the energy expended for the crack formation is approximately proportional to the surface area generated, i.e. G_f = constant. However, in the case of splitting compression and even more in the case of faulting modes of failure this problem is far from resolved and has been recently forwarded in the form of the provocative question, if the formation of "shear bands is sheer nonsense" in the case of brittle materials.

In the subsequent development the composite fracture model will be briefly outlined which incorporates the constant fracture energy release rate concept into the strain softening formulation of an equivalent elastic plastic solid. The general formulation will be subsequently applied to the solution of a one-dimensional model problem in which a uniaxial specimen is subjected to increasing tension. Because of tensile softening, strain localization takes place in a transverse crack band wherever the stress amplitude first exceeds the governing tensile strength. The trapping of tensile deformations appears irrespective of the underlying strain softening mechanics which may resort to singular fracture or distributed damage modes of failure. The strain localization simply reflects the continuum approximation of the actual crack discontinuity and the concomitant separation of the specimen into two unloading components.

In the recent past considerable discussion has centered about the well-posedness of quasistatic and dynamic strain softening computations [1], the uniqueness of rate-sensitive material formulations [2], the advantages of viscoelastic and/or viscoplastic strain softening models [3], and alternatively the need for non-local continuum theories along the line of the imbricate formulation of long range deformation measures [4,5]. Some of these arguments will be addressed in the context of the elementary model problem for which the composite fracture formulation provides both a unique and mesh-insensitive solution of the fracture energy [6]. In fact, we will observe that the wave propagation problem is computationally less demanding than the corresponding quasistatic strain softening analysis of continua.

COMPOSITE FRACTURE MODEL

The composite fracture formulation was recently developed by the authors in order to introduce the constant fracture energy release rate concept into strain softening computations of an energy-equivalent continuum. The original approach in ref. [7] started from two independent softening mechanisms for Mode I type debonding in tension and for Mode II type decohesion in shear considering some limited interaction [18]. Based on new experimental evidence on low strength concrete which was tested under stroke control in direct tension and low confined compression, a fracture energy based strain softening plasticity model was subsequently developed in ref. [8]. In this case decohesion under low confined compression was expressed in terms of Mode I type fracture which was monitored in terms of an equivalent tensile rather than a shear strain measure. The point of departure for the fracture based strain softening plasticity model was the Leon criterion of triaxial strength [9] which corresponds to a parabolic generalization of the Mohr-

Coulomb criterion augmented by the appropriate tension cut-off conditions. This formulation resorts to a single tensile strain controlled softening mechanism which describes splitting compression and shear faulting in terms of the fundamental Mode I type fracture process [19].

In view of the nature of the elementary model problem below we will focus on the composite fracture model for Mode I type cracking in tension. In this case the formulation corresponds to the strain softening plasticity model of Nilsson and Oldenburg [10] when the fracture condition degenerates to the maximum stress criterion of Rankine:

$$F(\sigma,q) = \sigma_n - \sigma_t(q) = 0 \quad \text{where} \quad \sigma_n = \sigma_1 \quad \text{and} \quad \sigma_1 \geq \sigma_2 \geq \sigma_3 \tag{1}$$

For isotropic conditions the normal tensile stress σ_n coincides with the major principal stress, i.e. $\sigma_n = \sigma_1$. For permanent crack memory subsequent cracking is monitored separately along the three directions defined by the first crack occurrence. The tensile strength parameter σ_t^i describes the degradation of bond stresses in terms of the internal variables q_i which characterize the tensile fracture deformations ε_f^i along the three crack directions. This "orthotropic" softening strategy deviates slightly from the isotropic formulation used previously [8] in which an equivalent tensile strain ε_f was extracted from the inelastic strain tensor which monitors the degradation of tensile strength. For rotating stress directions the orthotropic approach requires however additional provisions along the line of the rotating crack model of Schnobrich et al. [11].

In the case of localized macrodefects the fracture energy release rate G_f^I describes the degradation of tensile strength σ_t in terms of the crack opening displacement u_f. Therefore the fracture energy formulation of strain softening has to establish a relationship between the crack opening displacement u_f and the nominal tensile strain measure ε_f in the equivalent continuum. To this end let us consider the elementary volume $V_e = h_e bt$ depicted in Fig. 1 which is composed of an intact elastic region and a contained crack band of the area $A_f = bt$, where t denotes the thickness. Fracture of the composite fracture element should release the same amount of fracture energy as that of the equivalent continuum element when the crack band propagates through the elementary volume. A simple energy consideration leads to the following definition of the strain softening modulus E_f of the equivalent continuum in terms of the fracture modulus E_d and the underlying fracture energy release rate G_f^I

$$E_f = E_d \frac{V_e}{A_f} \quad \text{where} \quad E_d = \frac{d\sigma_f}{du_f} = \frac{d^2 G_f^I}{du^2_f} \tag{2}$$

Clearly in the case of a uniaxial tension specimen the characteristic length V_e/A_f corresponds to the height of the elementary volume h_e which converts the crack opening displacement into the overall extension of the composite fracture element after elastic unloading. Therefore the characteristic length plays the role of the gage length which calibrates the "nominal" fracture strain ε_f in the form

$$d\varepsilon_f^i = \frac{A_f}{V_e} du_f^i \qquad \text{where } \frac{A_f}{V_e} = \frac{1}{h_e} \tag{3}$$

A more fundamental viewpoint regards the volume fraction A_f/V_e as microcrack density which maps the fracture surface area into an equivalent volume quantity. Note that Eq. 3 is the key to the homogenization of localized macrodefects into a fracture energy equivalent continuum.

In a computational environment the characteristic length V_e/A_f corresponds to a representative dimension of the mesh size, i.e., the cubic root of the Jacobian if an isoparametric finite element formulation is utilized. This elemental approach ensures that the proper amount of fracture energy is released when a single element is subjected to complete softening. Clearly the localization of strain softening within the structural idealization is a separate issue which requires computational provisions in order to capture snap-back phenomena during the iterative correction phase of the incremental staging strategy [6].

The remaining formulation of fracture energy based strain softening follows the traditional derivation of strain controlled elastic plastic solids. Resorting to an associated flow rate and the usual additive decomposition of the deformation rate we find in the absence of elastic-plastic coupling the following evolution laws for the

$$\text{Elastic Response:} \quad \dot{\sigma} = \mathbf{E}(\dot{\varepsilon} - \dot{\varepsilon}_f) \tag{4}$$

$$\text{Fracturing Response:} \quad \dot{\varepsilon}_f = \dot{\lambda}\, \mathbf{n} \quad \text{where } \mathbf{n} = \frac{\partial F}{\partial \sigma} \tag{5}$$

The consistency condition $\dot{F} = 0$ leads to the strain-based loading condition for progressive cracking

$$\dot{\varepsilon}_f \neq 0 \qquad \text{if} \qquad n^t E \dot{\varepsilon} \geq 0 \tag{6}$$

when the trial stress rate $\dot{\sigma}_T = E \dot{\varepsilon}$ has a component in the positive direction of the normal n. The fracture parameter follows from

$$\dot{\lambda}_f = \frac{n^t E \dot{\varepsilon}}{E_f + n^t E n} \tag{7}$$

where the fracture-based strain softening modulus was defined in Eq. 2

$$E_f = \frac{\partial \sigma_t}{\partial u_f} \frac{\partial u_f}{\partial \varepsilon_f} = E_d \frac{V_e}{A_f} \tag{8}$$

This formulation for a single active crack readily extends to cracking in two and three orthogonal crack planes, whereby trial stress states in the vertex region require the simultaneous solution of two contiguous fracture parameters $\dot{\lambda}_f^i$ and $\dot{\lambda}_f^j$ along the line of simultaneous plastic flow in the case of multiple loading surfaces.

As a result the tangential material law of the equivalent elastic strain softening continuum is defined by

$$\dot{\sigma} = E_T \dot{\varepsilon} \qquad \text{where } E_T = E - \frac{E n n^t E}{E_f + n^t E n} \tag{9}$$

The fracture energy basis of the strain softening modulus in Eq. 8 ensures that the fracture energy released within each elementary volume remains constant irrespective of the size of the finite element. We note that the weak requirement for local uniqueness [6] infers that the denominator in Eq. 9 remains positive, i.e.,

$$E_f + n^t E n \geq 0 \tag{10}$$

This restriction infers for uniaxial conditions that

$$-E_f < E \tag{11}$$

which results in the following limitation of the characteristic dimension of the elementary volume

$$h_e = \frac{V_e}{A_f} = -\frac{E}{E_d} \tag{12}$$

This condition imposes severe restrictions on the choice of the maximum mesh size $h_{max} < h_e$.

MODEL PROBLEM

Let us examine the computational aspects of the composite fracture model when applied to the analysis of a uniaxial specimen subjected to increasing tension.

In the quasistatic case of a uniform tension specimen the localization of the softening zone is a problem of its own. The homogeneous deformation problem requires first deterministic or probabilistic identification of the crack location via initial imperfections in the form of variations of the tensile strength or the cross-sectional properties. In the case of the discrete fracture approach of Ingraffea and Saouma [12] and the fictitious crack model of Hilleborg et al. [13], a real or fictitious crack element would have to be incorporated into the mesh lay-out in the form of a discrete interface element which monitors the fracture energy release rate directly in terms of the ensuing crack opening displacement. In the case of the blunt crack approach of Bazant et al. [14] the initial mesh lay-out would also have to be changed in order to accommodate the blunt crack element at the crack location which now has finite rather than zero width in the order of three times the aggregate size.

In contrast the composite fracture model does not require remeshing as long as strain softening is localized within a single element. In this case the proper amount of fracture energy is released irrespective of the location of the "weak" element along the axis of the tension specimen. In view of the incremental format of strain-softening computations it is however crucial that strain softening and the concomitant deformation trapping will be localized within a single element. This infers that the iterative corrector phase of the solution strategy must capture elastic snap back within elements for which the initial predictor step might erroneously signal softening. As a result the tangent modulus return scheme might not only lead to premature difficulties with the loss of positiveness of the tangent stiffness matrix but also to wrong fracture energy release predictions when no special provisions are made for "iterative reversibility" within the load increment. In fact it was shown recently by the authors [6]

that the classic initial load method and the initial modulus return scheme are better suited for capturing strain localization in a single element when the contiguous elements are simultaneously unloading elastically.

Quasistatic Study

Fig. 2 illustrates the geometry and the material properties of the model problem. The tension specimen is subjected to monotonically increasing end displacements which result in a uniform tension in the absence of initial imperfections. The finite element idealization of half the bar with three elements of different length results in a uniform stress distribution in the entire bar, and only numerical round-off eventually leads to localized softening in the short element A. Fig. 3 depicts the overall solution in terms of the nominal stress versus axial extension diagram of half the bar, the area under which provides a measure of the fracture energy release rate. Reduction of the cross-sectional area from $A = 1.0$ to $A_w = 0.99$ leads to predetermined strain localization and deformation trapping in the weak element, a concept which has previously proposed by Prevost and Hughes [15] in order to initiate localization. In the case of the composite fracture model, in which the strain softening modulus E_f depends on the size of the weak element h_w the fracture energy release rate remains constant when either of the three elements is weakened. In the case of the traditional strain softening formulation in which E_f does not depend on mesh size, the corresponding results indicate that the ductility and thus the underlying fracture energy release rate strongly depends on the size of the weak element h_w, see also Crisfield [16].

The axial distribution of tensile strains is shown in Fig. 4 for the constant fracture energy and the constant strain softening formulations. The composite fracture model results in all three cases in identical fracture energy release values and thus in a corresponding decrease of tensile strain level when the size of the weak elements increases from $h_A = 5$ to $h_B = 15$ and $h_C = 30$ (see also Fig. 3a). The constant strain softening model in contrast leads to the same level of tensile straining in each of the weakened elements and thus to a drastic decrease of ductility and corresponding fracture energy as the size of the weak element decreases (see also Fig. 3b). In the limit this would result in zero fracture energy expended when softening localizes in an element of infinitesimal size. This disturbing aspect of the traditional strain-softening approach has been rightly criticized in the past by Bazant et al. [4,14]. We might add that the computational difficulties which arise with maintaining stable control of the post-critical response predictions are exacerbated by increasing

brittleness and could become prohibitive in the case of actual snap-back conditions. The numerical results above were obtained with the incremental initial load iteration method in which the initial elastic stiffness matrix remains constant during the entire solution phase. There was no need for arc length stabilization since the underlying tangent stiffness maintained positive definiteness in all three cases, as detailed in ref. [6].

Dynamic Study

In the second part of this study the same model problem was analyzed with the aid of the explicit finite element code DEGDYN which was developed by one of the authors [17] for the dynamic investigation of concrete dams. In this case the uniaxial bar was subdivided into 9, 21 and 97 elements of equal length and subjected to the constant velocity $c = 0.50$ at both ends, see Fig. 5. In contrast to the quasistatic problem, no special provision was necessary to capture localization of the strain softening zone in the stress wave problem. The analytic solution was recently reviewed by Bazant and Belytschko [5] for which a well posed solution was found irrespective of the loss of hyperbolicity of the underlying characteristic wave equation in the softening regime.

Figs. 6 and 7 compare the numerical results of the composite fracture model with those of the traditional strain softening approach in which the softening modulus is kept constant irrespective of the mesh size. The resulting stress histories and the associated values of the fracture energy release rates clearly demonstrate the extreme mesh sensitivity of those quantities when $E_f = \text{const}$. On the other hand, the composite fracture model maintains constant fracture energy release rates without resorting to non-local continuum theories along the line of the recent imbricate continuum proposal of ref. [4] for resolving this basic deficiency of the traditional strain softening approach.

Fig. 8 illustrates the various degrees of localized deformation trapping at the center of the tension specimen. Clearly it is a question of spatial resolution to capture tensile cracking and actual separation of the bar within the strain-softening formulation of an equivalent continuum. We observe that both formulations reproduce the actual separation phenomenon quite well. In fact, the conventional strain softening approach leads to a sharper approximation of the localized strain discontinuity at the center of the bar where $\varepsilon \to \infty$ as $h_e \to 0$. On the other hand, the composite fracture model enforces constant fracture energy release rates irrespective of the

particular element size h_e. In view of the actual separation process, it appears questionable if non-local continuum theories are really appropriate because they prevent sharp strain localization in the neighborhood of the actual discontinuity and distribute softening and thus failure over a long-range regime.

CONCLUDING REMARKS

A strain softening plasticity model was developed based on the composite fracture concept of homogenizing fracture discontinuities into an energy equivalent continuum. In view of the one-dimensional nature of the static and dynamic model problems the main thrust of the exposition was focused on mode I type cracking. The composite fracture formulation has been extended in [8,19] to mixed mode fracture in the form of splitting compression and shear faulting modes of failure in order to develop a unified approach towards softening in tension and compression.

Acknowledgement

This work was sponsored by the US Air Force Office of Scientific Research under Contract AFOSR 82-0273 with the University of Colorado, Boulder. The authors would like to acknowledge the support and liaison efforts of Lt-Col. Lawrence Hokanson in this endeavor.

REFERENCES

1 I. Sandler, "Strain Softening for Static and Dynamic Problems," ASME/WAM '84 Meeting, New Orleans, Symposium on Constitutive Equations Macro and Computational Aspects, ASME Vol. G00274, (K. Willam ed.), New York (1984), pp. 217-231.

2 K.C. Valanis, "On the Uniqueness of Solution of the Initial Value Problem in Softening Materials," Joint ASME/ASCE Summer Mechanics Conf., June 24-26, 1985, Albuquerque, JAM 85-APM-29 (1985), pp. 1-5.

3 H.E. Read and G.A. Hegemier, "Strain Softening of Rock, Soil and Concrete - A Review Article," Mechanics of Materials, Vol. 3 (1984), pp. 271-294.

4 Z.P. Bazant and T.B. Belytschko, "Continuum Theory for Strain-Softening," ASCE J. Eng. Mech. Vol. 110, No. 12 (1984), pp. 1666-1692.

5 Z.P. Bazant and T.B. Belytschko, "Wave Propagation in a Strain-Softening Bar: Exact Solution," ASCE J. Eng. Mech. Vol. 111, No. 3 (1985), pp. 381-389.

6 K.J. Willam, E. Pramono, S. Sture, "Stability and Uniqueness of Strain-Softening Computations," Europe-US Symposium on Finite Element Methods for Nonlinear Problems, NIT Trondheim, Aug. 12-16, 1985, Structures Research Series 8503, University of Colorado, Boulder (1985), pp. 1-24.

7 K.J. Willam, N. Bicanic, S. Sture, "Constitutive and Computational Aspects of Strain-Softening and Localization in Solids," ASME/WAM '84 Meeting, New Orleans, Symposium on Constitutive Equations, Macro and Computational Aspects, ASME Vol. G00274, (K.Willam ed.), New York (1984), pp. 233-252.

8 K.J. Willam, B. Hurlbut, S. Sture, "Experimental, Constitutive and Computational Aspects of Concrete Failure," US-Japan Joint Seminar on Finite Element Analysis of Reinforced Concrete Structures, University of Tokyo, May 21-24, 1985, Proc. Vol. 1 (1985), pp. 149-171.

9 M. Romano, "On Leon's Criterion," Meccanica, (1969), pp. 40-66.

10 L. Nilsson, M. Oldenburg, "On the Numerical Simulation of Tensile Fracture," Europe-US Symposium on Finite Element Methods for Nonlinear Problems, NIT, Trondheim Preprints Vol. 1, Aug. 12-16,(1985), pp. I.4-1 to I.4-15.

11 R.V. Milford and W.C. Schnobrich, "Numerical Model for Cracked Reinforced Concrete," Proc. Intl. Conf. on Computer Aided Analysis and Design of Concrete Structures," Part I, Pineridge Press, Swansea (1984), pp. 71-84.

12 A.R. Ingraffea and V. Saouma, "Numerical Modeling of Discrete Crack Propagation in Reinforced and Plain Concrete," Chapter 4 in Fracture Mechanics of Concrete, M. Nijhoff Publ., Dordrecht (1985), pp. 171-225.

13 H. Hillerborg, M. Modéer and P.E. Peterson, "Analysis of Crack Formation and Crack Growth in Concrete by Means of Fracture Mechanics and Finite Elements," Cement and Concrete Research, Vol. 6 (1976), pp. 773-781.

14 Z.P. Bazant and B.H. Oh, "Crack Band Theory for Fracture of Concrete," Rilem, Materiaux and Constructions, Vol. 16 (1983), pp. 155-177.

15 J.H. Prevost and T.J.R. Hughes, "Finite Element Solution of Elastic-Plastic Boundary Value Problems," ASME Paper No. 81-APM-17 (1981), pp. 1-6.

16 M.A. Crisfield, "Difficulties with Current Numerical Models for Reinforced Concrete and Some Tentative Solutions," Proc. Intl. Conf. on Computer Aided Analysis and Design of Concrete Structures," Part I, Pineridge Press, Swansea (1984), pp. 331-557.

17 N. Bicanic, "Nonlinear Finite Element Transient Response of Concrete Structures," Ph.D. Dissertation, C/Ph/50/78, University College of Swansea, Wales, 1978.

18 S.E. Day, "A Softening Plasticity Model for Concrete," M.S. Thesis, CEAE Department, University of Colorado, Boulder, 1985.

19 B.S. Hurlbut, "Experimental and Computational Investigation of Strain-Softening in Concrete," M.S. Thesis, CEAE Department, University of Colorado, Boulder, 1985.

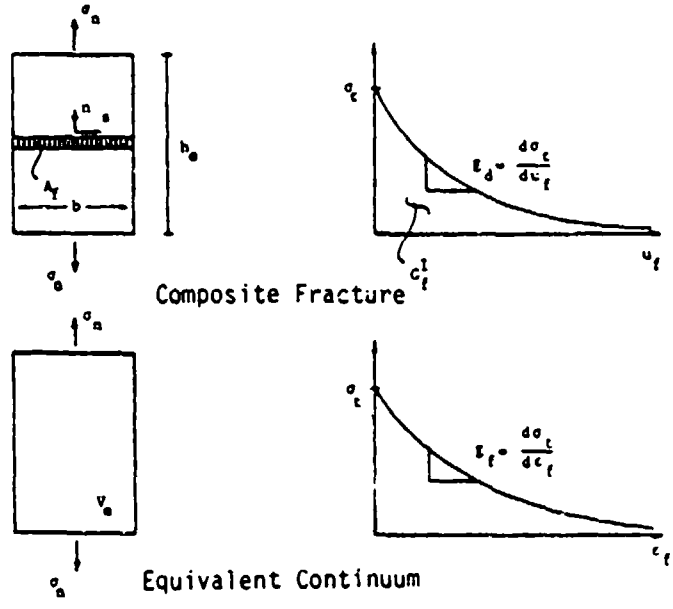

Fig. 1 Composite Fracture Model

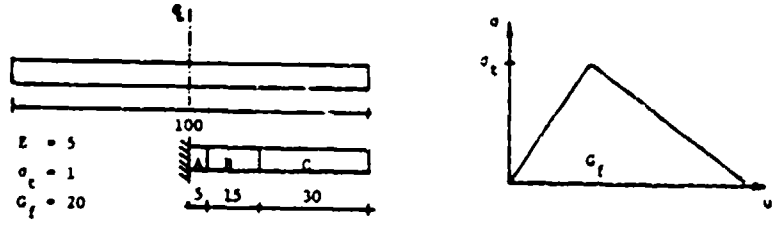

Fig. 2 Quasistatic Model Problem

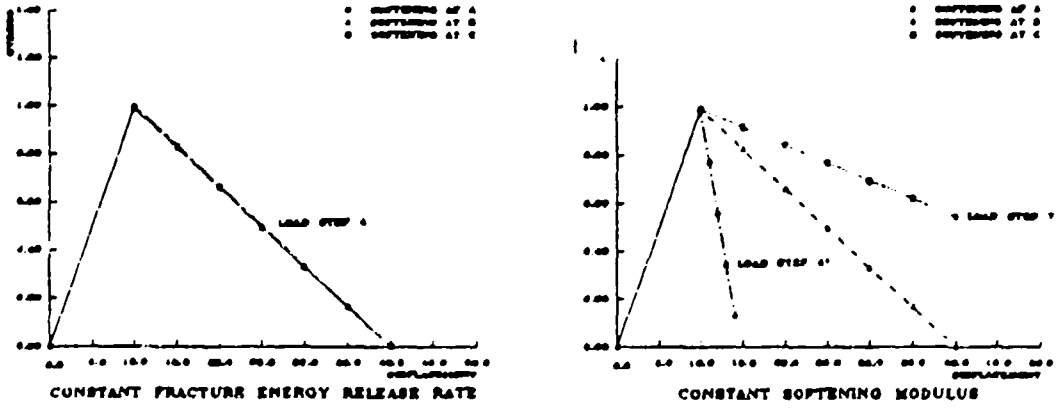

Fig. 3 Global Response Behaviour

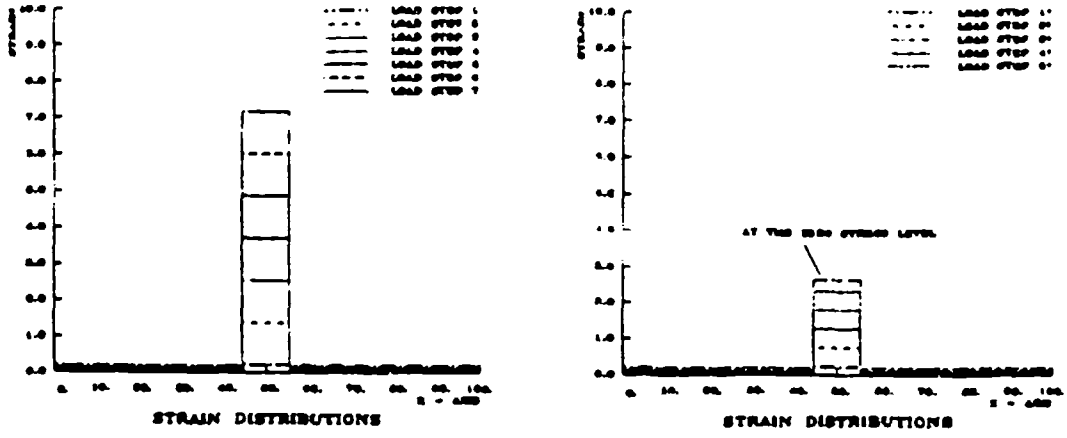

Localized Softening in Element A

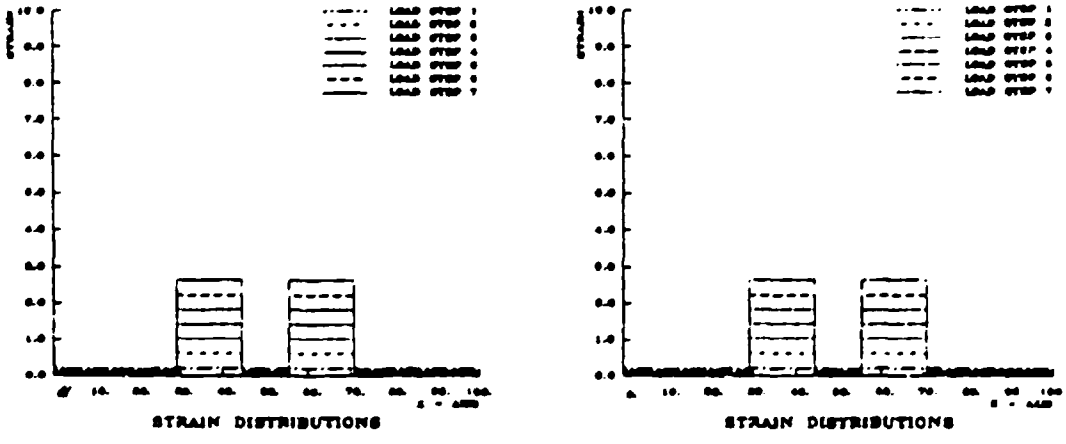

Localized Softening in Element B

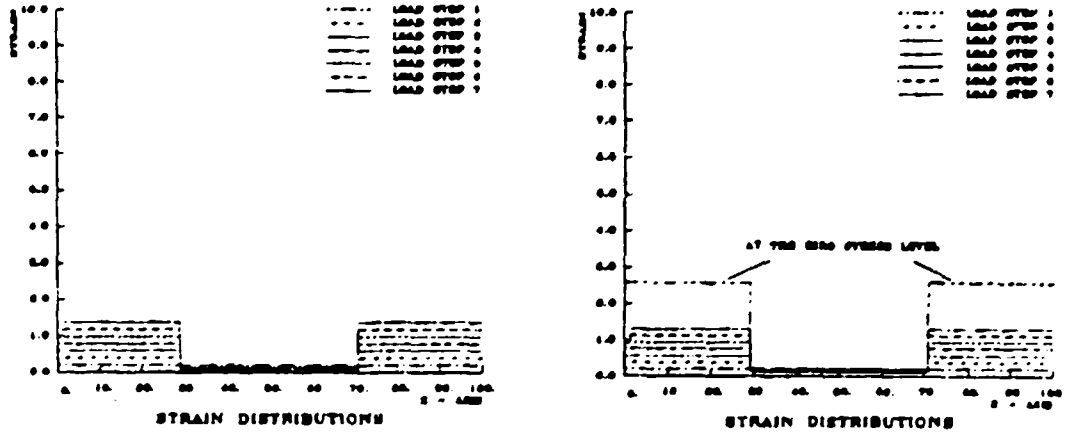

Localized Softening in Element C

Composite Fracture Model Constant Strain Softening

Fig. 4 Localization of Tensile Failure

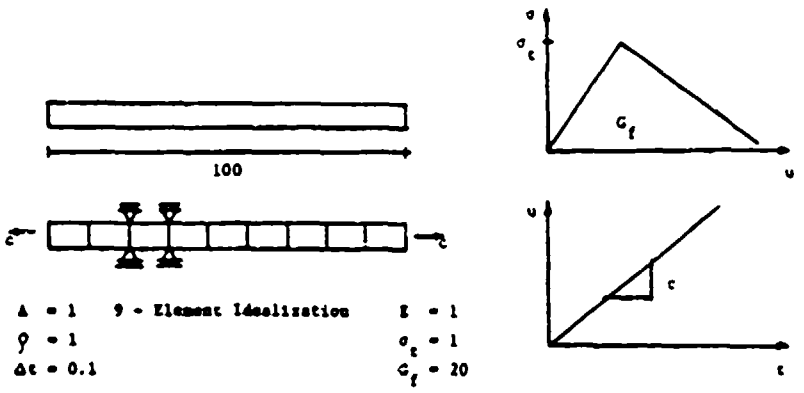

Fig. 5 Dynamic Model Problem

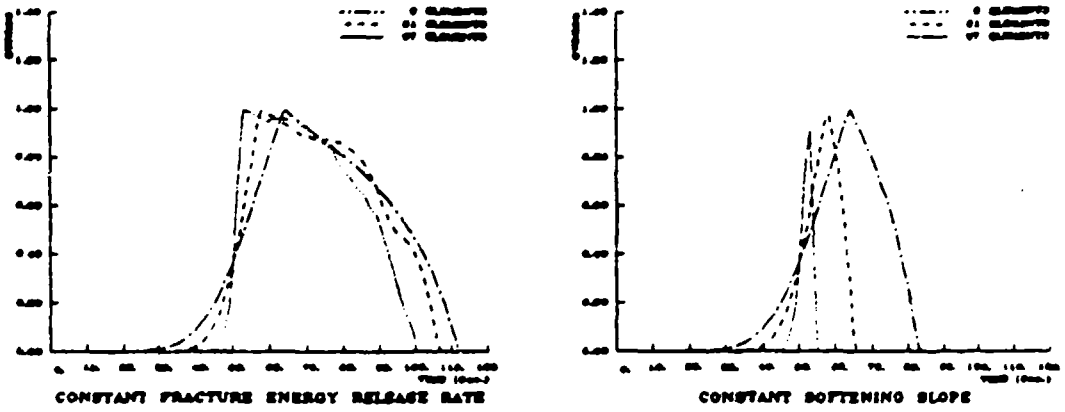

Fig. 6 Global Response Behaviour

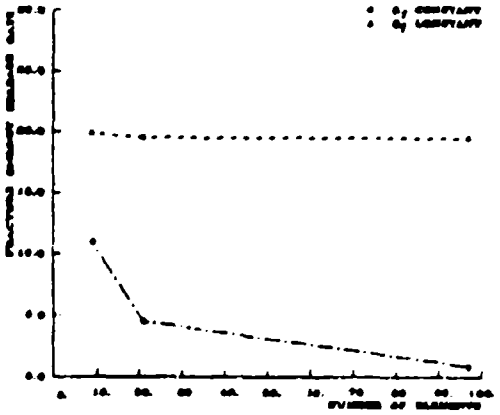

Fig. 7 Mesh Sensitivity of Fracture Energy

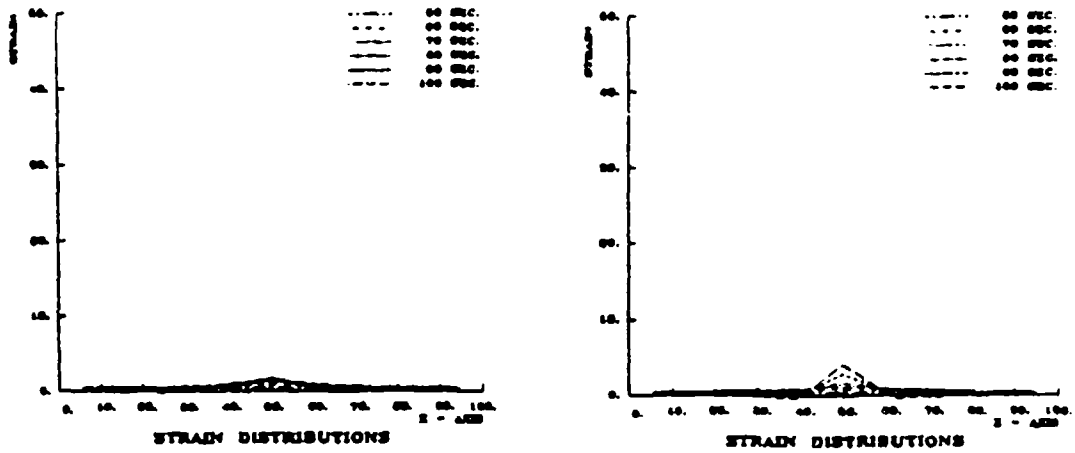

9 - Element Idealization

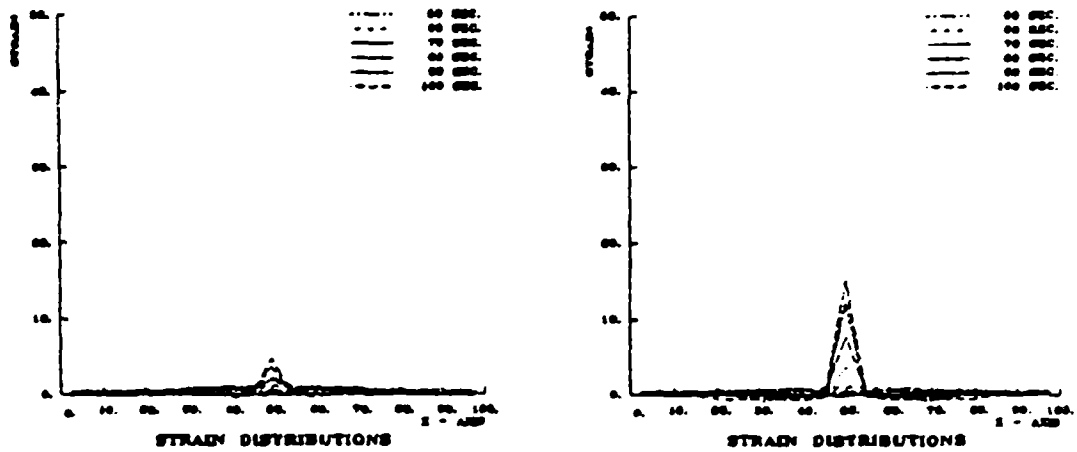

21 - Element Idealization

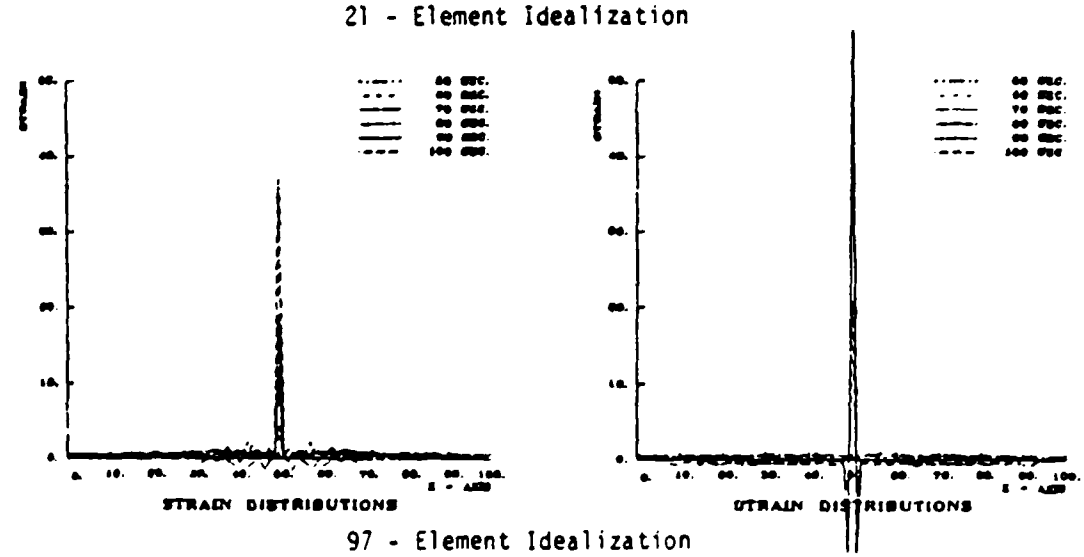

97 - Element Idealization

Composite Fracture Model

Constant Strain Softening

Fig. 8 Localization of Tensile Failure